AD-A190 505 PORT OF MIAMI NUMERICAL MODEL STUDY(U) COASTAL ENGINEERING RESEARCH CENTER VICKSBURG MS A SWAIN JAN 88 CERC-MP-88-2 1/2

UNCLASSIFIED F/G 13/2 NL

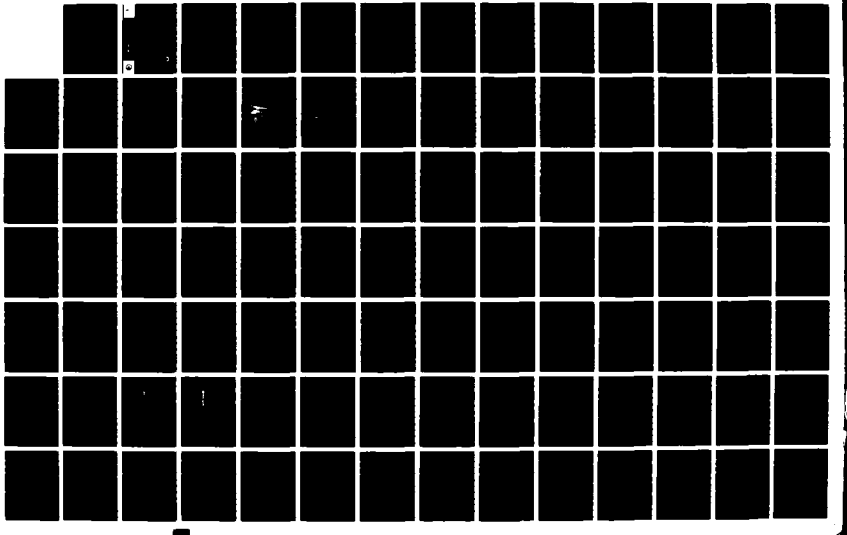

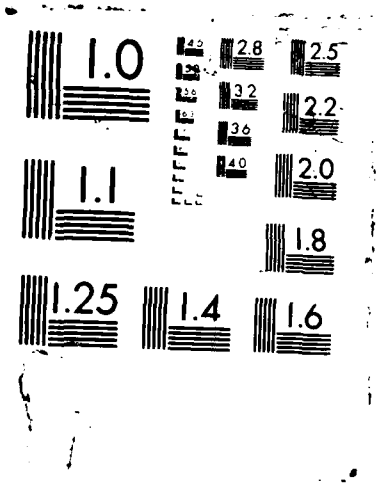
1.0
2.8
2.5
3.2
2.2
3.6
4.0
2.0
1.1
1.8
1.25
1.4
1.6

US Army Corps of Engineers

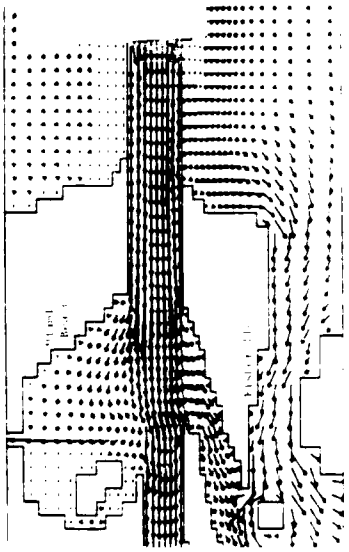

MISCELLANEOUS PAPER CERC-88-2

PORT OF MIAMI NUMERICAL MODEL STUDY

by

Abhimanyu Swain

Coastal Engineering Research Center

DEPARTMENT OF THE ARMY
Waterways Experiment Station, Corps of Engineers
PO Box 631, Vicksburg, Mississippi 39180-0631

January 1988
Final Report

Prepared for US Army Engineer District, Jacksonville
Jacksonville, Florida 32232-0019

Unclassified

SECURITY CLASSIFICATION OF THIS PAGE

REPORT DOCUMENTATION PAGE

Form Approved
OMB No 0704-0188
Exp Date Jun 30 1986

1a REPORT SECURITY CLASSIFICATION Unclassified	1b RESTRICTIVE MARKINGS
2a SECURITY CLASSIFICATION AUTHORITY	3 DISTRIBUTION/AVAILABILITY OF REPORT Approved for public release; distribution unlimited.
2b DECLASSIFICATION/DOWNGRADING SCHEDULE	
4 PERFORMING ORGANIZATION REPORT NUMBER(S) Miscellaneous Paper CERC-88-2	5 MONITORING ORGANIZATION REPORT NUMBER(S)
6a NAME OF PERFORMING ORGANIZATION USAEWES, Coastal Engineering Research Center 6b OFFICE SYMBOL (If applicable)	7a NAME OF MONITORING ORGANIZATION
6c ADDRESS (City, State, and ZIP Code) PO Box 631 Vicksburg, MS 39180-0631	7b ADDRESS (City, State, and ZIP Code)
8a NAME OF FUNDING/SPONSORING ORGANIZATION US Army Engineer District, Jacksonville 8b OFFICE SYMBOL (If applicable)	9 PROCUREMENT INSTRUMENT IDENTIFICATION NUMBER
8c ADDRESS (City, State, and ZIP Code) PO Box 4970 Jacksonville, FL 32232-0019	10 SOURCE OF FUNDING NUMBERS PROGRAM ELEMENT NO. / PROJECT NO / TASK NO / WORK UNIT ACCESSION NO
11 TITLE (Include Security Classification) Port of Miami Numerical Model Study	
12 PERSONAL AUTHOR(S) Swain, Abhimanyu	
13a TYPE OF REPORT Final report 13b TIME COVERED FROM _____ TO _____	14 DATE OF REPORT (Year, Month, Day) January 1988 15 PAGE COUNT 127
16 SUPPLEMENTARY NOTATION Available from National Technical Information Service, 5285 Port Royal Road, Springfield, VA 22161.	
17 COSATI CODES FIELD / GROUP / SUB-GROUP	18 SUBJECT TERMS (Continue on reverse if necessary and identify by block number) Hydrodynamics Numerical models Port of Miami, Florida Structural and nonstructural modification plans

19 ABSTRACT (Continue on reverse if necessary and identify by block number)

The US Army Engineer District, Jacksonville (CESAJ), is evaluating jetty modification plans at the entrance to the Miami Harbor to alleviate problems with strong cross currents at the ocean entrance and inner harbor channels. The US Army Engineer Waterways Experiment Station's (CEWES's), Coastal Engineering Research Center (CERC), was requested by CESAJ to conduct a tidal circulation numerical model study to better quantify the problem and to evaluate remedies.

Discussed herein is the WES Implicit Flooding Model (WIFM), a two-dimensional vertically integrated numerical model, along with a companion prototype data collection study in the Miami area, which CERC applied. The field data required for numerical model calibration and verification were collected by the National Oceanic and Atmospheric Administration (NOAA) and CERC.

(Continued)

20 DISTRIBUTION/AVAILABILITY OF ABSTRACT ☒ UNCLASSIFIED/UNLIMITED ☐ SAME AS RPT ☐ DTIC USERS	21 ABSTRACT SECURITY CLASSIFICATION Unclassified
22a NAME OF RESPONSIBLE INDIVIDUAL	22b TELEPHONE (Include Area Code) / 22c OFFICE SYMBOL

DD FORM 1473, 84 MAR 83 APR edition may be used until exhausted
All other editions are obsolete

SECURITY CLASSIFICATION OF THIS PAGE
Unclassified

SECURITY CLASSIFICATION OF THIS PAGE

19. ABSTRACT (Continued).

The numerical modeling approach consisted of applying WIFM in a two-phase modeling study. The first phase involved a global model. This model was calibrated against neap tidal events and was verified against spring tidal events using measured data.

The second phase of the modeling effort involved the development of a fine resolution grid in the entrance channel and port facility areas. Boundary conditions for this grid were supplied by the global model. This model was calibrated and verified for tidal events using observed data.

This report describes the use of the gobal and the refined numerical models to evaluate the tidal current regime at the entrance to the Port of Miami, and to assess the impact of structural (jetty extensions) and nonstructural modification plans for reducing strong cross-current effects on navigation.

PREFACE

This report describes the application of the US Army Engineer Waterways Experiment Station (CEWES) Coastal Engineering Research Center's (CERC's) Implicit Flooding Model to the entrance and port facility areas of Miami Harbor. The project was authorized and funded by the US Army Engineer District, Jacksonville (CESAJ), under project management of Mr. Ed Hodgens and under general direction of Mr. A. J. Salem, Chief, Planning Division.

Field data required for numerical model calibration and verification were provided by the National Oceanic and Atmospheric Administration (NOAA) and the Engineering Development Division (CD), CERC.

The study was performed and this report prepared by Dr. Abhimanyu Swain, Coastal Processes Branch (CR-P), Research Division (CR), CERC, under direct supervision of Dr. Steven A. Hughes, Chief, CR-P, and Mr. H. Lee Butler, Chief, CR; and under general supervision of Dr. James R. Houston and Mr. Charles C. Calhoun, Jr., Chief and Assistant Chief, CERC, respectively. Dr. Hughes provided technical review of the manuscript, and Dr. Norman W. Scheffner provided technical assistance throughout the project. This report was edited by Ms. Shirley A. J. Hanshaw, Information Products Division, Information Technology Laboratory, CEWES.

Commander and Director of CEWES during publication of this report was COL Dwayne G. Lee, CE. Technical Director was Dr. Robert W. Whalin.

TABLE OF CONTENTS

CONVERSION FACTORS, NON-SI TO SI (METRIC) UNITS OF MEASUREMENT

Non-SI units of measurement used in this report can be converted to SI (metric) units as follows:

Multiply	By	To Obtain
cubic feet per second	0.02831685	cubic metres per second
feet	0.3048	metres
knots (international)	0.5144444	metres per second
miles (US nautical)	1.852	kilometres
miles (US statute)	1.609347	kilometres
square miles (US statute)	2.589998	square kilometres

PORT OF MIAMI NUMERICAL MODEL STUDY

PART I: INTRODUCTION

Background

1. The Port of Miami, Florida, is located in the northern part of Biscayne Bay and along both banks of the lower part of the Miami River (Figure 1). The major deepwater navigation entrance to the port is via a dredged channel extending several miles from the ocean, through Government Cut, and across the bay to the turning basin at the municipal terminal. Because of problems with strong cross currents at the ocean entrance and inner harbor channels to Miami Harbor, the US Army Engineer District, Jacksonville (CESAJ), is evaluating jetty modification plans at the entrance channel. To better quantify the problems and to evaluate remedies, the US Army Engineer Waterways Experiment Station's (CEWES's) Coastal Engineering Research Center (CERC), was requested to conduct a tidal circulation numerical model study.

2. CERC applied the WES Implicit Flooding Model (WIFM) (Butler, in preparation), a two-dimensional (2-D) vertically integrated numerical model, along with a companion prototype data collection study in the Miami area. The field data required for numerical model calibration and verification were collected by the National Oceanic and Atmospheric Administration (NOAA) and CERC. All numerical computations were performed on the Control Data Corporation's CYBER 205.

3. The numerical modeling approach consisted of applying WIFM in a two-phase modeling study. The first phase involved a global model which included areas of the inner harbor and a substantial open ocean area with a 200- to 300-ft* minimum grid cell dimension. The horizontal grid spacing was variable, and the finer resolution was concentrated at the ocean entrance and port facilities. This model was calibrated against neap tidal events and was verified against spring tidal events using measured data.

4. The second phase of the modeling effort involved the development of a fine resolution grid (minimum grid dimension of 100 ft) in the entrance

---

* A table of factors for converting non-SI units of measurement to SI (metric) units is presented on page 3.

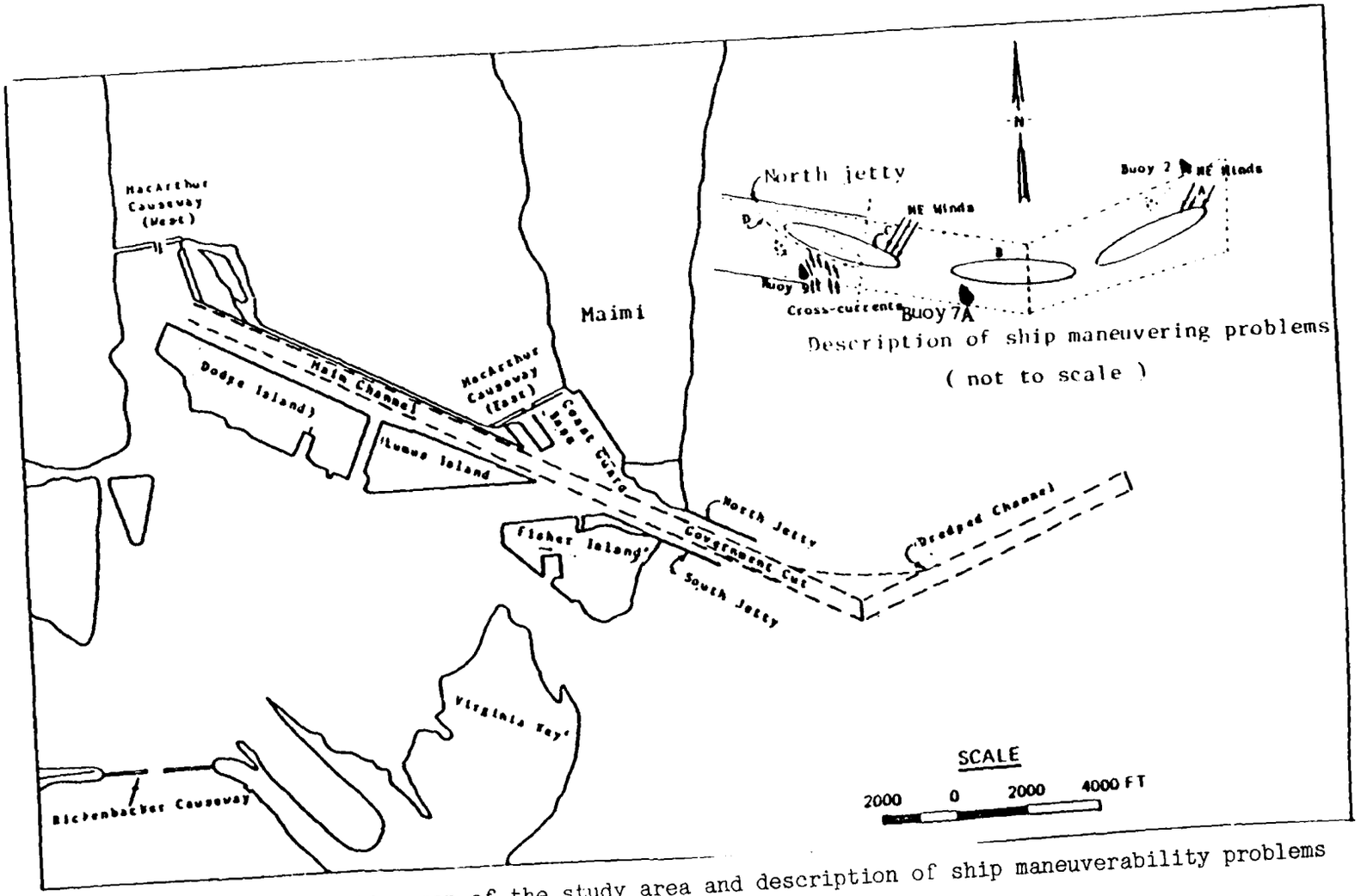

Figure 1. Location map of the study area and description of ship maneuverability problems

channel and port facility areas. Boundary conditions for this grid were supplied by the global model. This model was calibrated and verified for tidal events using observed data. The refined numerical model was necessary to permit accurate determination of the impact of small-scale changes to the port and entrance channel system on the coastal current regime and port hydrodynamics.

Scope

5. This report describes the use of the global and refined numerical models to evaluate the tidal current regime at the entrance to the Port of Miami and to assess the impact of structural (jetty extensions) and nonstructural modification plans for reducing strong cross-current effects on navigation. Hydrodynamic simulations using the refined grid model were made to provide input data into the vessel simulation study conducted by the US Department of Transportation Maritime Administration's Computer-Aided Operation and Research Facility (CAROF). This study was sponsored by CESAJ for the Port of Miami.

PART II: CHARACTERISTICS OF THE STUDY AREA

Study Area Description

6. The study area, Port of Miami, Florida, is located in the northern part of Biscayne Bay and along both banks of the lower 6-mile reach of the Miami River (Figure 1) which empties into the west side of the bay. The northern part of the Bay is separated from the Atlantic Ocean by Miami Beach Peninsula and the southern part by Fisher Island, Virginia Key, and Key Biscayne. Average water depths in Biscayne Bay range from 5 to 10 ft at mean low water (mlw).

7. The main mechanism responsible for flow in and out of the bay is the semidiurnal astronomical tide. The mean neap tide is about 0.8 ft (above the National Geodetic Vertical Datum (NGVD)), and the mean spring tide is about 1.3 ft in the bay. Tidal ranges in the bay are about 81 percent of the tidal range in the open coast. Mean tide variation between the harbor entrance and the bay is about 0.2 ft. Strong easterly winds raise the water level about 0.7 ft at the entrance to the port and 0.5 ft in the bay, while strong westerly winds lower the water level about 0.5 ft at the entrance and about 0.25 ft in the bay (Headquarters, US Army Corps of Engineers 1982).

8. The major deepwater navigation entrance to the port is via a dredged channel extending several miles from the ocean, through Government Cut, and across the bay to the turning basin between Fisher and Lumus islands. Government Cut is flanked on either side by two stone jetties (Figure 1), one extending from the southern end of Miami Beach and the other from the northeasterly side of Fisher Island. On the west side of this island are two man-made islands, triangular-shaped Lumus Island and rectangular-shaped Dodge Island, the main function of which is to handle cargoes.

Ship Maneuverability Problems

9. Large ships sailing into the Port of Miami encounter problems with cross currents at two distinct locations along the dredged channel. These two sites were identified by the ships' pilots as locations A and C (Figure 1). The problem at location A occurs when northeasterly winds blow over area A. These winds drive buoy 2 into the main channel, as shown in Figure 1. Ships

sailing toward the harbor are forced to maintain a crab angle about 4° S (according to pilots). Visible evidence on Gulf Stream currents also has been reported on the southern side of the dredged channel. The main edge and width of the Gulf Stream are unknown. There appears to be no literature on Gulf Stream migrations in the vicinity of the Port of Miami; however, pilot reports indicate that the Gulf Stream edge migrates westward as far as channel Buoy 7A along the channel.

10. Vessels leaving the dogleg turn (position B) enter Government Cut along the center line of the channel. During their sail they must maintain a course toward the south jetty to avoid collision with Buoy 8 (Figure 1) which penetrates into the main channel when northeasterly winds blow over the area. As ships come abreast of the north jetty, they must maintain a crab angle to avoid collision with Buoy 9 (position C). This near-collision is caused by northeasterly winds pushing the stern of the ship toward the south jetty, thereby causing the bow to move toward the north jetty. Northeast wind effects are partially blocked by the north jetty as the ship's stern passes the tip of the north jetty. At this time the vessel is pushed toward the north jetty (position D) by strong cross currents generated at the tip of the south jetty.

11. As southwesterly winds and cross currents intensify the movement of Buoy 9 into Government Cut Channel, vessels must follow a course closer to the north jetty to avoid colliding with the buoy. Under normal wind conditions ship collision is not a problem; however, if the wind and current forces on the ship are increased, the vessel can be pushed closer to the north jetty and possibly grounded. Pilot reports indicate grounding of ships at the north jetty under gusty southwesterly winds.

12. During flood tide with northeasterly winds, large vessels avoid meeting each other in the vicinity of the jetties for the reasons described above. This restriction prevents timely arrival and/or departure of ships and endangers ship safety. A similar but less serious situation occurs when vessels leave the port during ebb tides.

13. In its application of WIFM to these problems, CERC will (a) evaluate tidal current regime at the entrance to the Port of Miami, (b) assess the impact of proposed jetty extensions on reducing strong cross-current effects on navigation, and (c) evaluate the impact of proposed port facility changes on tidal circulation.

PART III: COMPUTATIONAL METHODS

Governing Equations

14. The governing equations WIFM uses for hydrodynamic calculations are as follows:

Continuity Equation

$$\frac{\partial \eta}{\partial t} + \frac{\partial}{\partial x}(ud) + \frac{\partial}{\partial y}(vd) = R \qquad (1)$$

Momentum Equation (x-direction)

$$\frac{\partial u}{\partial t} + u\frac{\partial u}{\partial x} + v\frac{\partial u}{\partial y} - fv + g\frac{\partial}{\partial x}(\eta - \eta_a) + \frac{gu}{C^2 d}(u^2 + v^2)^{1/2}$$

$$- \varepsilon\left(\frac{\partial^2 u}{\partial x^2} + \frac{\partial^2 u}{\partial y^2}\right) + F_x = 0 \qquad (2)$$

Momentum Equation (y-direction)

$$\frac{\partial v}{\partial t} + u\frac{\partial v}{\partial x} + v\frac{\partial v}{\partial y} + fu + g\frac{\partial}{\partial y}(\eta - \eta_a) + \frac{gv}{C^2 d}(u^2 + v^2)^{1/2}$$

$$- \varepsilon\left(\frac{\partial^2 v}{\partial x^2} + \frac{\partial^2 v}{\partial y^2}\right) + F_y = 0 \qquad (3)$$

in which η* , u , and v are the dependent variables representing water surface elevation above datum and vertically integrated velocities in

---

* For convenience, symbols and abbreviations are listed in the Notation (Appendix A).

the x- and y-directions, respectively. Independent variables in the above equations are:

$d = \eta - h$, total water depth

h = bed elevation above datum

t = time

f = Coriolis parameter

g = acceleration due to gravity

η_a = hydrostatic water elevation due to atmospheric pressure differences

C = Chézy coefficient

ε = eddy viscosity coefficient

F_x, F_y = external forces in the x- and y-directions, respectively (i.e., wind stress)

Numerical Formulation

15. WIFM uses the alternating-direction-implicit (ADI) scheme to solve Equations 1-3. However, because of the inclusion of the advective terms in these equations, the ADI scheme encountered stability problems. To minimize these problems, WIFM uses a centered stabilizing-correction (SC) scheme, that is accurate to second order in space and time. Boundary conditions can be formulated to the same order of accuracy. A brief description of this technique is given below. Butler (in preparation) provides additional details on the SC scheme.

16. Equations 1, 2, and 3 can be written in matrix form as

$$U_t + AU_x + BU_y = 0 \tag{4}$$

where

$$U = \begin{bmatrix} \eta \\ u \\ v \end{bmatrix}, \quad A = \begin{bmatrix} o & d & o \\ g & o & o \\ o & o & o \end{bmatrix}, \quad B = \begin{bmatrix} o & o & d \\ o & o & o \\ g & o & o \end{bmatrix}$$

The SC scheme for solving Equation 4 is

$$(1 + \lambda_x)\, U^* = (1 - \lambda_x - 2\lambda_y)\, U^{K-1} \tag{5}$$

$$(1 + \lambda_y)\, U^{\kappa+1} = U^* + \lambda_y\, U^{\kappa-1} \tag{6}$$

where

$\lambda_x = \frac{1}{2}\frac{\Delta t}{\Delta x} A\delta_x$, 2-D difference operator

Δt = time-step

Δx = length of computational cell in x-direction

δ_x = centered difference operator

U^* = Value of u at an intermediate time-step level ($\kappa + 1$ time level)

κ = integer time-step counter

$*$ = intermediate time-step level

$\lambda_y = \frac{1}{2}\frac{\Delta t}{\Delta_y} B\delta_y$, 2-D difference operator

Δ_y = length of a computational cell in y-direction

δ_y = centered difference operator

17. The SC scheme consists of two steps: approximating the grid in the x-direction and sweeping the grid in the y-direction. Completing both sweeps constitutes a full time-step and marches the solution from the κ^{th} time level to the $\kappa + 1^{th}$ time level. The forms of the continuity and momentum equations employed in the multioperational hydrodynamic scheme are given by

X-sweep

$$\frac{1}{2\Delta t}(\eta^* - \eta^{\kappa-1}) + \frac{1}{2\Delta x}\delta_x(u^* d + u^{\kappa-1} d) + \frac{1}{\Delta y}\delta_y(v^{\kappa-1} d) = 0 \tag{7}$$

$$\frac{1}{2\Delta t}(u^* - u^{\kappa-1}) + \frac{g}{2\Delta x}\delta_x(\eta^* + \eta^{\kappa-1}) = 0 \tag{8}$$

$$\frac{1}{2\Delta t}(v^* - v^{\kappa-1}) + \frac{g}{\Delta y}\delta_y(\eta^{\kappa-1}) = 0 \tag{9}$$

and

Y-sweep

$$\frac{1}{2\Delta t}(\eta^{\kappa-1} - \eta^*) + \frac{1}{2\Delta y}\delta_y(v^{\kappa-1} d - v^{\kappa-1} d) = 0 \tag{10}$$

$$u^{\kappa+1} = u^* \tag{11}$$

$$\frac{1}{2\Delta t}(v^{\kappa+1} - v^*) + \frac{g}{2\Delta y}\delta_y(\eta^{\kappa+1} - \eta^{\kappa-1}) = 0 \tag{12}$$

18. Notably, v^* in Equation 9 represents a functional value computed for the $\kappa - 1^{th}$ time-level. If the value of v^* from Equation 9 and the value of u^* from Equation 11 are substituted into Equations 7 and 8, the following simplified equations are obtained:

X-sweep

$$\frac{1}{2\Delta t}(\eta^* - \eta^{\kappa-1}) + \frac{1}{2\Delta x}\delta_x(u^{\kappa+1}d + u^{\kappa-1}d) + \frac{1}{\Delta y}\delta_y(v^{\kappa-1}d) = 0 \quad (13)$$

$$\frac{1}{2\Delta t}(u^{\kappa+1} - u^{\kappa-1}) + \frac{g}{2\Delta x}\delta_x(\eta^* + \eta^{\kappa-1}) = 0 \quad (14)$$

Y-sweep

$$\frac{1}{2\Delta t}(\eta^{\kappa+1} - \eta^*) + \frac{1}{2\Delta y}\delta_y(v^{\kappa+1}d - v^{\kappa-1}d) = 0 \quad (15)$$

$$\frac{1}{2\Delta t}(v^{\kappa+1} - v^{\kappa-1}) + \frac{g}{2\Delta y}\delta_y(\eta^{\kappa+1} + \eta^{\kappa-1}) = 0 \quad (16)$$

Equations 13 and 14 and 15 and 16 are alternatively solved in WIFM by applying these finite difference equations to one column (X-sweep) or row (Y-sweep), respectively, of the numerical grid. Butler (1984) gives the solution method.

Grid Schematization

19. WIFM uses a stretching transform

$$x = a + b\,Z^c \quad (17)$$

where

x = physical distances

a,b,c = arbitrary constants

Z = computational distance

for mapping distances along the coordinate directions. A detailed description of the program MAPIT, which maps a variable grid in real space into a uniform

grid in computational space, is described by Butler (in preparation). MAPIT maps each coordinate direction independently and maximizes grid resolution (finer cells) in areas of hydrodynamic importance and minimizes the number of computational cells (coarser cells) in areas of less importance.

Global grid

20. A global grid was constructed to model the hydrodynamic impact of the large open ocean. Since it is not practical to make numerical computations in real space, real spaces were mapped into computational spaces by using Equation 17. This technique generated a variably spaced grid which included areas of Biscayne Bay north and south of Lumus Island, the entrance channel and Norris Cut, and approximately 40 square miles of open ocean around the entrance. There were 80 computational cells in the longitudinal direction and 50 cells in the transverse direction. This grid approximates the entire area of interest with 4,000 cells. Finer cells (300-ft minimum cell dimension) were provided in areas of hydrodynamic importance and coarser cells in areas of less importance. Figure 2 shows a portion of the global grid laid over NOAA Chart 11467 (US Department of Commerce 1984).

Refined grid

21. The second phase of the numerical modeling effort consisted of the development of a fine resolution grid (150-ft minimum cell dimension) in the entrance channel and port facility areas. The finer resolution permits accurate determination of the impact of small-scale changes to the port and entrance channel system on the coastal current regime and port hydrodynamics. This grid, which includes the inlet and port facility areas described for the global grid and approximately 4 square miles around the entrance to the port, is composed of 83 cells in the longitudinal direction and 58 cells in the transverse direction. It covers the area of interest with 4,814 computational cells. Figure 3 presents the refined grid laid over NOAA Chart 11467.

Grid coupling

22. Using the embedded grid concept to transfer hydrodynamic information from the global grid to the refined grid, WIFM required coupling between global grid cells and other boundary cells (open ocean boundary) of the refined grid. Coupling of one grid to another is done such that the cell size is the same in the coupling cells of both grids. Leenknecht, Earickson, and Butler (1984) provide additional requirements on coupling grids.

23. The hydrodynamic data transfer between global and refined models

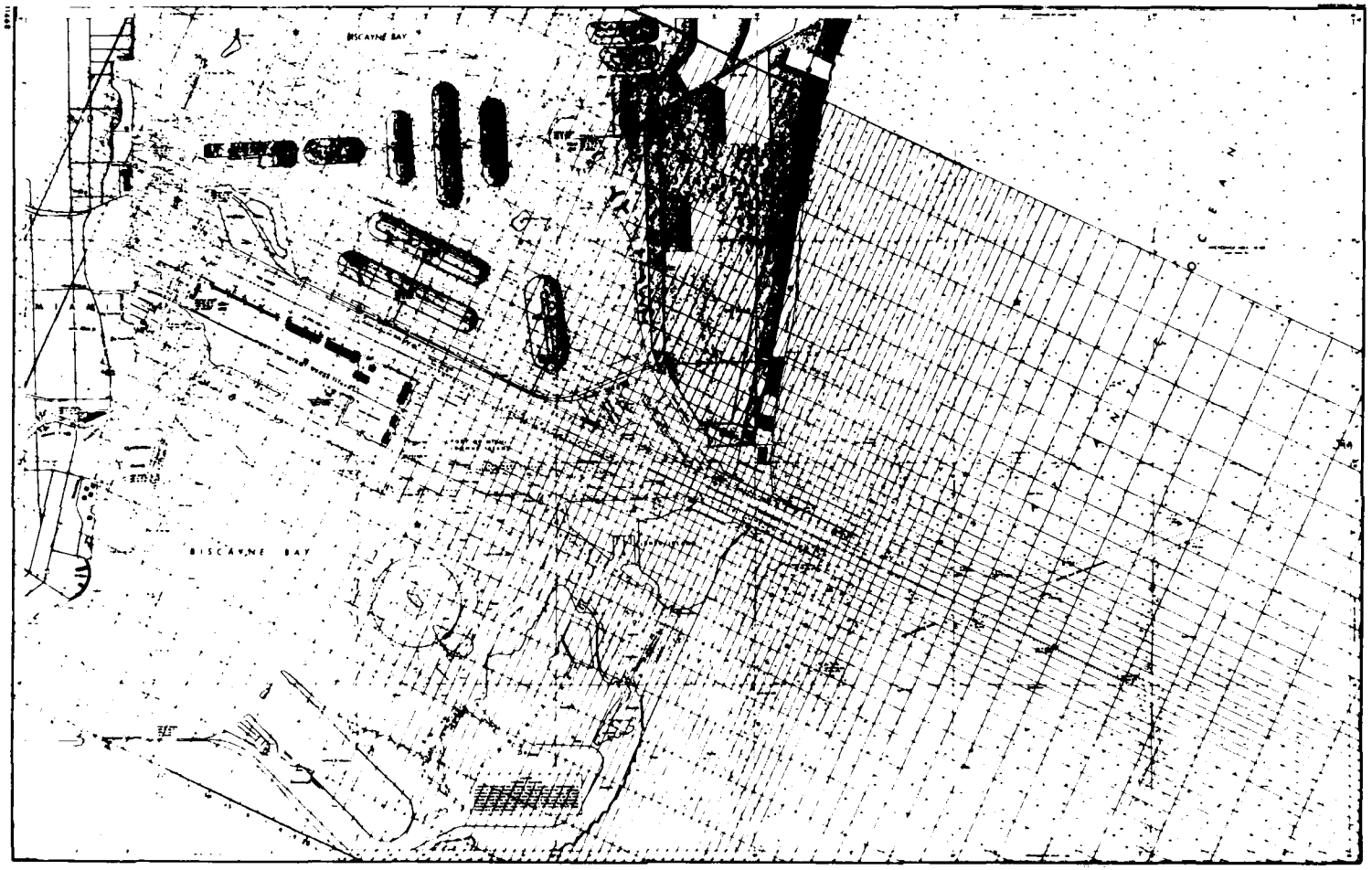

Figure 2. Global numerical model computational grid laid over NOAA Chart 11467

Figure 3. Refined numerical model computational grid laid over NOAA Chart 11467

consists of η , u , and v at each coupling cell. In the present study, global data were saved at each coupling cell and obtained for use in the refined grid by means of a utility program in WIFM. It should be noted that grid coupling is not totally dynamic in the sense that hydrodynamic simulations in the coupling cells of both grids are independent and not concurrent. Data transfer is unidirectional from the global to the refined model.

PART IV: PROTOTYPE DATA

24. Field measurement data required for numerical model calibration and verification were collected by NOAA and CERC. Following is a summary of prototype data used in this study.

NOAA Current Data and Analysis

25. NOAA conducted an intensive field data collection effort in the Miami area which included 19 stations located throughout the study area (Figure 4). The data collection periods are shown in Figure 5. Current speed and direction were recorded at 15-min intervals. These raw data were obtained from NOAA, and a data base was constructed from it for data analysis.

26. A low-pass filtering technique was performed for all prototype current and direction data. This technique was necessary to remove data spikes caused by vibration and/or other extraneous behavior of the instrument and high and low frequency trends. In addition, all observed data were analyzed separately for the east-west and north-south velocity components which corresponded in orientation to the numerical model current component. This separate analysis allowed for easy comparison between observed and predicted currents.

27. The analysis indicated that several of the 19 current stations were affected by the instrumentation and calibration errors. Therefore, these stations were discarded from the analysis. Plates 1-3 show the magnitude and direction of current recorded at stations which were not affected by the instrumentation and calibration errors.

CERC Current Data and Analysis

28. To supplement NOAA's effort, WES collected current data from in situ current meters deployed at four locations: (a) south side of Government Cut channel, (b) Norris Cut, and (c) two locations in the coastal area north of the ocean entrance. Figure 4 presents the locations of current meter stations. Table 1 shows CERC's current data collection period and current meter position and identification. Data collection periods relative to NOAA's effort are shown in Figure 5.

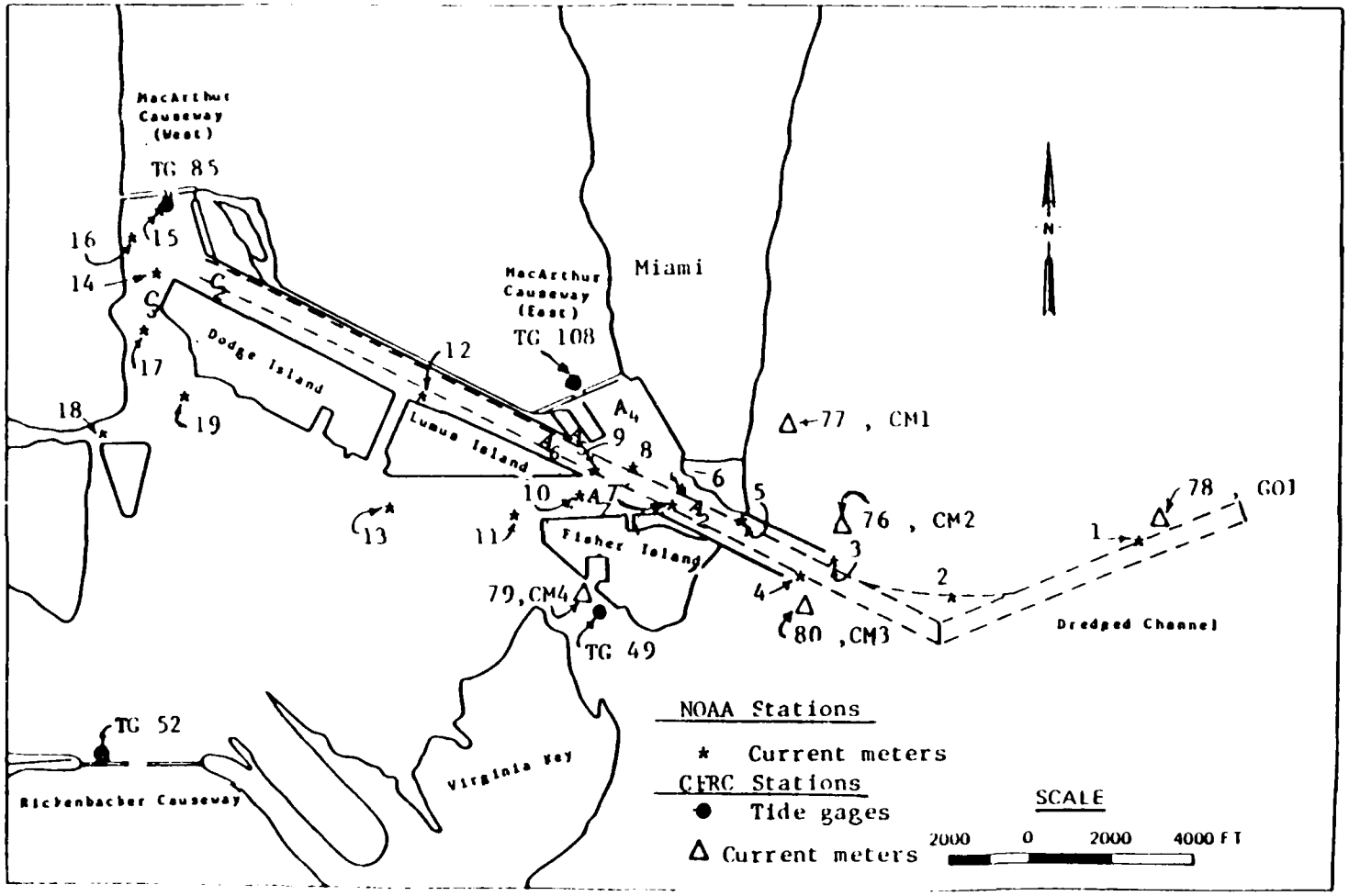

Figure 4. CERC's tide gage current meter stations and NOAA's current meter stations

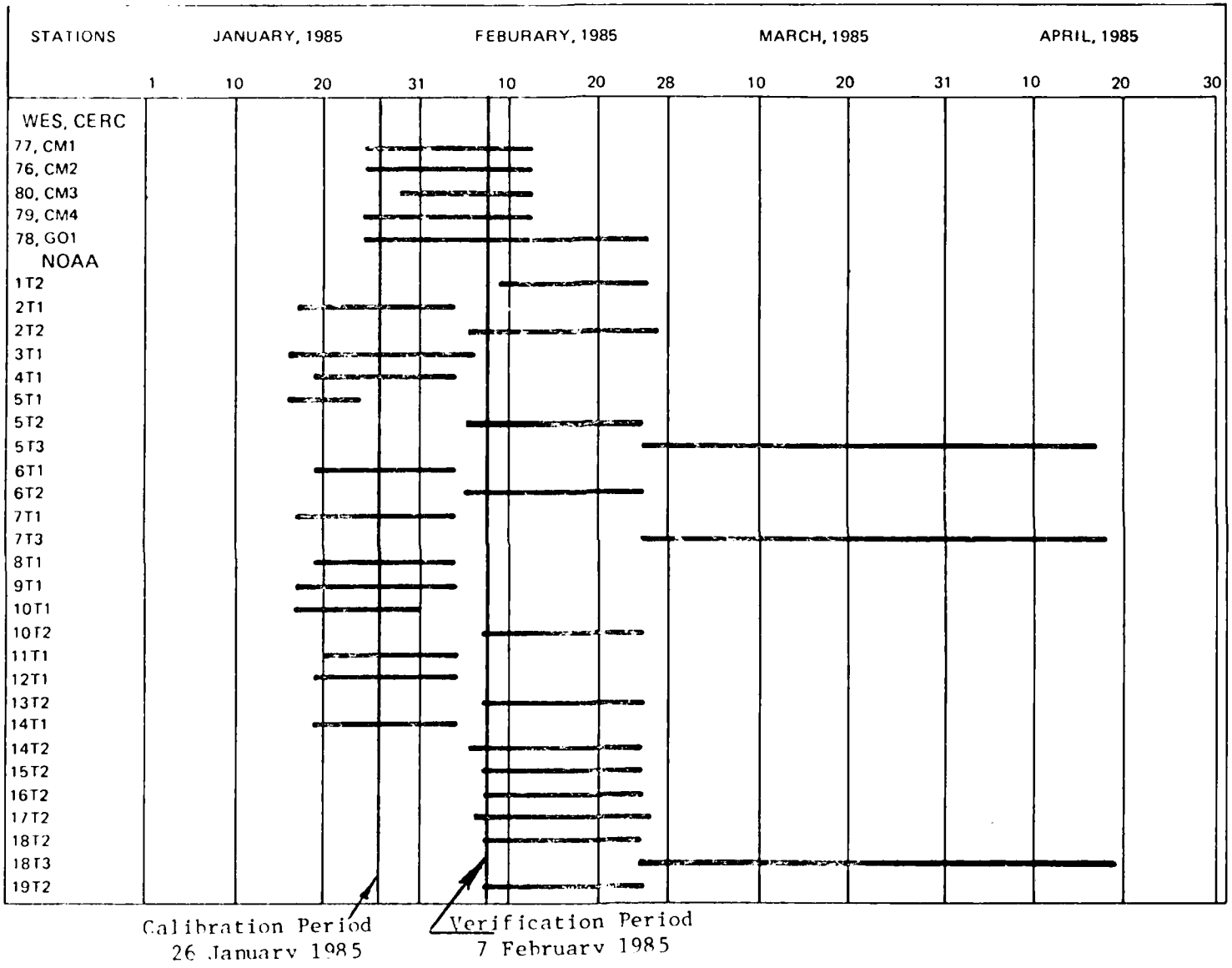

Figure 5. CERC and NOAA prototype data collection periods

29. Additional current measurements were taken by a boat survey team at three ranges in the entrance channel and at other locations throughout the harbor (Figure 4). Some of the NOAA current station locations coincide with some of those where CERC took hand-held current measurements. Overlap of current meter locations allowed verification of the prototype data accuracy.

30. Because of the failure of a number of NOAA's current meter stations, a considerable amount of additional data analysis was required of both the NOAA and CERC data in order to develop a common data base for numerical model calibration and verification. The analysis and reduction of all raw data were performed in a way similar to the techniques used for NOAA's current data analysis. Plates 4-8 present the magnitude of velocity and direction for field current measurement locations 76, 77, 78, 79, and 80 (Figure 4).

31. Hand-held current measurement data also were analyzed for use in numerical model verification. Figure 6 shows the magnitude of current measured at selected hand-held current meter stations.

CERC Tide Data and Analysis

32. CERC carried out a prototype water surface elevation data collection program to obtain field measurements required for boundary conditions and calibration and verification. This effort included installation of five tide gages at appropriate locations within the study area (Figure 4). These instruments were maintained from 23 January to 12 February 1985 for a period of 3 weeks (Table 2). Tide elevation data were recorded at every 5-min interval during the data collection period.

33. A harmonic analysis of tide data was conducted to remove data spikes and high and low frequency trends, and to subtract the mean from the data record. The mean water level was referenced to NGVD. Filtered tide data were then analyzed for the amplitude and epoch (phase) of their respective tidal constituents. This harmonic analysis was necessary to obtain boundary conditions for input to WIFM. The constituents, amplitudes, and epoch obtained from the harmonic analysis are presented in Table 3. The principal tidal constituents analyzed were three semidiurnal (M2, S2, and N2) and three diurnal (O1, K1, and P1). These six major tidal constituents were selected to provide boundary conditions for numerical model calibration and verification. Details of the tidal constituent analysis are reported by Schmalz (1985).

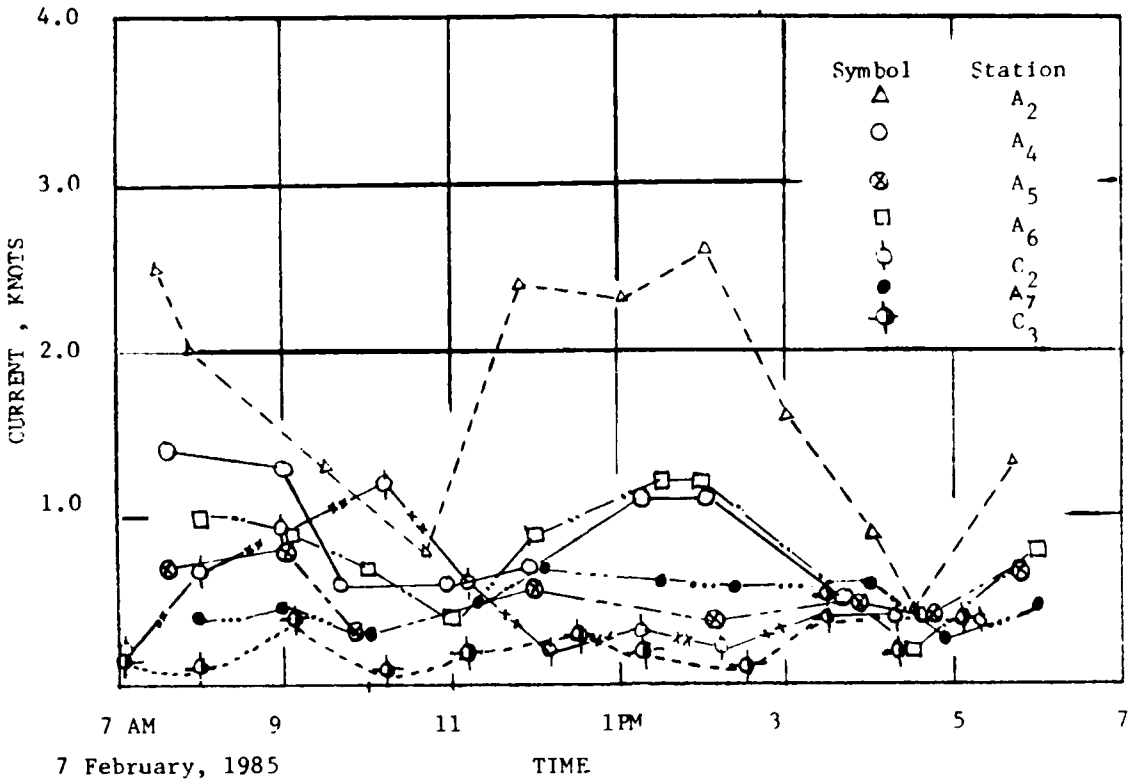

Figure 6. WES hand-held current meter locations

34. Plates 9-12 show the results of a harmonic analysis and the measured water surface elevation records for the offshore, Rickenbacker Causeway, MacArthur Causeway East, and Fisher Island gages. These results indicate that the comparison between measured and calculated water elevations above NGVD is quite good, as should as expected.

Effect of Gulf Stream on Tidal Circulation

35. Coastal currents under the influence of winds, waves, and sea level fluctuations generate boundary currents such as those of the Gulf Stream. Most of the water in the Gulf Stream comes through Yucatan Channel from the Caribbean Sea (Stommel 1965). The water is forced through the long channel caused by a differential head of about 19 cm (0.62 ft) between the Florida Peninsula on one side and the island of Cuba on the other. This channel becomes narrower and shallower downstream and attains a minimum cross section off the Coast of Miami (about 20 miles) at longitude 80°30' and latitude 25°15' where the width is about 130 miles and the maximum depth is 2,500 ft.

The average velocity of the Gulf Stream in this region is about 0.3 fps, and water mass transport is estimated to be 9.2×10^8 cfs (Stommel 1965). The order of magnitude of the maximum surface velocity in the channel off Miami is about 1.5 fps. The axis of maximum surface velocity is not in the center of the upper layer of the Gulf Stream but is displaced toward Miami. This eccentricity of velocity generates anticyclonic vorticity in the upper layer. However, this upper layer does not extend into the study area. (The study area is less than 10 miles off the coast, while the predominant Gulf Stream influence is 20 miles off the coast.)

36. Sea level change along the Miami coastline is minimum during July and August (about 5 cm) and maximum during October (8 cm). The diurnal sea level signal compared with the semidiurnal signal is very small at the Miami coast. The magnitude of current (other than tide induced) generated from sea level changes is on the order of 7 cm/sec (0.23 fps) during summer and about 5 cm/sec (0.16 fps) during winter (Blaha 1984). These results indicate that the contribution of sea level fluctuations to the observed east-west and north-south component of current velocity is insignificant.

37. The period selected for numerical model calibration (26 January 1985) and verification (7 February 1985) does not show Gulf Stream influence. Nonexistance of Gulf Stream Influence is further demonstrated by the close agreement between the measured tides and calculated time series of water surface elevations generated from tidal constituents. It is concluded that Gulf Stream currents have a negligible effect on the overall tidal circulation at the entrance to the port and in the port facility areas during most parts of the year. While it is possible that the Gulf Stream might occasionally migrate closer to the harbor entrance, it is impossible to predict these occurrences or to quantify their effect on tidal circulation.

PART V: INPUT REQUIREMENTS AND BOUNDARY CONDITIONS

Input Requirements

38. The numerical model WIFM used in this study requires an input data set consisting of 27 card groups. Also associated with WIFM are preprocessing and postprocessing codes which provide data to or a means of interpreting the results of WIFM. Care must be taken in noting which groups of data should be omitted and the number of cards needed for these groups of data. The complete input requirements for WIFM are explained in detail by Butler (in preparation).

Boundary Conditions

39. A number of boundary conditions are allowed in WIFM which can be classified into three categories: open-water boundaries, water-land boundaries, and subgrid barrier boundaries. A complete description is given by Butler (in preparation).

Open boundaries

40. The open boundary category includes seaward boundaries terminating the computational grid or channels exiting the two-dimensional grid at any point in the grid system. Water elevations or flow velocities can be prescribed as functions of location and time. This information can be input to WIFM either as tabular data or as constituent tidal components from which water surface elevations can be calculated within the code during the time-marching process. In the present study, tabular water levels were prescribed at the open-water boundary.

Land/Water boundaries

41. Included in the land/water boundaries are either fixed or variable boundaries to allow flooding and drying of cells. The usual condition at these boundaries is "no-flow" normal to the boundary which is accomplished by setting $u = o$ or $v = o$ at the appropriate cell face. Low-lying terrain may alternately dry and flood within a tidal cycle or surge history. Flooding in WIFM is simulated by making the location of the land/water boundary a function of local water depth. Once the water levels in adjacent cells rise above the level of adjacent land height (possibility of flooding), water is allowed

to flow into the "dry" cell according to a broad created weir formula (Reid and Bodine 1968). When the water level on the dry cell exceeds some small prescribed value, the boundary face is treated as open; and computations for n , u , and v are made for the cell (wet cell). The drying of cells is the inverse process, and water mass balance is conserved in these procedures.

Subgrid barriers

42. Subgrid barriers are defined along cell faces and are of three types: exposed, submerged, and overtopping. Exposed barriers permit no flow across a cell face. Submerged barriers are simulated by controlling flow across cell faces with the use of a time-dependent frictional coefficient. Overtopping barriers are treated by using the broad-crested weir formula which calculates the proper flow rate across the barrier. The barrier's characteristics are determined by its height and water elevations in the two adjoining cells.

43. At the open-water boundaries, tidal constituents, tidal elevations, or discharge input data may be used to drive WIFM. In this study the generated tidal constituents were specified at the open-water boundaries. The code uses these constituents to generate time series of surface elevations at the boundaries.

Tidal Constituents

Global grid

44. Tidal constituents were specified as the boundary condition at the following global grid boundaries: open ocean, Rickenbacker Causeway, MacArthur Causeway East, MacArthur Causeway West, and Coast Guard station. Figure 1 shows these boundaries.

Refined grid

45. Tidal constituents were specified as the boundary condition at the following refined grid boundaries: MacArthur Causeway East, MacArthur Causeway West, and Coast Guard station. Hydrodynamic values were transferred from the global grid to the refined grid at the open-ocean boundary, northern boundary, and at the southern boundary, including Rickenbacker Causeway. Hydrodynamic data transfer was accomplished by linking computational grids of the global grid with the refined grid as described in Part III of this report.

PART VI: NUMERICAL MODEL CALIBRATION AND VERIFICATION

Global Grid Calibration

46. WIFM was calibrated against the time series of water surface elevations developed from the tidal constituents generated from the harmonic analysis of prototype data for water surface elevations at Rickenbacker Causeway, MacArthur Causeway East, Fisher Island, and an offshore gage. Six predominant tidal constituents (M_2, S_2, N_2, K_1, O_1, and K_2) were used for the numerical model calibration. These constituents were selected because they provided a good representation of tide for the Miami coast.

47. The capability of the numerical model to accurately predict prototype data depends on many factors: (a) boundary specified conditions, (b) cell size in the grid, (c) water depths assigned to each cell, and (d) Manning's roughness coefficient for each cell. A detailed description of the sensitivity of WIFM results to these parameters can be found in Leenknecht et al. (1984). In this study the elevations assigned to each cell and the Manning's coefficient were adjusted to match predicted tides with prototype data.

48. The WIFM calibration period was chosen to be in the neap tidal period beginning at midnight 26 January 1985. This period was selected because the agreement between measured and calculated tides is the best, and accurate velocity measurements were available. In addition, a majority of the field stations have recorded prototype data during this period (Figure 5). Tidal constituents (magnitude and phase) were specified at Rickenbacker Causeway, MacArthur Causeway East, Fisher Island, Miami Marina, and the offshore boundary of the computational grid (see Figure 1). Tidal constituents for Miami Marina were obtained from NOAA. The tidal constituents specified at the different gage locations within the global grid served as boundary conditions for the numerical model calibration.

49. A 60-sec time-step was used in WIFM, and 26 hr of the tide were simulated at 20 locations within the global grid. Four stations (Rickenbacker Causeway, MacArthur Causeway, Fisher Island, and offshore) were selected for comparisons with WIFM computations during the entire calibration period. The number of cells and water depth for cells were adjusted to adequately describe flow conditions at the internal boundaries (MacArthur Causeway East and West,

Coast Guard station, and Rickenbacker Causeway).

50. Plates 13-16 compare predicted and measured tides at the boundaries. Plate 17 presents a multiplot of calculated tidal elevations for boundary gages. Plate 18 compares measured tide at a nonboundary gage (Fisher Island) and calculated results. The model reproduced the offshore tide with reasonable accuracy. Model performance at other locations is good with amplitude variation less than 0.1 ft and a slight phase shifting caused by channel and shoaling features of the study area.

51. Plates 19 and 20 present the results of WIFM compared to the prototype current measured by NOAA. It is seen that velocity records of peak flood and ebb flows and calculated peak flood and ebb flows match quite well for the stations shown. Because of the failure of several NOAA field stations, only selective comparisons are shown.

52. Plates 21 and 22 show computed current fields over a portion of the grid in the form of vector plots for a flood and an ebb flow, respectively. Simulation time and vector scale are given at the bottom of each plate. Tidal circulation patterns appear quite reasonable in direction and in magnitude.

53. The above results indicate that WIFM's ability to describe the hydrodynamics of the area of interest is quite good. The model quite accurately reproduced the observed tide and velocity at all stations where measurements were available.

Global Grid Verification

54. Verification of WIFM consists of its ability to reproduce accurately the hydrodynamics of the area of interest without adjusting model parameters. To test this accuracy, a period on 7 February 1985 was simulated by WIFM. This verification period was selected because extreme spring tidal events were recorded along the Miami coast, and they have significant effects on tidal circulation in the study area. In addition, a majority of the field stations have accurate prototype velocity data measured during this period (Figure 5).

55. To verify the model, computation in WIFM began at midnight on 7 February 1985 using the predominant tidal constituents described earlier. The simulation continued for a period of 26 hr. A 60-sec time-step was used in the model.

56. Computed tidal elevation and flow velocities were compared with prototype data at various locations over the grid. Plates 23-26 compare calculated and measured tidal elevations at the boundary gages. Plate 27 shows a multiple plot of WIFM-calculated tidal elevations of boundary gages. Plate 28 compares the measured and calculated tides at a nonboundary gage (Fisher Island).

57. Plates 29-31 show the measured and computed flow velocities which were obtained for the model verification period. Comparison between the measured and calculated currents is quite good except at NOAA Stations 10 and 17.

58. Figure 7 was constructed to show a comparison of WIFM current computations, prototype data measured by NOAA, and hand-held data collected by WES at NOAA Station 10. The comparison between WIFM computation and the hand-held data is quite good, while prototype data from the NOAA gage show some differences. Plate 32 displays a good comparison of WIFM computations with hand-held data at various locations along the grid (Figure 2). NOAA's prototype data are not available at these locations.

59. Plates 33 and 34 show computed current fields in the form of vector plots for a selected portion of the grid. These plots represent peak flood- and ebb-tidal flow through the entrance. Simulation time and vector scale are given at the bottom of each plate.

Refined Grid Verification

60. Verification of the refined numerical model was accomplished by using the refined grid boundary conditions. The minimum cell dimension was restricted to 120 ft. A 60-sec time-step gave simulation stability and provided sufficient resolution to accurately describe tidal circulation in the area of interest. To keep the expenses of verification to a minimum, WIFM simulated 16 hr of tide during spring tide (7 February 1985).

61. Plates 35-38 compare calculated and measured tidal elevations of the boundary gages. These results show insignificant variation in amplitude and phase between the measured and calculated water surface elevations. Plate 39 compares the measured tide at a nonboundary gage (Fisher Island) and WIFM-calculated results. Peak amplitude variation between measured and calculated results is less than 0.15 ft with little phase shifting.

62. Plates 40 and 41 compare WIFM-calculated current magnitudes and

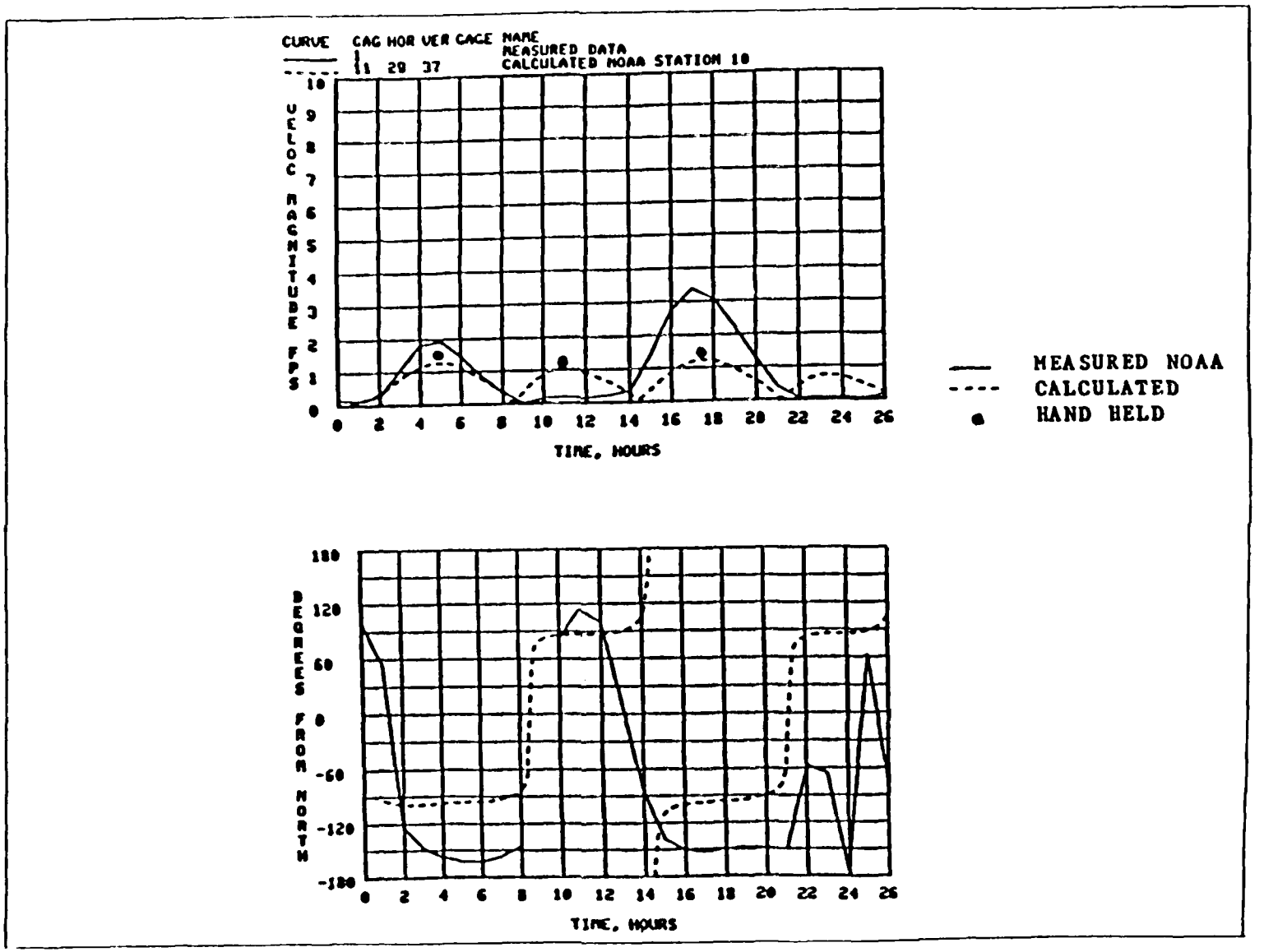

Figure 7. Comparison of calculated, measured (NOAA), and hand-held (CERC) current data

directions with prototype data measured by NOAA. The model reproduced prototype velocity records with proper phasing of the peak flood and ebb flows.

63. Based on the results described above, it was concluded that the refined numerical model accurately simulated the hydrodynamics of the area of interest, and calibration of the refined numerical model was not required. Therefore, no hydrodynamic simulations were performed for neap tide conditions (25 January 1985).

PART VII: EVALUATION OF ENTRANCE CHANNEL CROSS-CURRENT PROBLEMS AND INNER-HARBOR CHANNEL NAVIGATION PROBLEMS

Cross-Current Problems

64. Production tests were conducted to assist CESAJ in assessing the cross-current problems at the entrance to the Port of Miami. The investigation involved a numerical modeling effort to identify the problems and to evaluate the impact of proposed corrective alternatives (structural and nonstructural) on the hydrodynamic regime near the port entrance. In addition to the entrance problem, CESAJ is interested in evaluating the hydrodynamic impact of proposed changes (widening and deepening of harbor channels) to port facilities. Therefore, the numerical model test results cover a substantial portion of the Port of Miami and adjacent areas. On the basis of the results presented for refined numerical model verification, it is concluded that WIFM correctly simulates Port of Miami hydrodynamics and that the refined numerical model can therefore be used for evaluating cross-current problems at the entrance to the port and navigation problems in the inner harbor channels.

No change in topography

65. For the the *no change in topography* test, and subsequent tests, the testing period for hydrodynamic scenarios was 7 February 1985 (spring tide event), the refined numerical grid was used, and the forcing boundary conditions were identical to those used in the refined grid verification. The above testing period was selected because extreme spring tidal events, which have significant effects on tidal circulation in the study area, were recorded along the Miami coast.

66. A numerical simulation was conducted with WIFM to determine the coastal current regime and harbor hydrodynamics for the existing topography. The simulation allowed comparison of subsequent test results obtained for various structural and nonstructural modification plans. Hydrodynamic results were simulated for one tidal cycle (12.8 hr) using a 60-sec time-step. This testing period included flood and ebb flows through the entrance channel. Plates 42 and 43 show computed current field for the flood and ebb flows in the form of vector plots for a selected portion of the grid. Simulation time and vector scale are given at the bottom of each plate.

Structural changes

67. Modified jetty configurations were simulated using existing bathymetry features. The structural changes tested included four alternative jetty modification plans to alleviate problems with strong cross currents at the ocean entrance. These alternative plans are given in Table 4 (Cases 2-5).

68. Plates 44 and 45 show computed current field for the flood and ebb flows in the form of vector plots for the second test (Table 4). A comparison between test results obtained for the existing topography (Plates 42 and 43) and the second test (Plates 44 and 45) indicates that the strong cross currents generated at the tip of the south jetty due to unequal jetty lengths were eliminated when the jetties were of equal length. This finding clearly indicates that the effects of cross currents on navigation are greater when the jetties are of unequal lengths. A possible solution for alleviating cross currents at the entrance is even length jetties.

69. Plates 46 and 47 present computed current field for the flood and ebb flows which were obtained for the third test (Table 4). In this case the jetties were of even length, and the north jetty was flared. The purpose of providing flare at the north jetty was to demonstrate the effect of confined flow on tidal circulation at the entrance. A comparison between Plates 42 and 43 and 46 and 47 shows that the magnitude of currents near the tip of the north jetty was decreased because of the addition of flare at the north jetty.

70. Results for the fourth test (Table 4) are shown in Plates 48 and 49 for the flood and ebb flows, respectively. For this test the jetties were of even length, and the south jetty was flared. Results showed that providing flare at the tip of the south jetty reduces the magnitude of current at the flared end. However, strong cross currents at the tip of the unflared jetty were not evident.

71. Plates 50 and 51 present computed current field for the fifth test (Table 4). In this case, jetties were of even length and flared at the jetty ends. As anticipated, flare at the jetty ends reduced the magnitude of currents and alleviated cross currents. These wider jetty flares produced smaller velocities at the vicinity of the flares and negligible velocity changes along Government Cut. This combination of even jetty length and flare at jetty ends appears to be a corrective measure for alleviating the problem with strong cross currents at the ocean entrance to the port of Miami.

Nonstructural changes

72. In the event jetty modification is precluded because of lack of funding, consideration should be given to nonstructural modifications (widening and deepening of navigation channels). This alternative may be less costly than structural changes while providing the additional room required for safe maneuvering of large vessels through strong cross currents at the ocean entrance.

73. Test 6 (Table 4) was conducted with WIFM to examine tidal circulation changes resulting from a hole at the tip of the north jetty. The size of the hole and the water depth in the hole are shown in Plate 52. Plates 52 and 53 show computed current fields for the flood and ebb conditions, respectively. A comparison of Plate 42 with Plates 52 and 53 shows that the magnitude of current in the hole is reduced because of increased water depth in the hole.

Navigation Problems

74. CESAJ provided a list of projected water depths in the harbor channels along with information that defines the proposed channel and turning basin widths to be tested using WIFM. Table 5 lists the maximum project water depths which were used with WIFM for channel deepening. Figure 8 shows assigned water depths (which are circled) at various locations in the harbor and the boundary lines of widened channels.

Nonstructural changes

75. Test 7 (Table 4) was conducted with WIFM to examine the nonstructural impact on tidal circulation at the entrance and in the harbor channels. The nonstructural changes included channel deepening and widening as shown in Figure 7. Table 5 lists the maximum project water depths used for channel deepening. All tests were conducted for the spring tide events (7 February 1985). Plates 54 and 55 present computed tidal currents for the flood and ebb flows, respectively. A comparison of test results obtained for the existing topography (Plates 42 and 43) and the results (Plates 54 and 55) of this test indicate that the overall tidal circulation in the harbor does not change significantly, and the magnitude of the current increases slightly in areas subjected to channel deepening and widening.

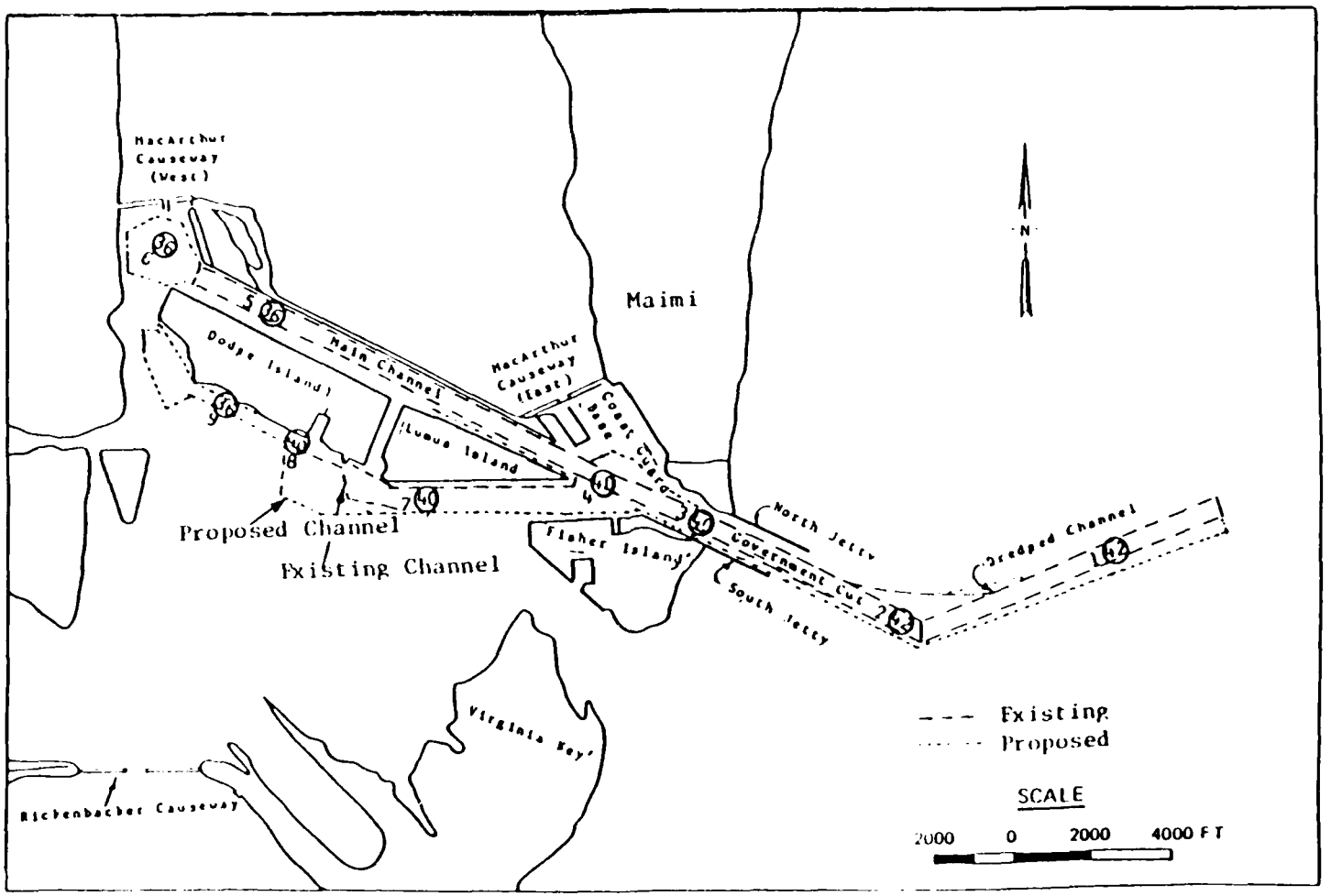

Figure 8. Boundary lines of proposed channel deepening and widening

Structural and nonstructural changes

76. For practical purposes, sometimes a combination of structural and nonstructural changes is warranted for a coastal project. Table 4 lists two of these modification plans (Tests 8 and 9) tested in WIFM.

77. In Test 8, the jetty lengths were made even, and the nonstructural changes included deepening at the jetty ends, as shown in Plate 56. No other changes were made in the harbor channels (existing topography was used). Plates 56 and 57 present computed current field for the flood- and ebb-tidal events, respectively. A comparison of this test to test results obtained for the second test indicates that the strong cross currents at the entrance to the port were reduced by deepening at the inlet throat. Results in this comparison also indicate the holes have no impact on currents in the main channel. Consequently, widening and deepening the entrance channel appear to be appropriate to mitigate cross-current problems at the entrance.

78. The final test (Test 9) conducted in WIFM included even length jetties, flared jetty ends, and deepening and widening of the inlet and harbor channels (similar to Test 7). Plates 58 and 59 present the computed tidal circulation structure at the entrance and port facility areas for the flood- and ebb-tidal flows, respectively. It is seen that the overall circulation in the harbor did not change (compare results of Tests 7 and 9) with the structural changes provided at the entrance to the port. However, the problem with strong cross currents at the entrance to the Port of Miami was alleviated.

79. Table 6 shows the relative changes in peak flood and ebb velocities at selected points with and without harbor improvements. An examination of results presented in Table 6 indicates that harbor improvements would not have significant impact on current flow through the harbor.

PART VIII: PRODUCTION RUNS FOR INPUT TO VESSEL SIMULATION STUDY

80. CAORF is conducting a vessel simulation study sponsored by CESAJ for the Port of Miami. This study requires the refined numerical model test results obtained for the existing navigation channels with existing jetties, with jetties extended to be equal and flared, and for deepened and widened channels. These various tests are listed in Table 7. For each test, the input data into the vessel simulation study were obtained during two different peak tidal flood conditions (at hour 4), one in the absence of wind and one with a constant wind of 20 knots from the northeast.

Global Model Test Runs

81. Two test runs with the global numerical model were conducted in WIFM using the global grid. For these tests, and subsequent ones (global or refined), the testing period for hydrodynamic scenarios was 7 February 1985 (at peak spring tide), and the forcing boundary conditions without the wind were identical to those used in the global/refined grid verification. The first test dealt with the existing topography and the boundary conditions described above. The second test was similar to the first but included the appropriate wind.

82. Plate 60 shows computed current field vector plots of the first test for the maximum flood flows for a selected portion of the grid. Simulation time and vector scale are given at the bottom of the plate. The hydrodynamic results from the global model were saved for input into the fine resolution model.

83. The second test included a wind of 20 knots from the northeast, which was superimposed on the existing topography of the study area and the previously used boundary conditions for the first test. Plate 61 presents the computed current vector fields for the peak flood flows. A comparison of Plates 60 and 61 indicates that the effect of storm winds at the entrance to the Port of Miami is significant. These plots show a distinct difference in the magnitude and direction of the velocity vectors at the entrance to the Port. The hydrodynamic results for the second test were saved for input into the refined model.

Refined Model Test Runs

84. A numerical test (Test 3, Table 7) was conducted in the refined numerical model to determine the coastal current regime and harbor hydrodynamics for the existing topography. The forcing boundary conditions at MacArthur Causeway East, MacArthur Causeway West, and the Coast Guard station were identical to those used in the refined model verification. However, the boundary conditions specified at Rickenbacker Causeway and at the offshore boundary of the computational grid were the hydrodynamic results obtained from the global grid for peak flood flow through the entrance channel. Hydrodynamic scenarios were obtained for hour 4 using a 60-sec time-step. Plate 62 shows computed tidal currents for the flood flow through the entrance channel in the form of vector plots for a selected portion of the grid. Simulation time and vector scale are given at the bottom of the plate.

85. Results for the fourth test (Table 7) are shown in Plate 63 for the peak flood flow conditions. For this test, the jetties were extended to be equal in length, and the boundary conditions used in WIFM were for calm conditions.

86. Plate 64 presents computed current field for the peak flood flow through the entrance for the fifth test (Table 7). In this case, the jetties are set equal in length and flared, and the entrance and harbor channels are widened and deepened. The effect by winds on the overall tidal circulation of the study area was not included in this test.

87. Plates 65, 66, and 67 present corresponding plots which were obtained for a constant wind 20 knots from the northeast. A comparison of these results (Plates 65-67) to test results (Plate 62-64) obtained for the 3rd, 4th, and 5th tests indicates that the magnitude and direction of currents at the entrance to the port were intensified in the presence of the 20-knot wind from the northeast. Table 8 lists the magnitude and direction (measured from true north) of velocity (with and without wind effects) at selective numerical grid point locations. The model indicates that the magnitude of the velocity at the tip of the north jetty was increased by about 0.5 fps, and the direction changed by about 10 deg because of the wind. This effect is seen for Cases 2 and 4 (Table 8). For Case 6, the magnitude of velocity was increased by 0.2 fps, and the change in direction was insignificant. At the south jetty, the magnitude and direction of the velocity (Table 8, Cases 1 and 2)

were changed. However, when the jetties were extended to equal length (Table 8, Cases 3 and 4), the magnitude of velocity was increased by about 0.2 fps and the direction was unchanged. Results for Cases 5 and 6 indicate that the magnitude of velocity increased by about 0.2 fps at the three locations selected for model analysis, while the direction of velocity remained practically the same. The magnitude of velocity at midchannel increased by about 0.2 fps for all cases. For Cases 1-4, the direction of velocity changed by about 5 deg because of the wind. However, no change in direction was evident for Cases 5 and 6.

PART IX: SUMMARY AND CONCLUSIONS

88. WES applied WIFM in a two-phase numerical modeling study to evaluate tidal current regime at the entrance to the Port of Miami and to examine the impact of the proposed port facility changes on tidal circulation in the harbor. The first phase consisted of a global model and the second phase a fine resolution model. The global model was calibrated against tidal constituents generated from a harmonic analysis of the prototype data. WIFM-predicted neap tides (26 January 1985) were compared against the measured data. The comparison was good.

89. The global and refined numerical models were verified during spring tides (7 February 1985). Computed water surface elevations above NGVD and flow velocities were compared with the field data at several locations across the grid. These comparisons were good. It was concluded that the refined numerical model can accurately describe the hydrodynamics of the area of interest and that calibration of this model is not required.

90. Nine alternative plans (structural, nonstructural, and the combination of both) were tested in the refined numerical model. The testing period for all cases was 7 February 1985 (spring tide).

91. Structural alternatives at the entrance to the port were found to effectively reduce cross currents when the jetties were made equal length. In addition, flared jetties of equal length provided more effective results.

92. The nonstructural modification included channel deepening and widening at the entrance to the port and in the port facility areas. Hydrodynamic scenarios obtained for this case indicated that the overall tidal circulation in the harbor did not change significantly and that the magnitude of current increased slightly in areas subjected to channel deepening and widening.

93. The structural and nonstructural changes included jetty extensions as well as deepening and widening inlet and harbor channels. The hydrodynamic results obtained for Case 9 (Table 4) (flared jetties of equal length and changes made to inlet and harbor channels) were effective in alleviating strong cross currents at the entrance.

94. The numerical modeling effort required for the Port of Miami Ship Simulation Study was investigated during two different peak tidal flood conditions (spring tide at hour 4), one in the absence of wind and one with a

constant wind of 20 knots from the northeast. A total of eight test runs (two global and six refined) was conducted with WIFM (Table 7).

95. Hydrodynamic results obtained for these tests were provided for input information into the vessel simulation study.

REFERENCES

Blaha, J. P. 1984 (Sep). "Fluctuation of Monthly Sea Level as related to the Intensity of the Gulf Stream from Key West to Norfolk", Journal of Geophysical Research, Vol 89, No. C5.

Butler, H. L. In preparation. "WIFM-WES Implicit Flooding Model: Theory and Program Documentation," Miscellaneous Paper, US Army Engineer Waterways Experiment Station, Coastal Engineering Research Center, Vicksburg, Miss.

Headquarters, US Army Corps of Engineers. 1982. "The Port of Miami, Port Everglades Palm Beach, and Port Canaveral, Florida," Port Series, US Government Printing Office, Washington, DC.

Leenknecht, D. A., Earickson, J. A., and Butler, H. L. 1984. "Numerical Simulation of Oregon Inlet Control Structures' Effects on Storm and Tide Elevations in Pamlico Sound," Technical Report CERC-84-2, US Army Engineer Waterways Experiment Station, Coastal Engineering Research Center, Vicksburg, Miss.

Reid, R. O., and Bodine, B. R. 1968 (Feb). "Numerical Model for Storm Surges in Galveston Bay," Journal of Waterways and Harbor Division, American Society of Civil Engineers, Vol 94, No. WW 1, pp 33-57.

Schmalz, R. A. 1985. "Numerical Model Investigation of Mississippi Sound and Adjacent Areas," Miscellaneous Paper CERC-85-2, US Army Engineer Waterways Experiment Station, Coastal Engineering Research Center, Vicksburg, Miss.

Stommel, H. 1965. The Gulf Stream: A Physical and Dynamic Description, University of California Press, Berkeley, California.

US Department of Commerce. 1984. "United States East Coast, Miami Harbor," Chart 11467, National Oceanic and Atmospheric Administration, Washington, DC.

Table 1

Summary of Prototype Current Data, WES Effort

Current Meter Position	Current Meter Identification	Latitude	Longitude	Data Collection Began	Data Collection Ended	Collection Period days
Nearshore, north of Government Cut	77,CM1	25°46.2'	80°7.7'	1-23-85	2-12-85	21
Near tip of north jetty	76,CM2	25°45.8'	80°7.4'	1-23-85	2-12-85	21
Near tip of south jetty	80,CM3	25°45.4'	80°7.6'	1-27-85	2-12-85	17
Norris Cut	79,CM4	25°45.5'	80°8.7'	1-23-85	2-12-85	17
Near Outer Bar	78,G01	25°45.7'	80°5.9'	1-23-85	2-25-85	34

Table 2

Summary of Prototype Tide Data, WES Effort

Tide Gage Location	Tide Gage Identification	Latitude	Longitude	Data Collection Began	Data Collection Ended	Collection Period, days
Fisher Island	TG 49	25°45.3'	80°8.5'	1-22-85	2-12-85	22
Rickenbacker Causeway	TG 52	25°14.7'	80°11.1'	1-22-85	2-12-85	22
Offshore	TG 72	25°45.8'	80°8.0'	1-22-85	2-12-85	22
MacArthur Causeway, W	TG 85	25°47.3'	80°10.9.5'	1-22-85	2-12-85	22
MacArthur Causeway, E	TG 108	25°46.4'	80°8.7'	1-22-85	2-07-85	17

Table 3

Summary of Tidal Constituents Generated from Harmonic Analysis

Gage Location	Constituents	Amplitude ft	Epoch deg	Root-Mean Square Error
Fisher Island	M2	1.04797	226.16911	
	S2	0.10315	310.35679	
	N2	0.22081	217.81348	0.20096
	K1	0.14593	177.94606	
	O1	0.09358	188.68112	
	K2	0.11529	153.59656	
Rickenbacker Causeway	M2	0.92165	240.21394	
	S2	0.10950	305.95851	
	N2	0.16834	236.34916	0.219685
	K1	0.12809	188.70476	
	O1	0.09437	199.32917	
	K2	0.07310	189.35635	
Offshore	M2	1.18837	216.75510	
	S2	0.06828	159.38349	
	N2	0.28860	204.94294	0.202639
	K1	0.15418	173.94872	
	O1	0.10946	180.10808	
	K2	0.22850	174.89292	
MacArthur Causeway, E	M2	1.01556	233.43168	
	S2	0.20003	291.18362	
	N2	0.21499	230.57715	
	K1	0.13321	184.66181	
	O1	0.09421	189.17045	0.175297
	K2	0.00889	203.56246	
Miami Marina*	M2	1.00000	245.27000	
	S2	0.17300	227.25000	
	N2	0.20000	277.85000	
	K1	0.10700	185.99000	
	O1	0.08900	209.09000	
	K2	0.05000	273.39000	

* Supplied by NOAA.

Table 4

Port of Miami Numerical Model Study, Refined Grid

Production Test Cases

Test Cases	Modification Plan	Tests
1	None	Existing topography
2	Structural	North and south jetties of equal length
3	Structural	North and south jetties of equal length and flared at the north jetty
4	Structural	North and south jetties of equal length and flared at the south jetty
5	Structural	North and south jetties of equal length and flared at jetty ends
6	Nonstructural	Existing topography and a hole provided at the tip of the north jetty
7	Nonstructural	Deepening and widening of harbor channels and turning basins, ocean entrance channel and outer bar channel
8	Structural and nonstructural	Existing topography, both jetties of equal length, throat width increased at the entrance on either side of jetty, and water depth increased to 47 ft
9	Structural and nonstructural	Both jetties extended to same length, flared at jetty ends, and deepening and widening of harbor channels, ocean entrance channel and outer bar channel

Table 5

Maximum Project Water Depths Used for Channel Deepening

Location	Water Depth ft	Identification Number
Outer Bar Cut	42	1
Bar Cut	42	2
Government Cut	42-40	3
Fisher Island Turning Basin	40	4
Main Channel	36	5
Main Turning Basin	36	6
Fisherman's Channel	40	7
Turning Basin	40	8
Fisherman's Channel (West of turning basin)	36	9

Table 6

Port of Miami Numerical Model Study, Refined Grid Numerically Calculated*

Peak Flood and Ebb Velocity With and Without Harbor Improvements

Test Cases**	Station Numbers According to Figure 4													
	4		7		8		10		11		12		18	
	Flood	Ebb	Flood	Ebb	Flood	Ebb	Flood	Ebb	Flood	Ebb	Flood	Ebb	Flood	Ebb
1	1.7	1.6	4.1	4.5	4.7	5.0	1.0	1.0	1.0	1.0	1.5	1.6	1.2	1.2
3	1.7	1.6	4.3	4.5	5.0	5.1	1.1	1.1	1.1	1.1	1.5	1.7	0.8	0.8
5	1.7	1.6	4.2	4.5	4.8	5.0	1.0	1.0	1.0	1.0	2.0	2.0	0.8	0.8
7	1.7	1.6	4.2	4.6	4.0	4.2	1.0	1.0	1.2	1.2	2.2	2.2	1.2	1.2
9	1.8	1.7	4.4	4.7	4.0	4.3	1.2	1.2	1.0	1.0	1.5	1.6	0.9	0.9

* Measurements in feet per second.

** Test cases are referenced to Table 4.

Table 7

Production Test Cases for Ship Simulation Study*

Test Cases	Numerical Model	Modification Plan	Tests
1	Global	None	Existing topography without wind
2	Global	None	Existing topography with wind
3	Refined	None	Existing topography without wind
4	Refined	Structural	Existing topography, even length Jetties without wind
5	Refined	Structural and nonstructural	Even length jetties, jetties flared at ends, and deepening and widening of harbor channels without wind
6	Refined	None	Existing topography with wind
7	Refined	Structural	Existing topography, even length jetties, with wind
8	Refined	Structural and nonstructural	Even length jetties, jetties flared at ends, and deepening and widening of harbor channels, with winds

* For peak flood conditions with and without 20-knot northeasterly winds.

Table 8

Magnitude of Velocity and Direction, With and Without Wind

Effects Refined Grid*

Case	Test	Grid Indices: At North Jetty N = 74, M = 25** Magnitude fps	At North Jetty N = 74, M = 25** Direction deg	At Midchannel N = 74, M = 28 Magnitude fps	At Midchannel N = 74, M = 28 Direction deg	At South Jetty N = 74, M = 31 Magnitude fps	At South Jetty N = 74, M = 31 Direction deg
3	Existing condition, no wind	2.96	260.70	3.98	290.00	3.91	119.92
6	Existing condition, with wind	3.49	248.2	4.09	284.08	3.92	120.00
4	Jetty equal length no wind	3.31	263.8	4.24	290.6	4.18	120.60
7	Jetty equal length with wind	3.98	254.20	4.53	286.00	4.39	120.60
5	Jetty equal length, flared at ends, and deepening and widening of inlet and harbor channels, no wind	3.13	286.40	4.21	293.70	4.15	118.60

* Direction measured from true north.

** N = grid index in y-direction, M = grid index in x-direction.

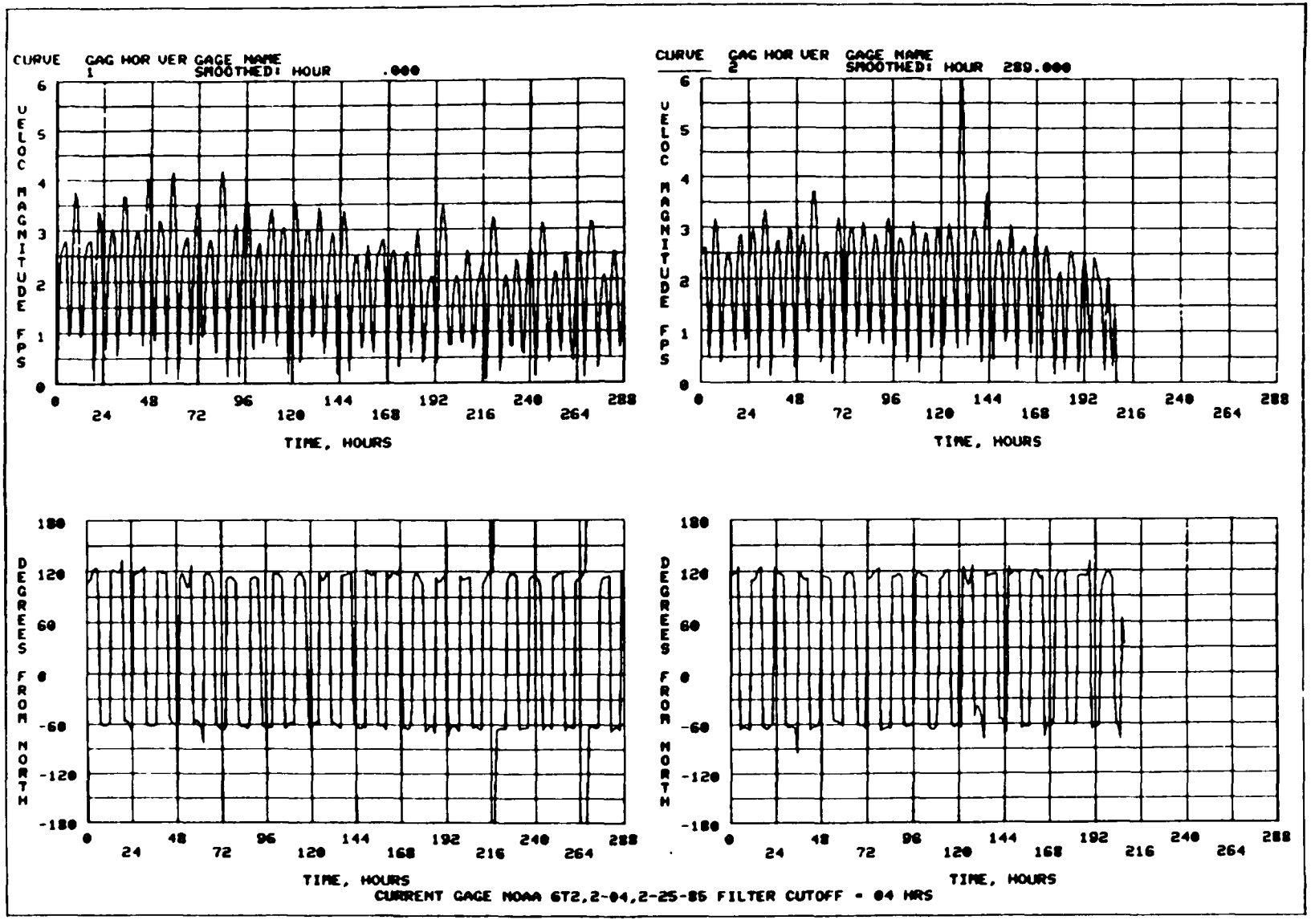
CURVE GAG HOR VER GAGE NAME
1 SMOOTHED: HOUR .000
CURVE GAG HOR VER GAGE NAME
2 SMOOTHED: HOUR 289.000
VELOC MAGNITUDE FPS
0 1 2 3 4 5 6
0 24 48 72 96 120 144 168 192 216 240 264 288
TIME, HOURS
DEGREES FROM NORTH
180 120 60 0 -60 -120 -180
CURRENT GAGE NOAA GT2,2-04,2-25-85 FILTER CUTOFF = 04 HRS

PLATE 1

PLATE 2

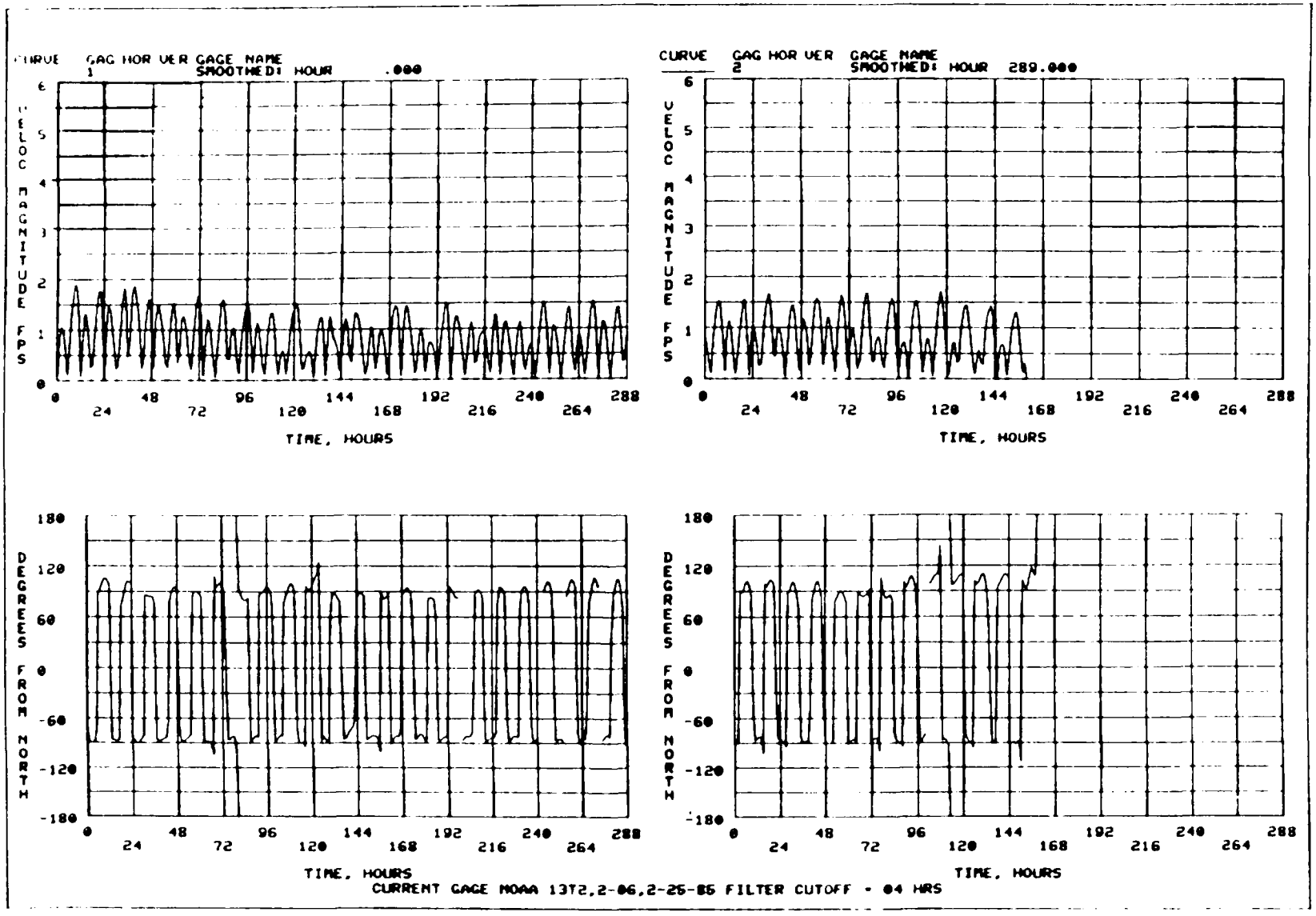
CURVE GAG HOR VER GAGE NAME
1 SMOOTHED: HOUR .000
VELOC MAGNITUDE FPS
TIME, HOURS
CURVE GAG HOR VER GAGE NAME
2 SMOOTHED: HOUR 289.000
VELOC MAGNITUDE FPS
TIME, HOURS
DEGREES FROM NORTH
TIME, HOURS
DEGREES FROM NORTH
TIME, HOURS
CURRENT GAGE MOAA 13T2,2-06,2-25-85 FILTER CUTOFF - 04 HRS

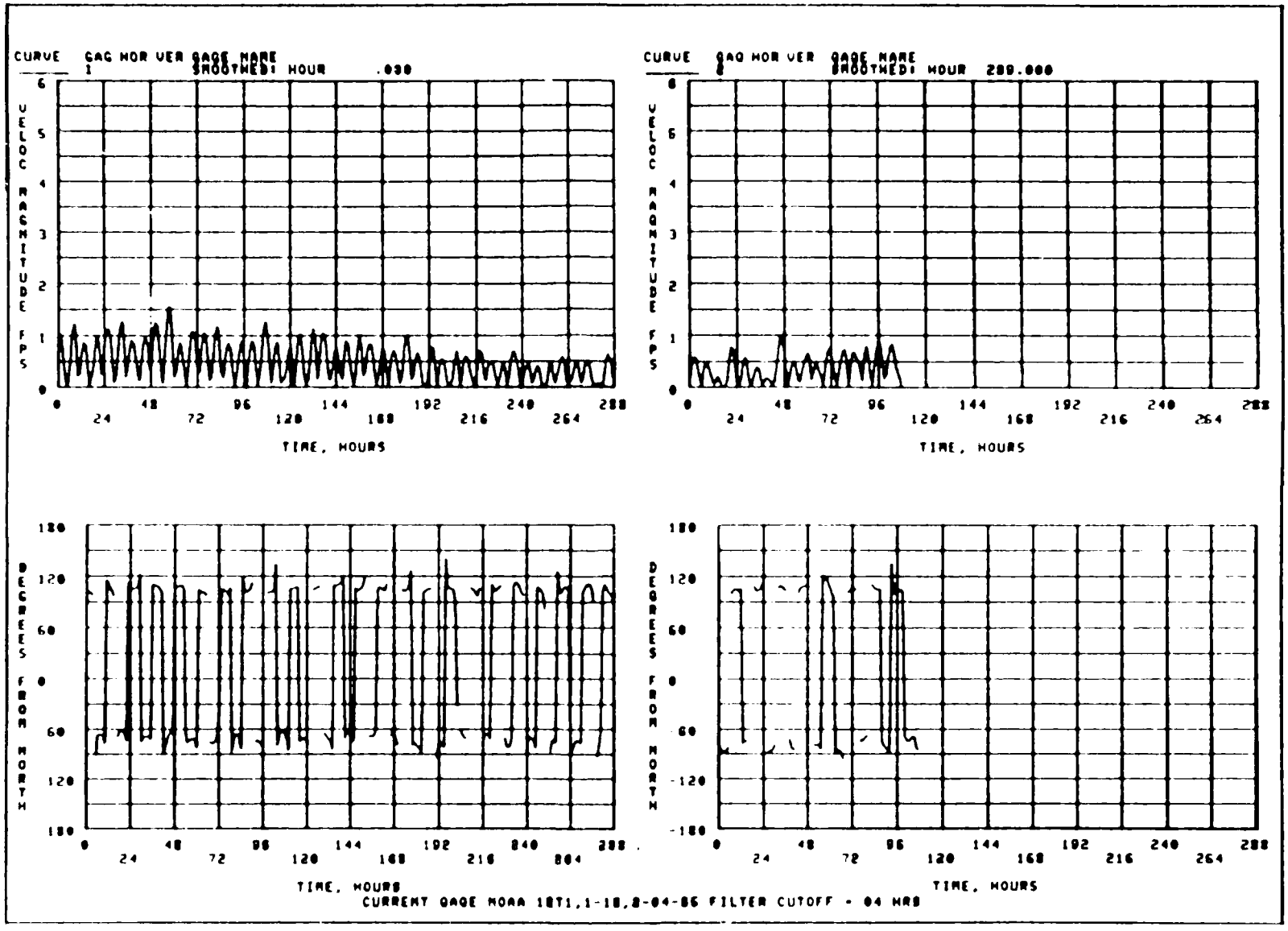
CURVE GAG HOR VER GAGE NAME
1 SMOOTHED HOUR .000
VELOC MAGNITUDE FPS
TIME, HOURS
CURVE GAG HOR VER GAGE NAME
2 SMOOTHED HOUR 288.000
VELOC MAGNITUDE FPS
TIME, HOURS
DEGREES FROM NORTH
TIME, HOURS
DEGREES FROM NORTH
TIME, HOURS
CURRENT GAGE NOAA 1BT1,1-18,8-04-86 FILTER CUTOFF - 04 HRS

PLATE 3

PLATE 4

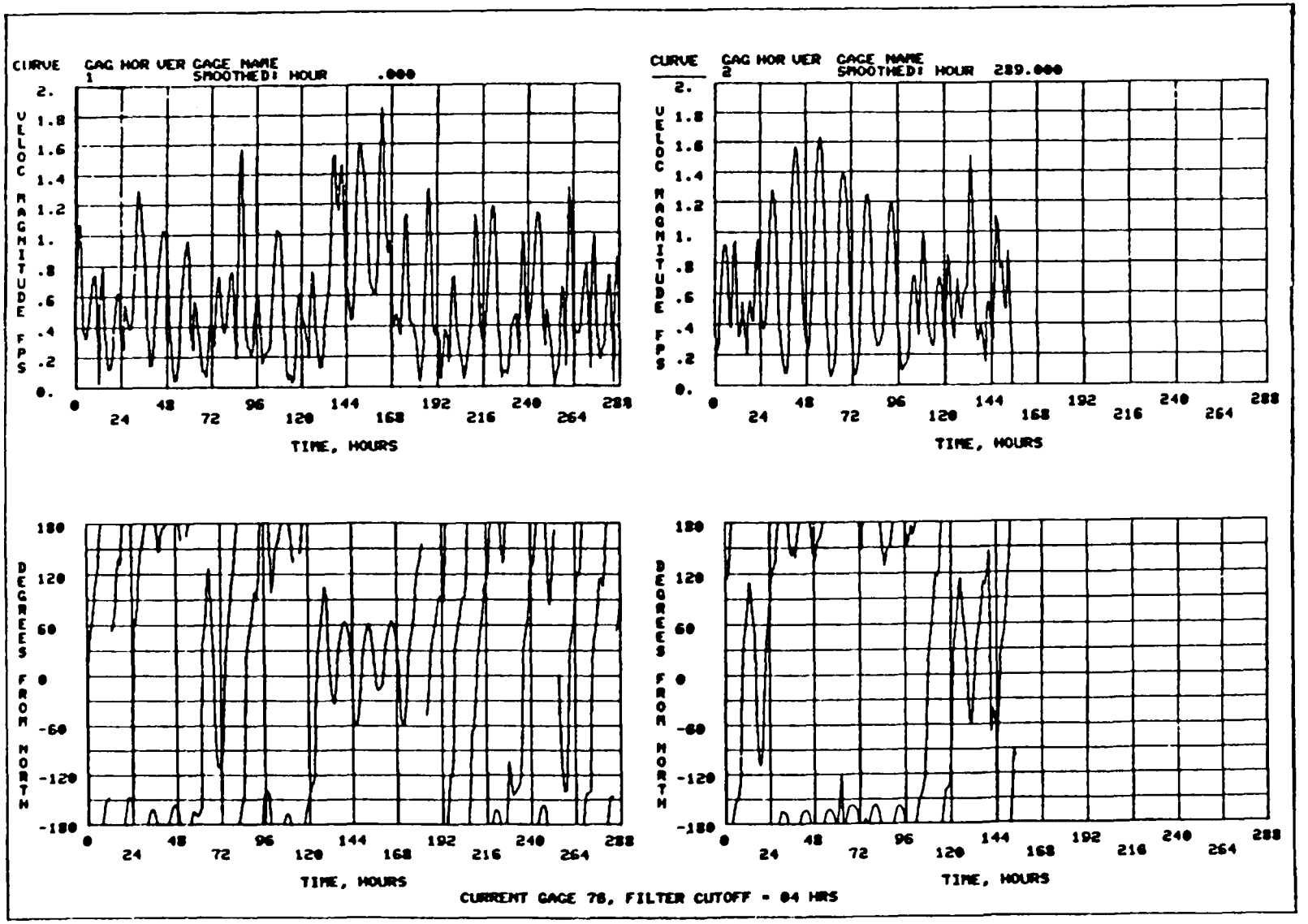
CURVE GAG HOR VER GAGE NAME
1 SMOOTHED: HOUR .000
VELOC MAGNITUDE FPS
TIME, HOURS
CURVE GAG HOR VER GAGE NAME
2 SMOOTHED: HOUR 289.000
VELOC MAGNITUDE FPS
TIME, HOURS
DEGREES FROM NORTH
TIME, HOURS
DEGREES FROM NORTH
TIME, HOURS
CURRENT GAGE 78, FILTER CUTOFF - 04 HRS

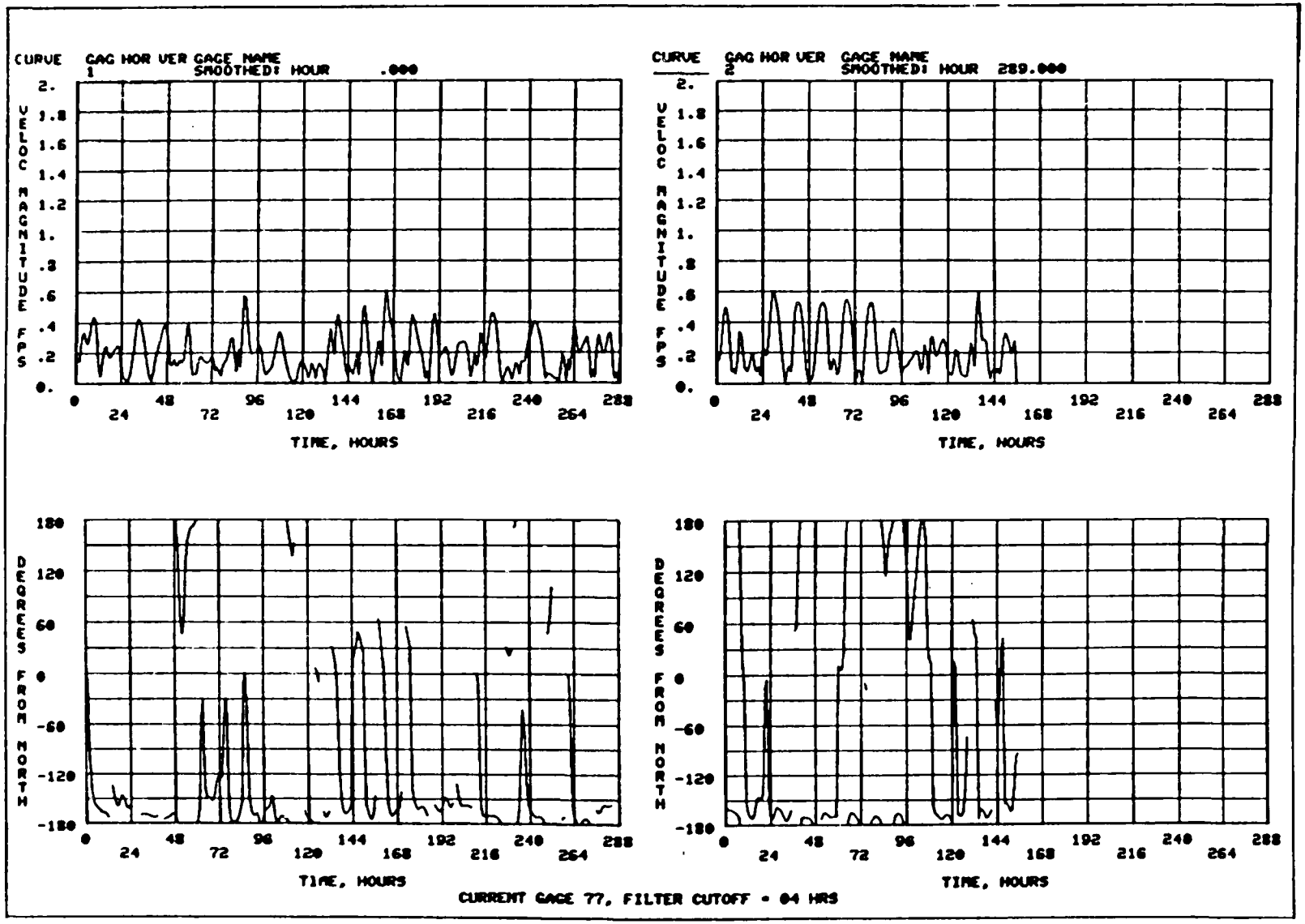
CURVE GAG HOR VER GAGE NAME
1 SMOOTHED: HOUR .000
VELOC MAGNITUDE FPS
2.
1.8
1.6
1.4
1.2
1.
.8
.6
.4
.2
0.
0 24 48 72 96 120 144 168 192 216 240 264 288
TIME, HOURS
CURVE GAG HOR VER GAGE NAME
2 SMOOTHED: HOUR 289.000
VELOC MAGNITUDE FPS
2.
1.8
1.6
1.4
1.2
1.
.8
.6
.4
.2
0.
0 24 48 72 96 120 144 168 192 216 240 264 288
TIME, HOURS
DEGREES FROM NORTH
180
120
60
0
-60
-120
-180
0 24 48 72 96 120 144 168 192 216 240 264 288
TIME, HOURS
DEGREES FROM NORTH
180
120
60
0
-60
-120
-180
0 24 48 72 96 120 144 168 192 216 240 264 288
TIME, HOURS
CURRENT GAGE 77, FILTER CUTOFF = 04 HRS

PLATE 5

PLATE 6

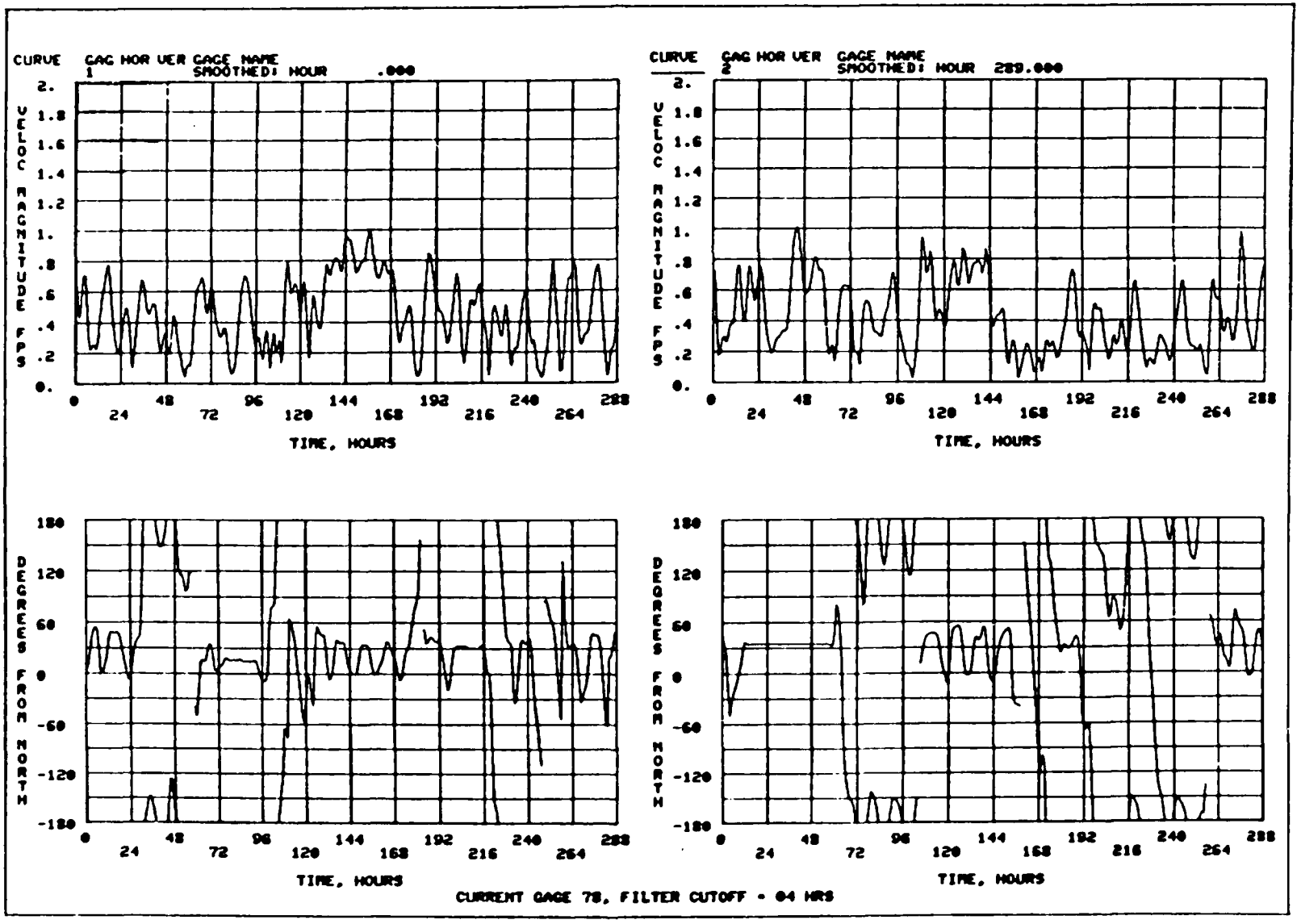
CURVE GAG HOR VER GAGE NAME
1 SMOOTHED: HOUR .000
CURVE GAG HOR VER GAGE NAME
2 SMOOTHED: HOUR 289.000
VELOC MAGNITUDE FPS
2.
1.8
1.6
1.4
1.2
1.
.8
.6
.4
.2
0.
0 24 48 72 96 120 144 168 192 216 240 264 288
TIME, HOURS
DEGREES FROM NORTH
180
120
60
0
-60
-120
-180
CURRENT GAGE 78, FILTER CUTOFF - 04 HRS

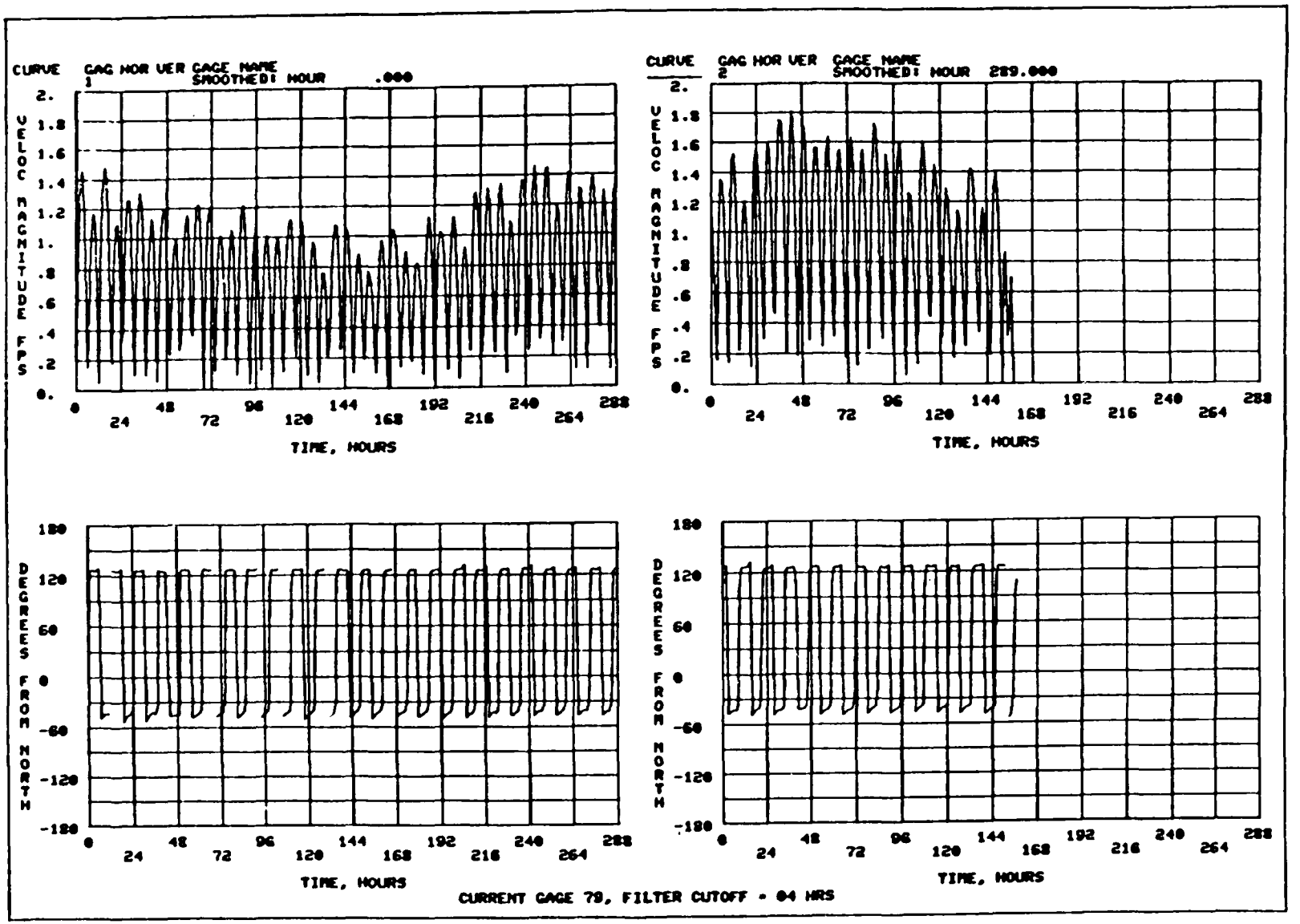
CURVE 1 GAG HOR VER GAGE NAME
SMOOTHED: HOUR .000
VELOC MAGNITUDE FPS
TIME, HOURS
CURVE 2 GAG HOR VER GAGE NAME
SMOOTHED: HOUR 289.000
VELOC MAGNITUDE FPS
TIME, HOURS
DEGREES FROM NORTH
TIME, HOURS
DEGREES FROM NORTH
TIME, HOURS
CURRENT GAGE 79, FILTER CUTOFF - 04 HRS

PLATE 7

PLATE 8

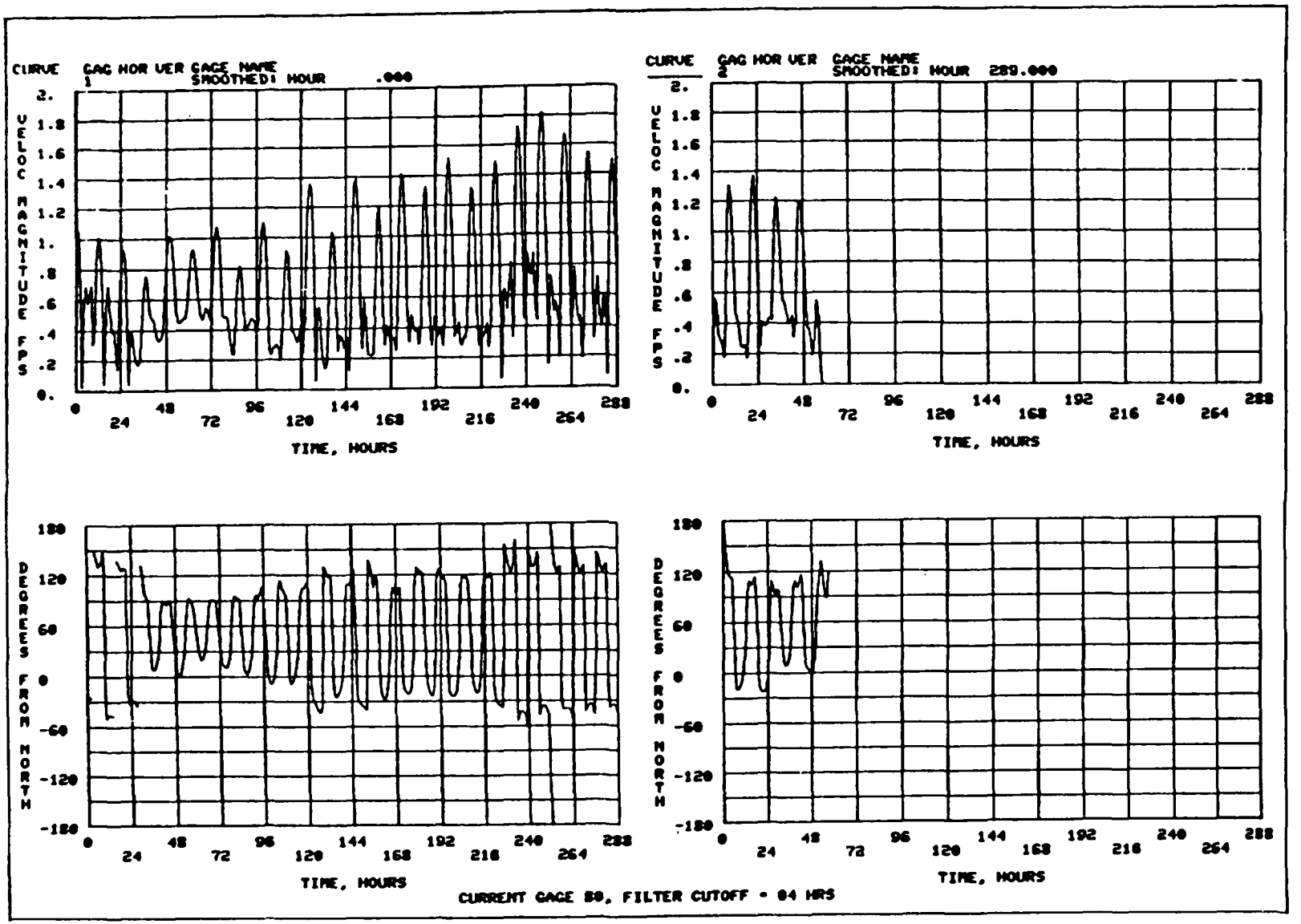
CURVE 1 GAG HOR VER GAGE NAME SMOOTHED: HOUR .000
CURVE 2 GAG HOR VER GAGE NAME SMOOTHED: HOUR 289.000
VELOC MAGNITUDE FPS
DEGREES FROM NORTH
TIME, HOURS
CURRENT GAGE 80, FILTER CUTOFF = 04 HRS

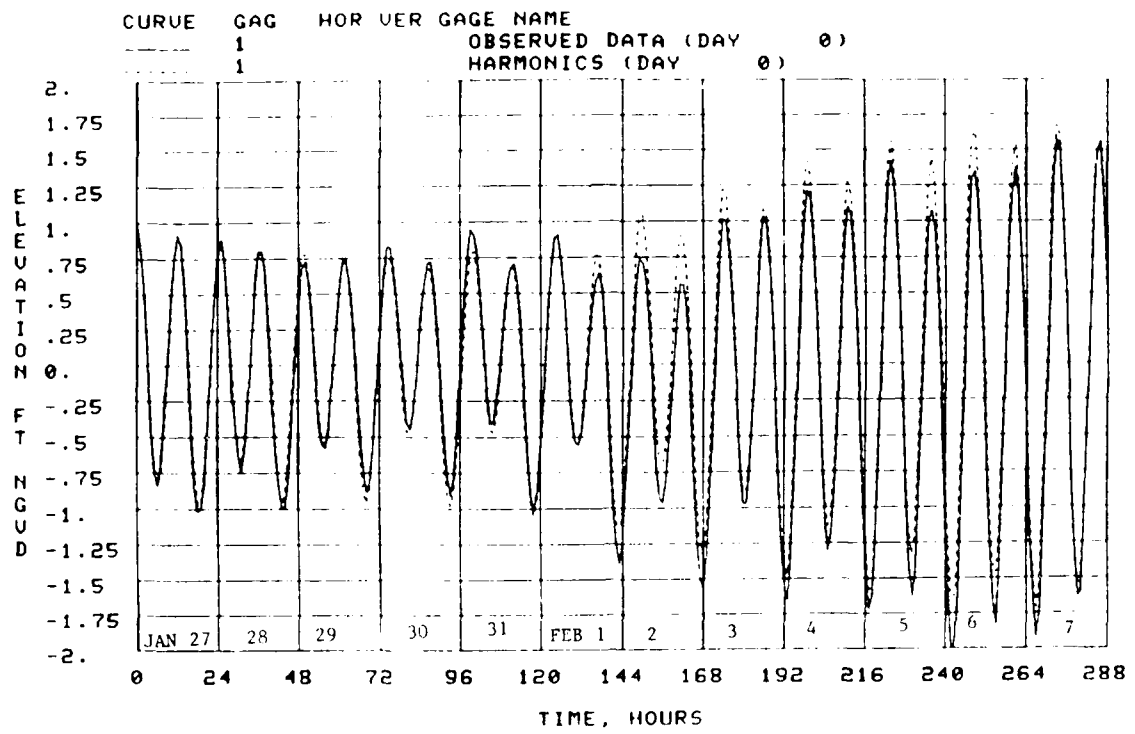

MIAMI OFFSHORE TG72

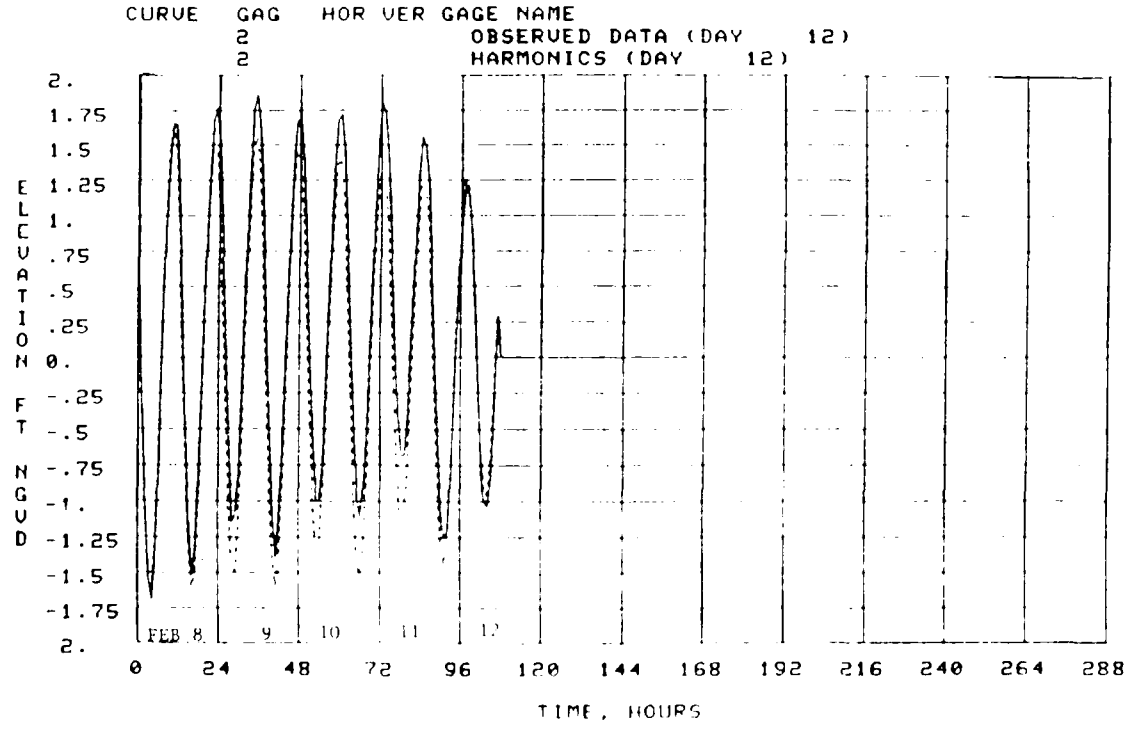

MIAMI OFFSHORE TG72

PLATE 9

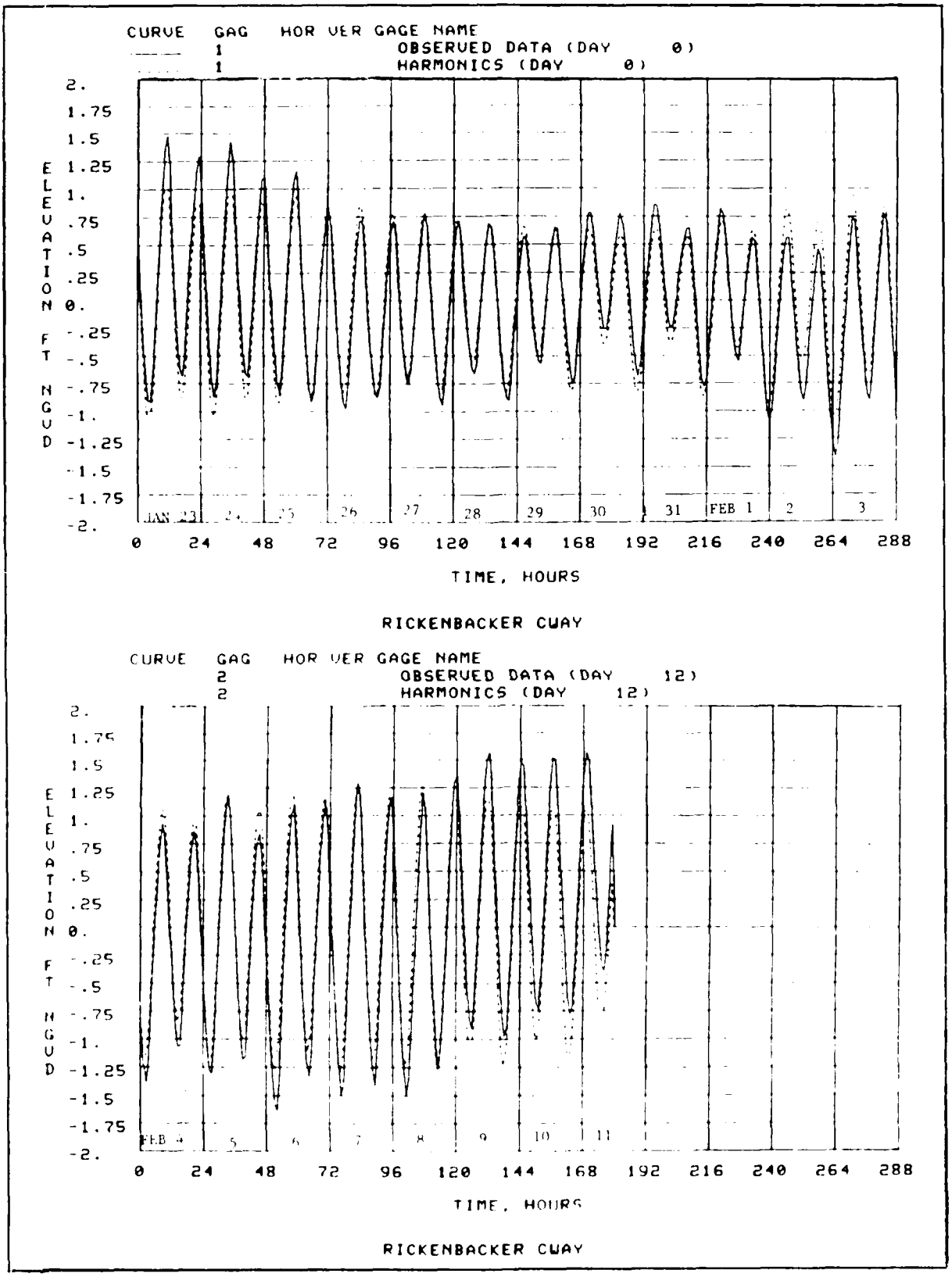
CURVE GAG HOR VER GAGE NAME
1 OBSERVED DATA (DAY 0)
1 HARMONICS (DAY 0)
ELEVATION FT NGVD
2.
1.75
1.5
1.25
1.
.75
.5
.25
0.
-.25
-.5
-.75
-1.
-1.25
-1.5
-1.75
-2.
JAN 23
24
25
26
27
28
29
30
31
FEB 1
2
3
0
24
48
72
96
120
144
168
192
216
240
264
288
TIME, HOURS
RICKENBACKER CWAY
CURVE GAG HOR VER GAGE NAME
2 OBSERVED DATA (DAY 12)
2 HARMONICS (DAY 12)
ELEVATION FT NGVD
FEB 4
5
6
7
8
9
10
11
TIME, HOURS
RICKENBACKER CWAY

PLATE 10

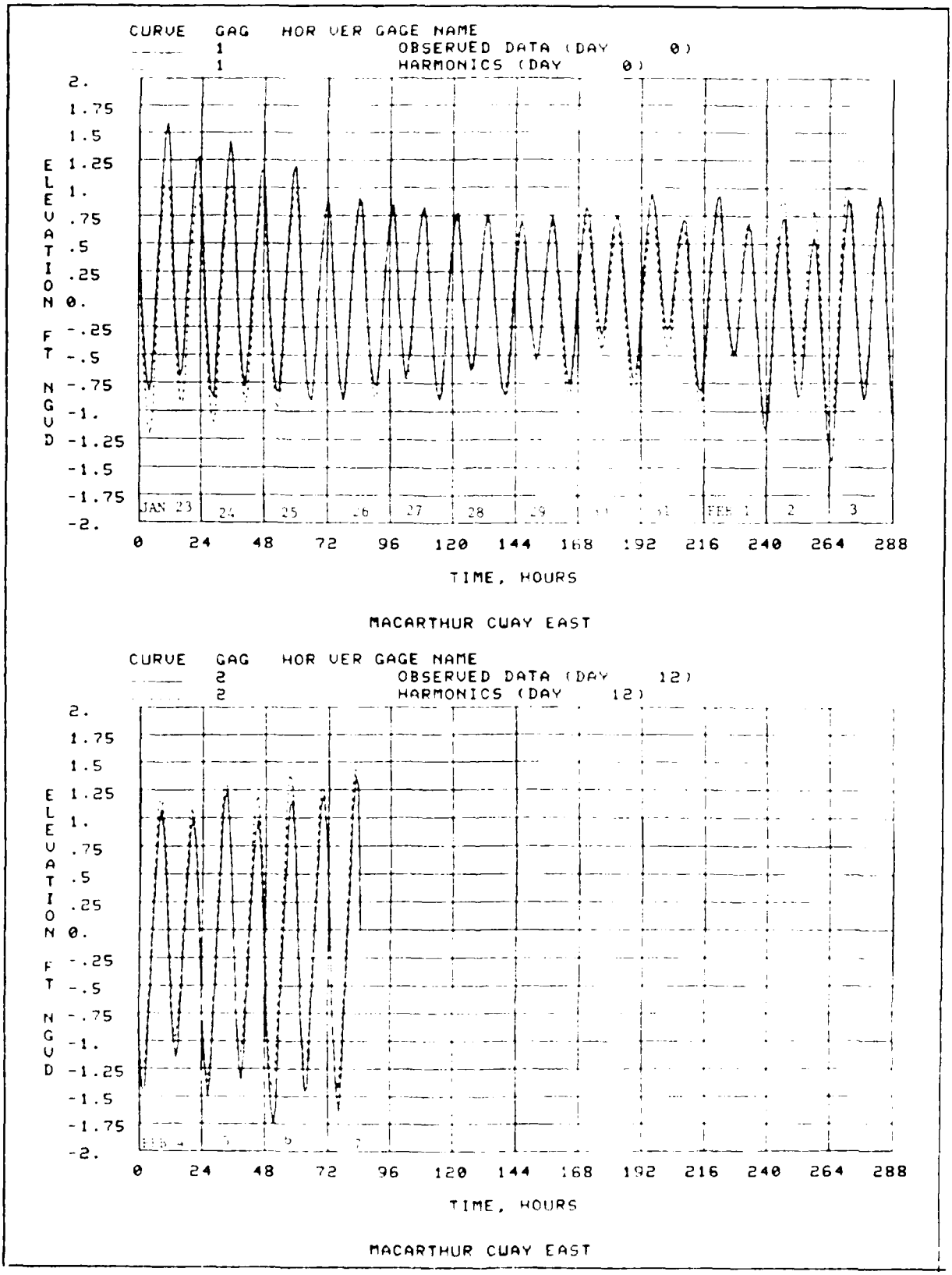
CURVE GAG HOR VER GAGE NAME
1 OBSERVED DATA (DAY 0)
1 HARMONICS (DAY 0)
ELEVATION FT NGVD
2.
1.75
1.5
1.25
1.
.75
.5
.25
0.
-.25
-.5
-.75
-1.
-1.25
-1.5
-1.75
-2.
JAN 23
24
25
26
27
28
29
FEB 1
2
3
0 24 48 72 96 120 144 168 192 216 240 264 288
TIME, HOURS
MACARTHUR CWAY EAST
CURVE GAG HOR VER GAGE NAME
2 OBSERVED DATA (DAY 12)
2 HARMONICS (DAY 12)
ELEVATION FT NGVD
0 24 48 72 96 120 144 168 192 216 240 264 288
TIME, HOURS
MACARTHUR CWAY EAST

PLATE 11

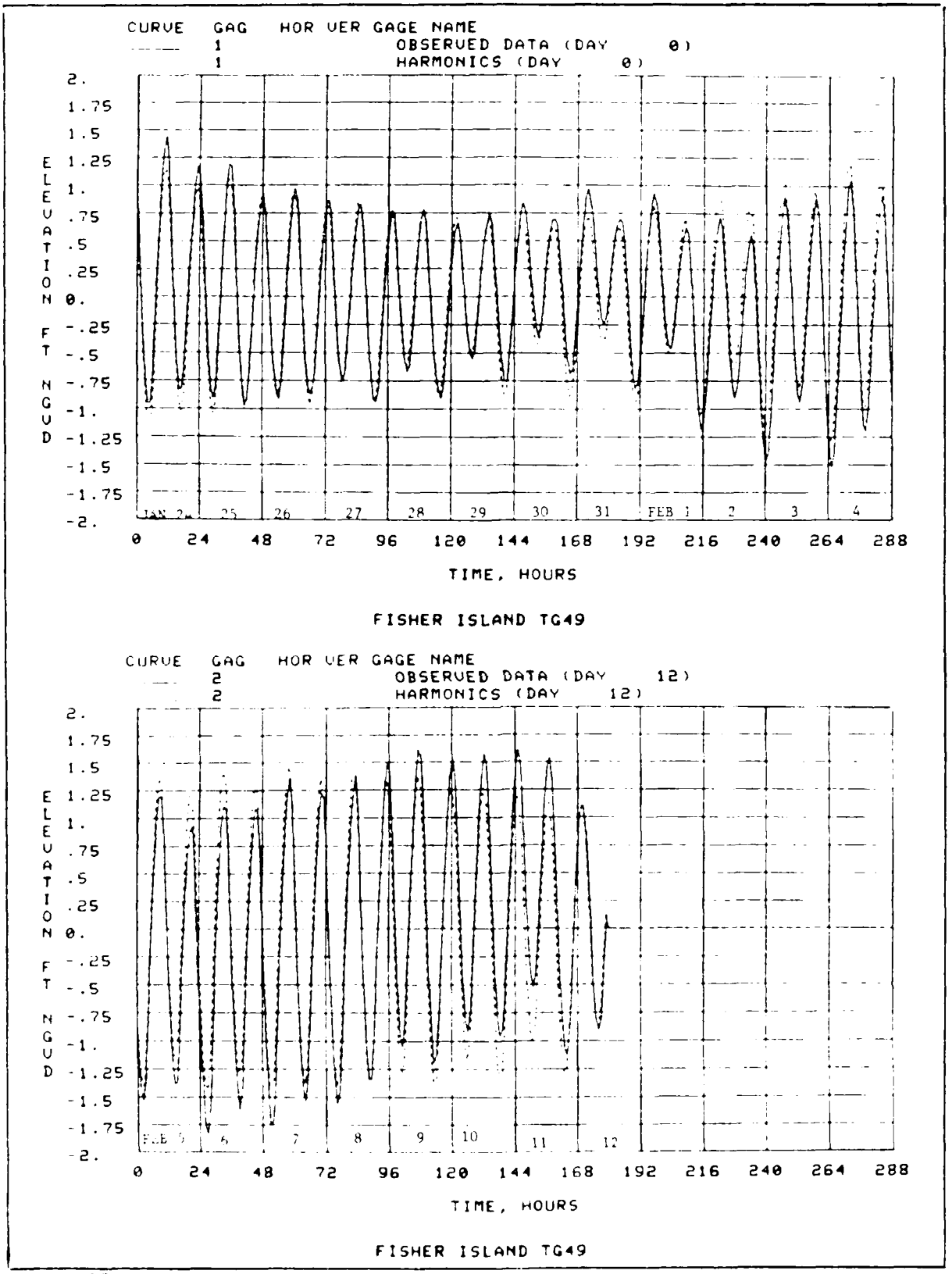
CURVE GAG HOR VER GAGE NAME
1 OBSERVED DATA (DAY 0)
1 HARMONICS (DAY 0)
ELEVATION FT NGVD
2.
1.75
1.5
1.25
1.
.75
.5
.25
0.
-.25
-.5
-.75
-1.
-1.25
-1.5
-1.75
-2.
JAN 24 25 26 27 28 29 30 31 FEB 1 2 3 4
0 24 48 72 96 120 144 168 192 216 240 264 288
TIME, HOURS
FISHER ISLAND TG49
CURVE GAG HOR VER GAGE NAME
2 OBSERVED DATA (DAY 12)
2 HARMONICS (DAY 12)
ELEVATION FT NGVD
FEB 5 6 7 8 9 10 11 12
0 24 48 72 96 120 144 168 192 216 240 264 288
TIME, HOURS
FISHER ISLAND TG49

PLATE 12

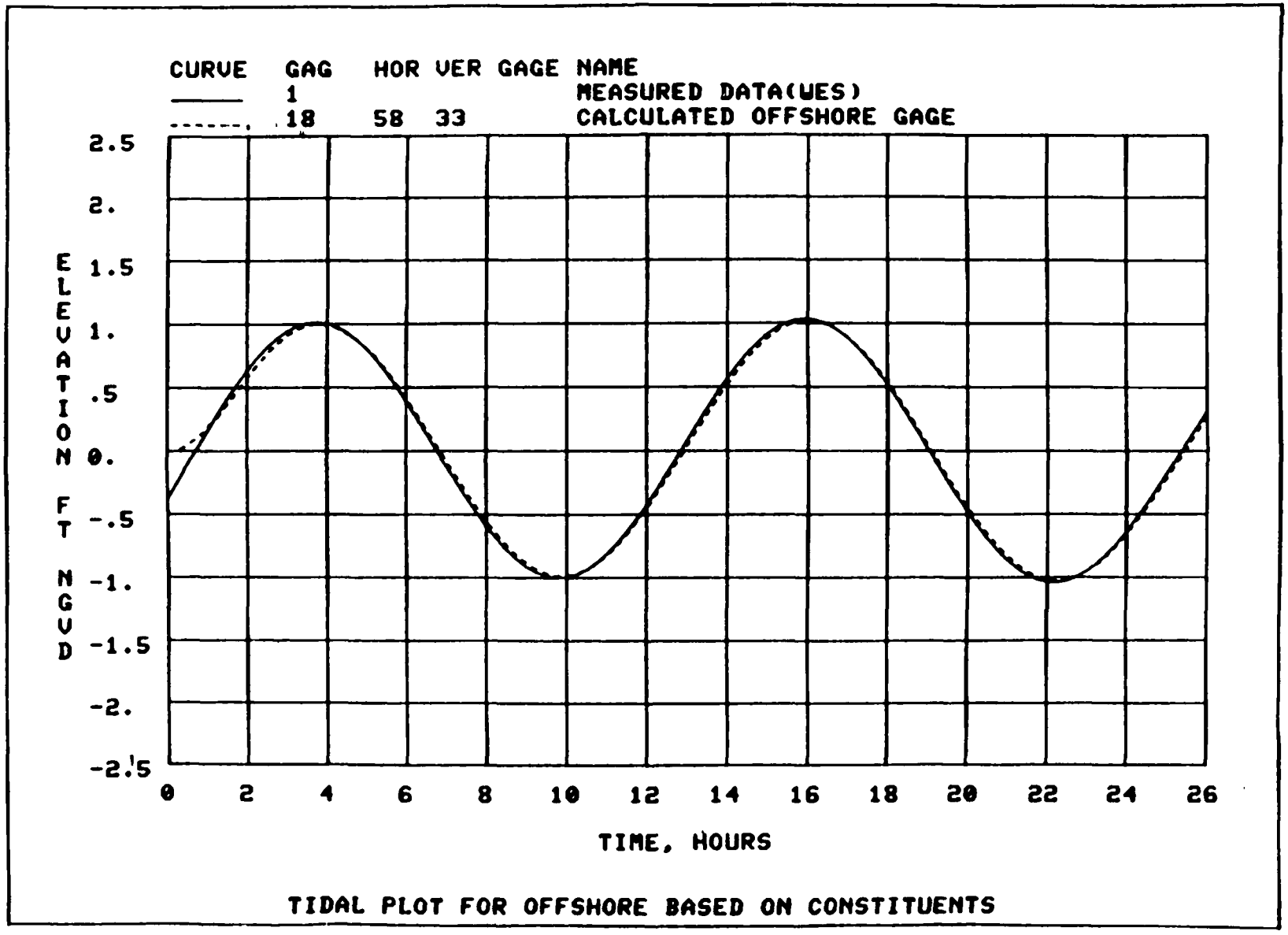

TIDAL PLOT FOR OFFSHORE BASED ON CONSTITUENTS

PLATE 13

PLATE 14

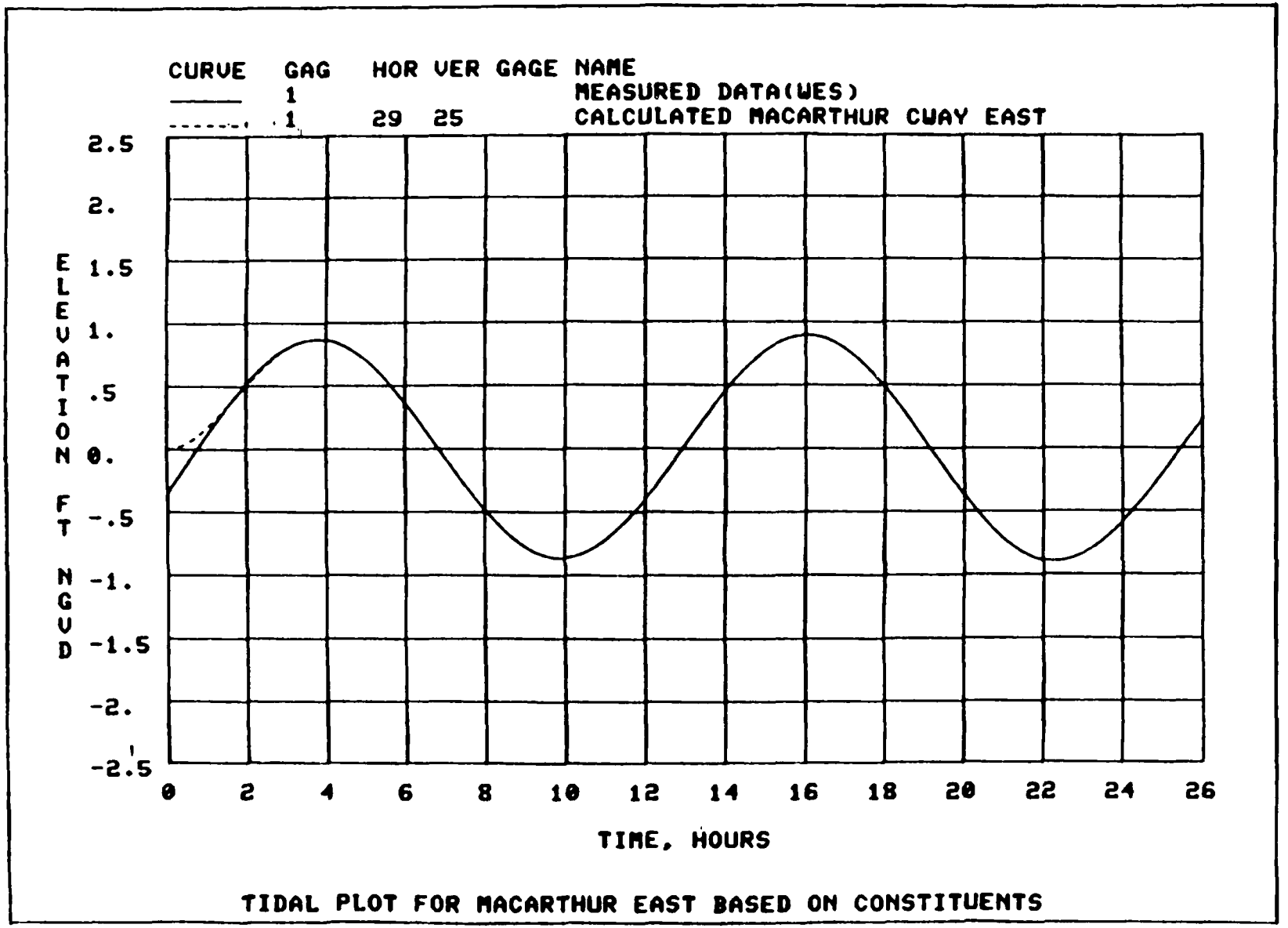

TIDAL PLOT FOR MACARTHUR EAST BASED ON CONSTITUENTS

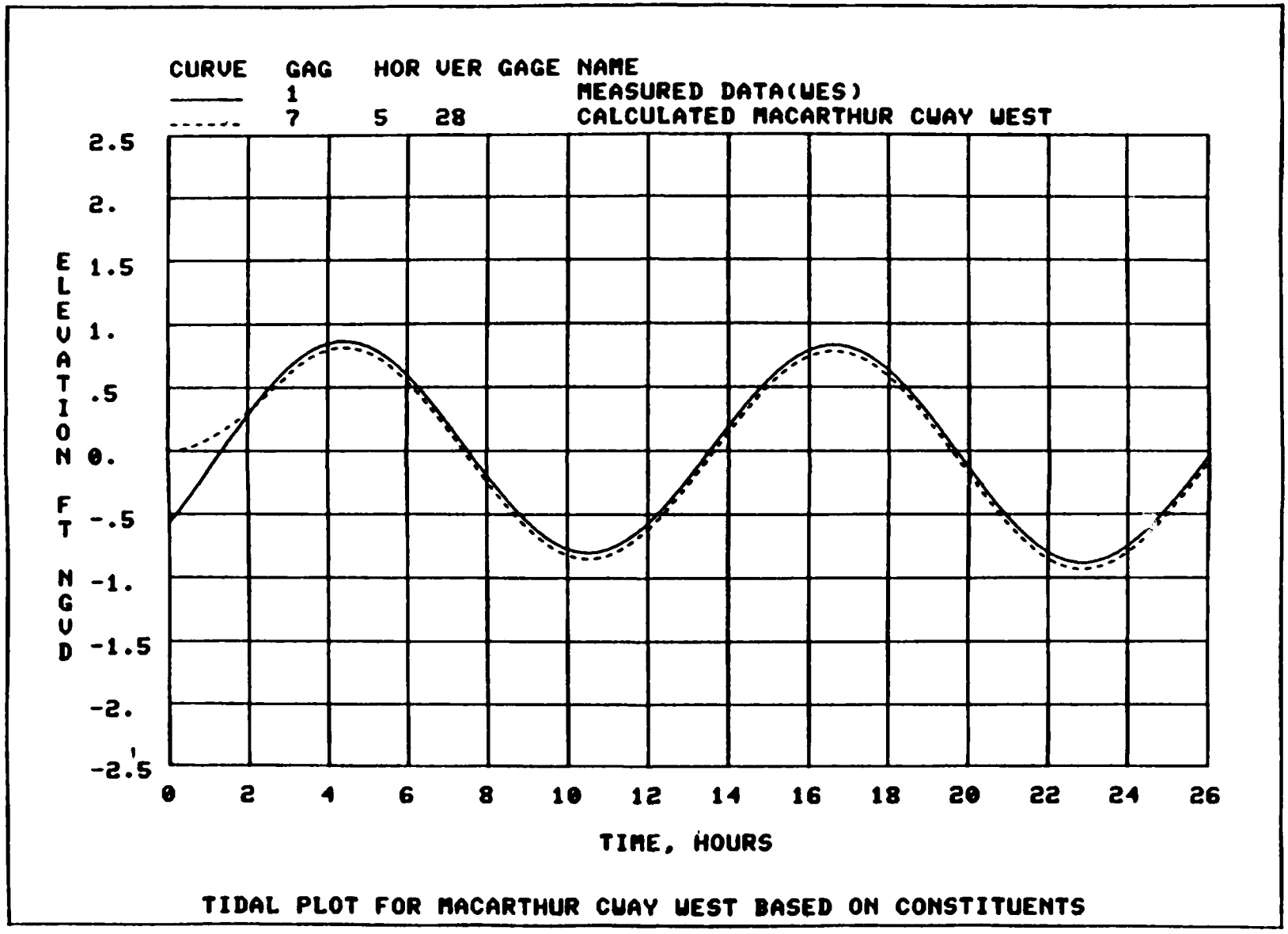

TIDAL PLOT FOR MACARTHUR CWAY WEST BASED ON CONSTITUENTS

PLATE 15

PLATE 16

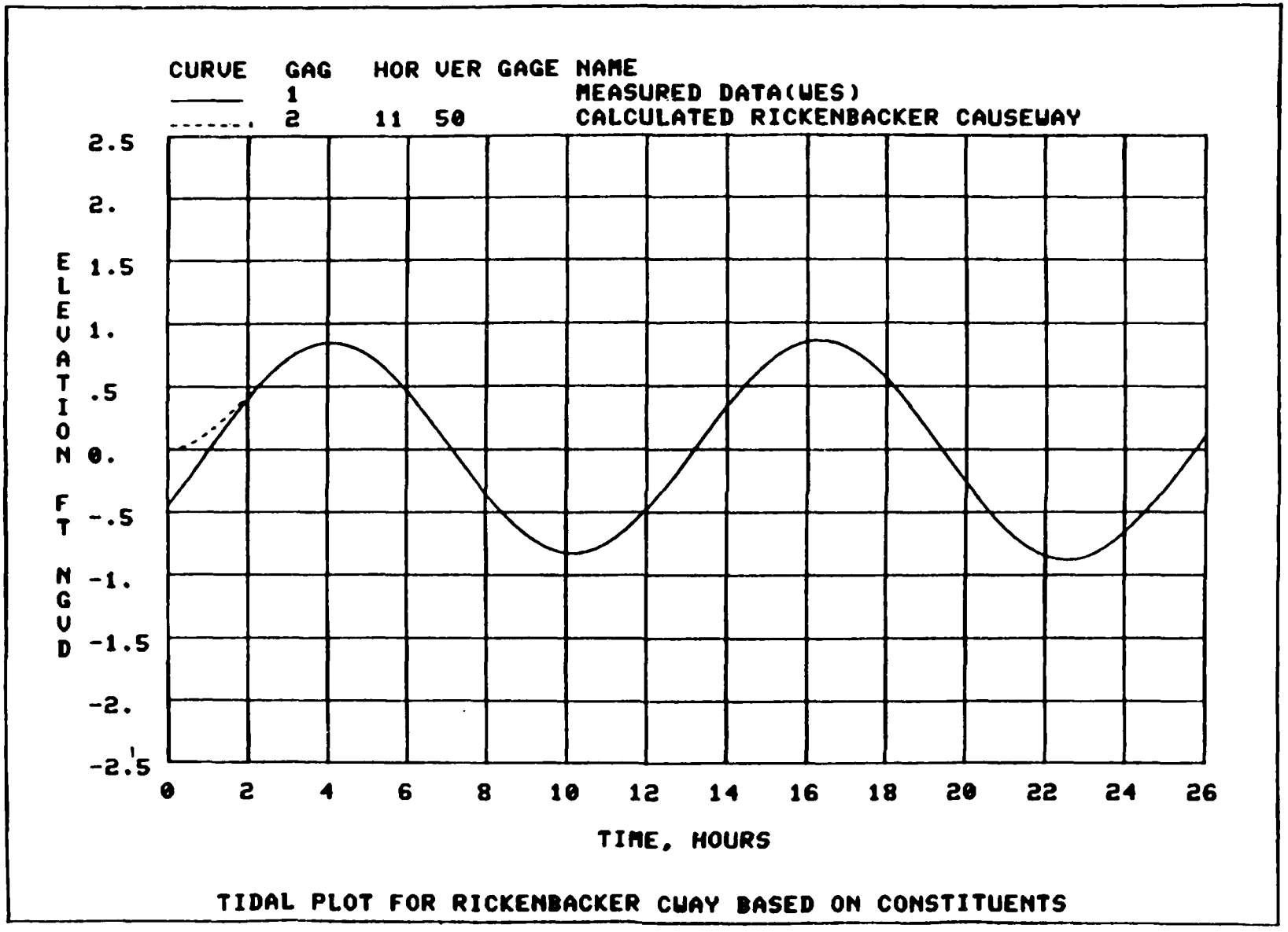

TIDAL PLOT FOR RICKENBACKER CWAY BASED ON CONSTITUENTS

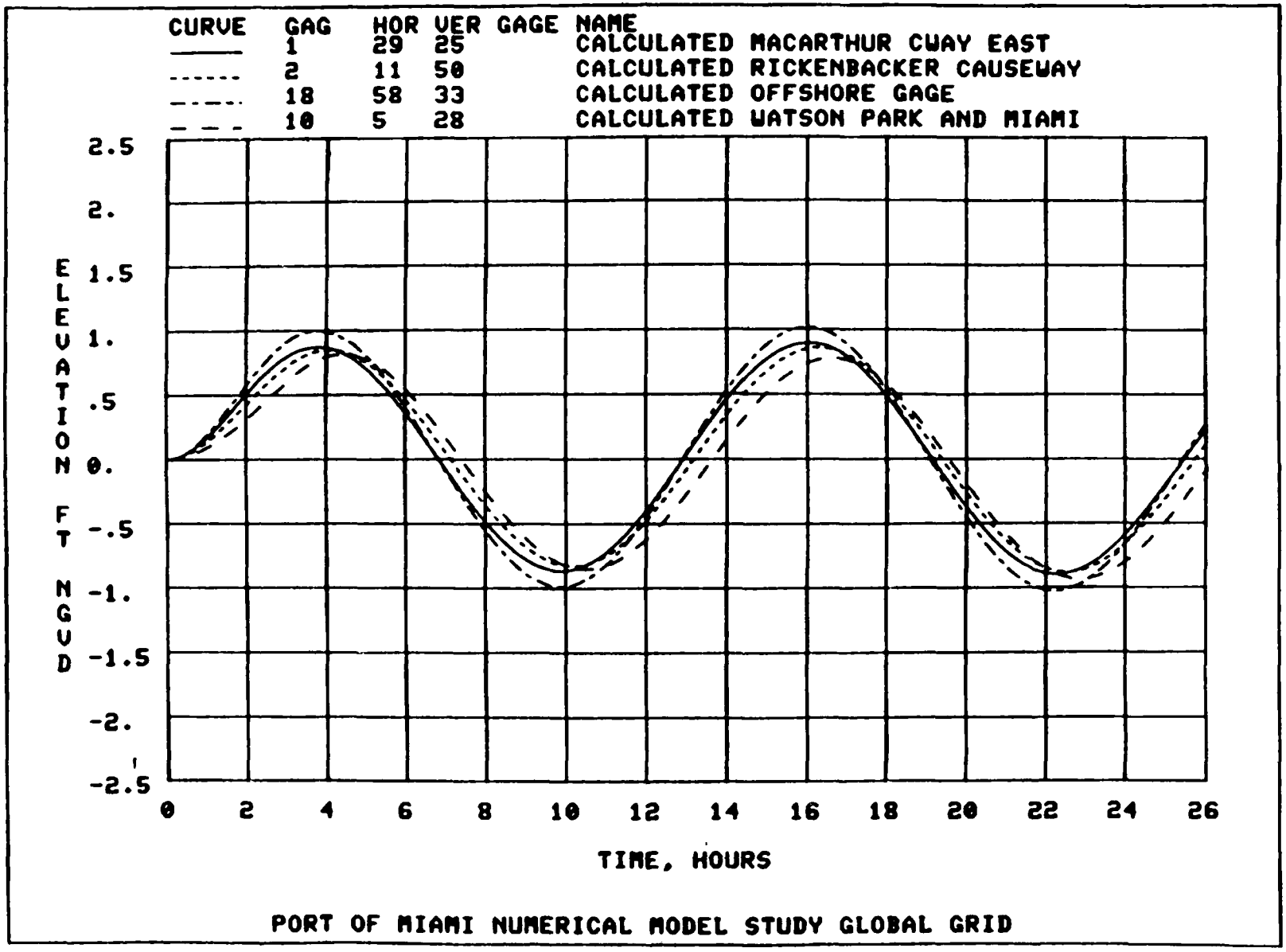
CURVE GAG HOR VER GAGE NAME
1 29 25 CALCULATED MACARTHUR CWAY EAST
2 11 50 CALCULATED RICKENBACKER CAUSEWAY
18 58 33 CALCULATED OFFSHORE GAGE
10 5 28 CALCULATED WATSON PARK AND MIAMI
2.5
2.
1.5
1.
.5
0.
-.5
-1.
-1.5
-2.
-2.5
ELEVATION FT NGVD
0 2 4 6 8 10 12 14 16 18 20 22 24 26
TIME, HOURS
PORT OF MIAMI NUMERICAL MODEL STUDY GLOBAL GRID

PLATE 17

PLATE 18

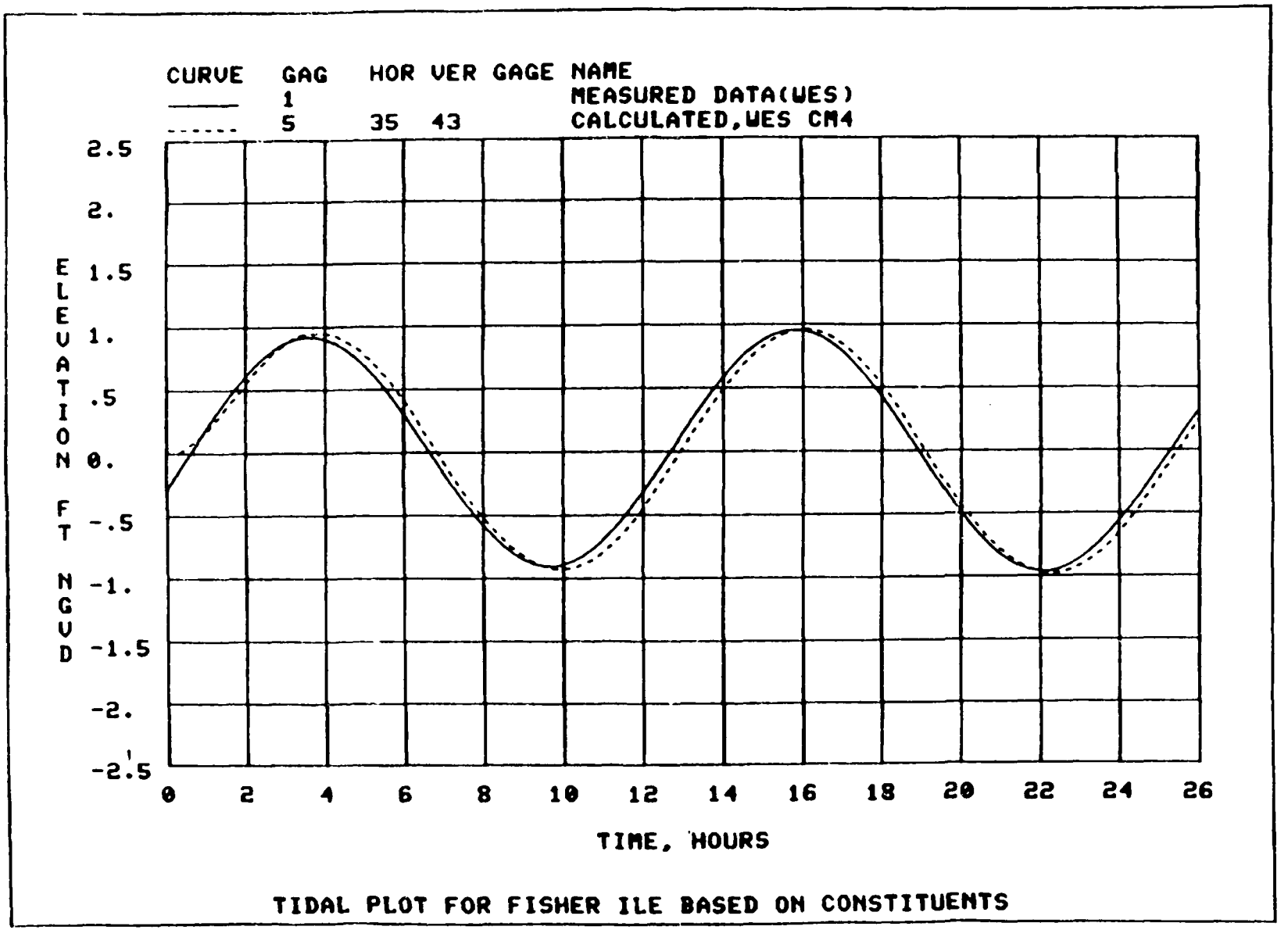

TIDAL PLOT FOR FISHER ILE BASED ON CONSTITUENTS

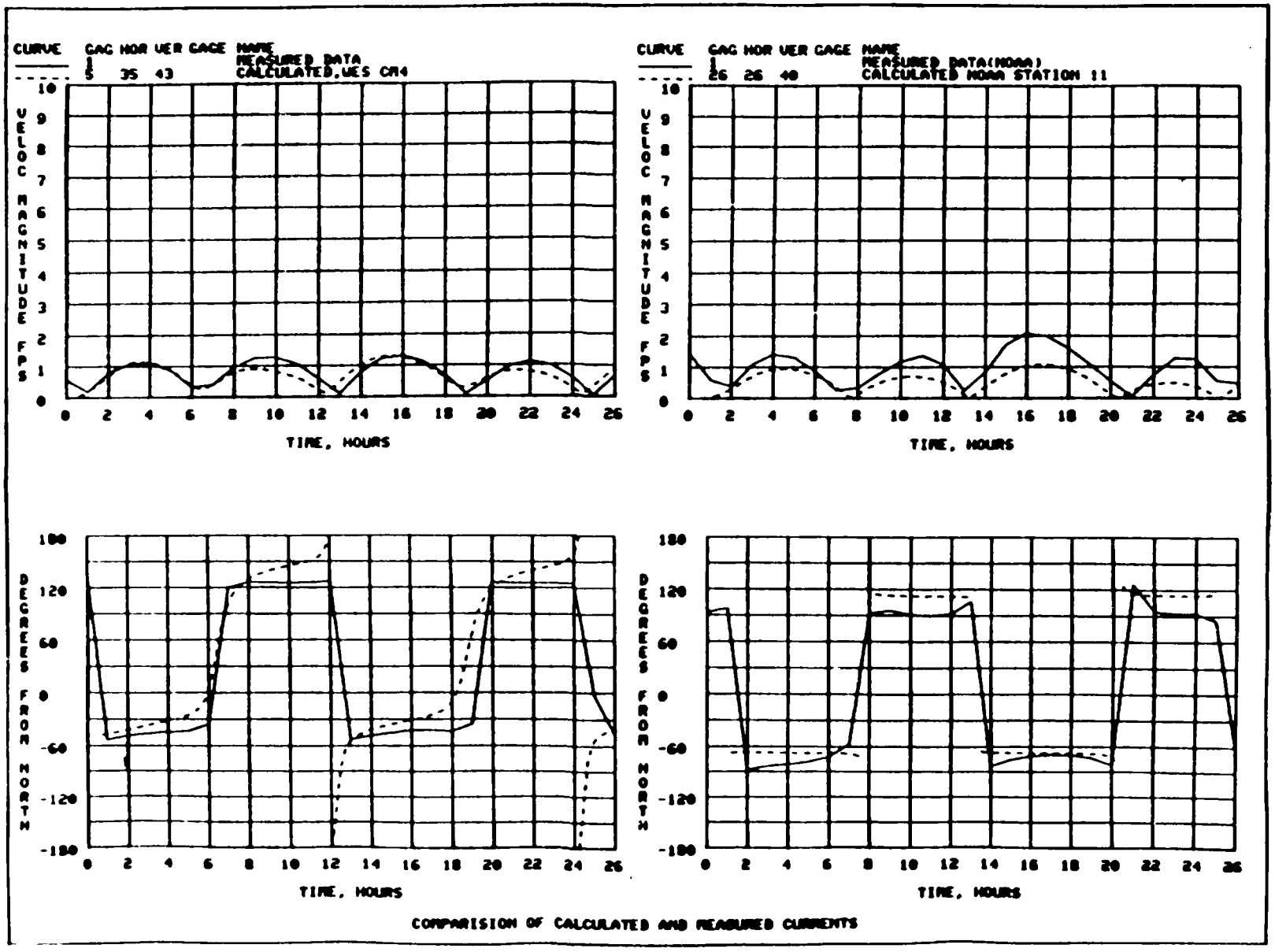

COMPARISION OF CALCULATED AND MEASURED CURRENTS

PLATE 19

PLATE 20

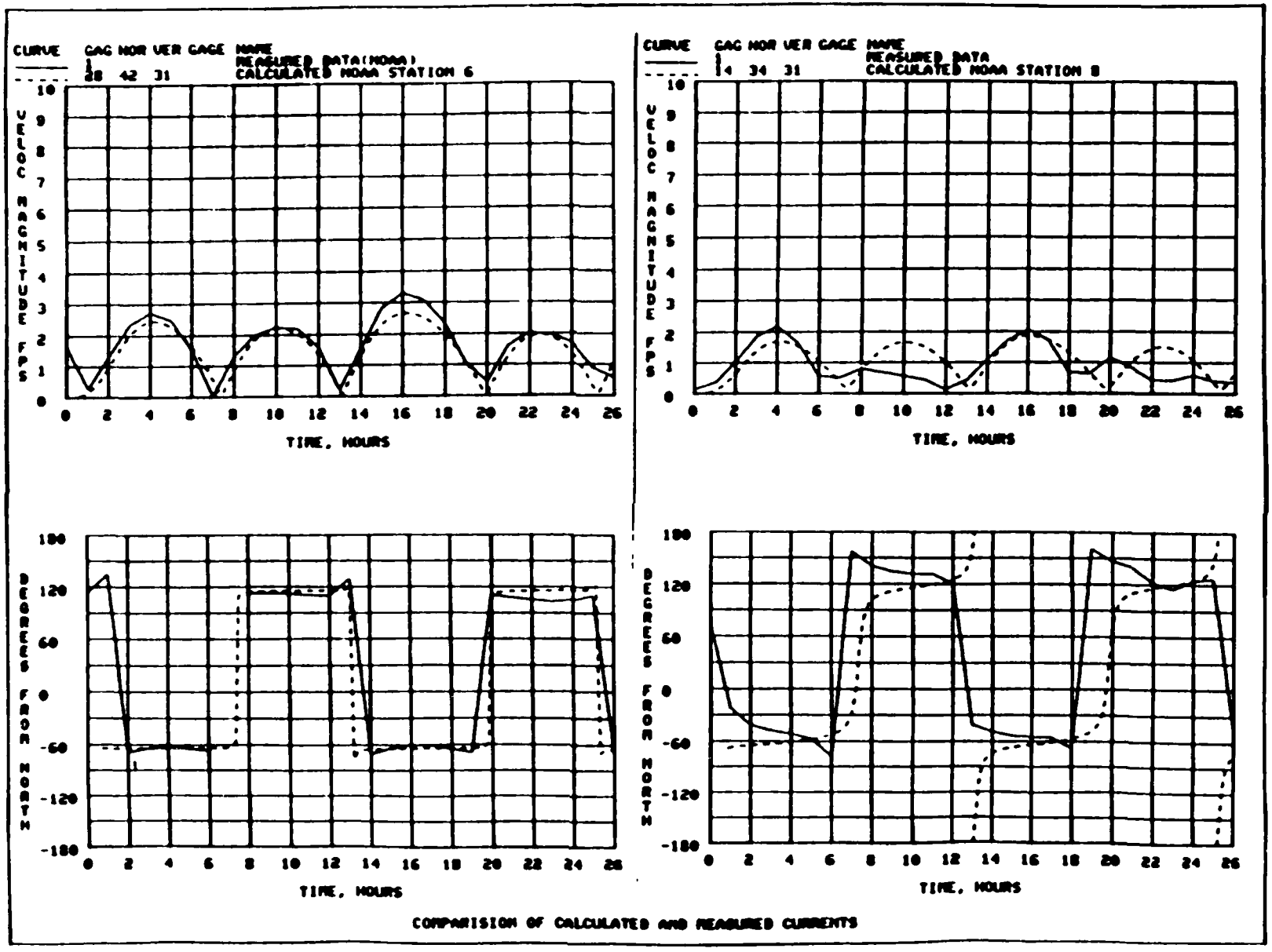

COMPARISION OF CALCULATED AND MEASURED CURRENTS

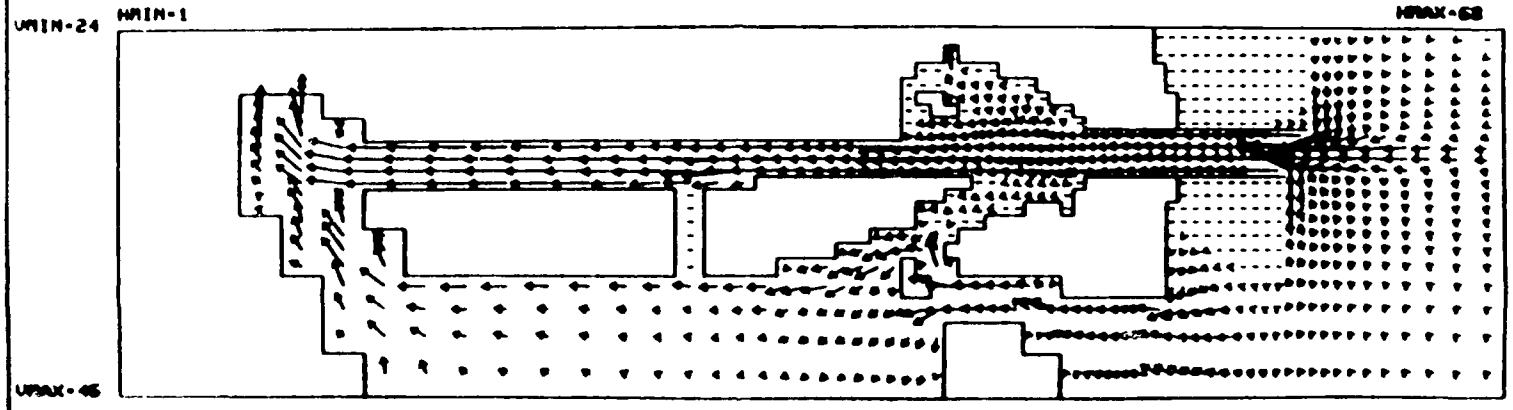

MODEL VELOCITY VECTORS

SIMULATION TIME: 4. HRS
VECTOR SCALE: ——→ 6. FPS
VECTOR THRESHOLD: .2 FPS

PLATE 21

PORT OF MIAMI NUMERICAL MODEL STUDY GLOBAL GRID

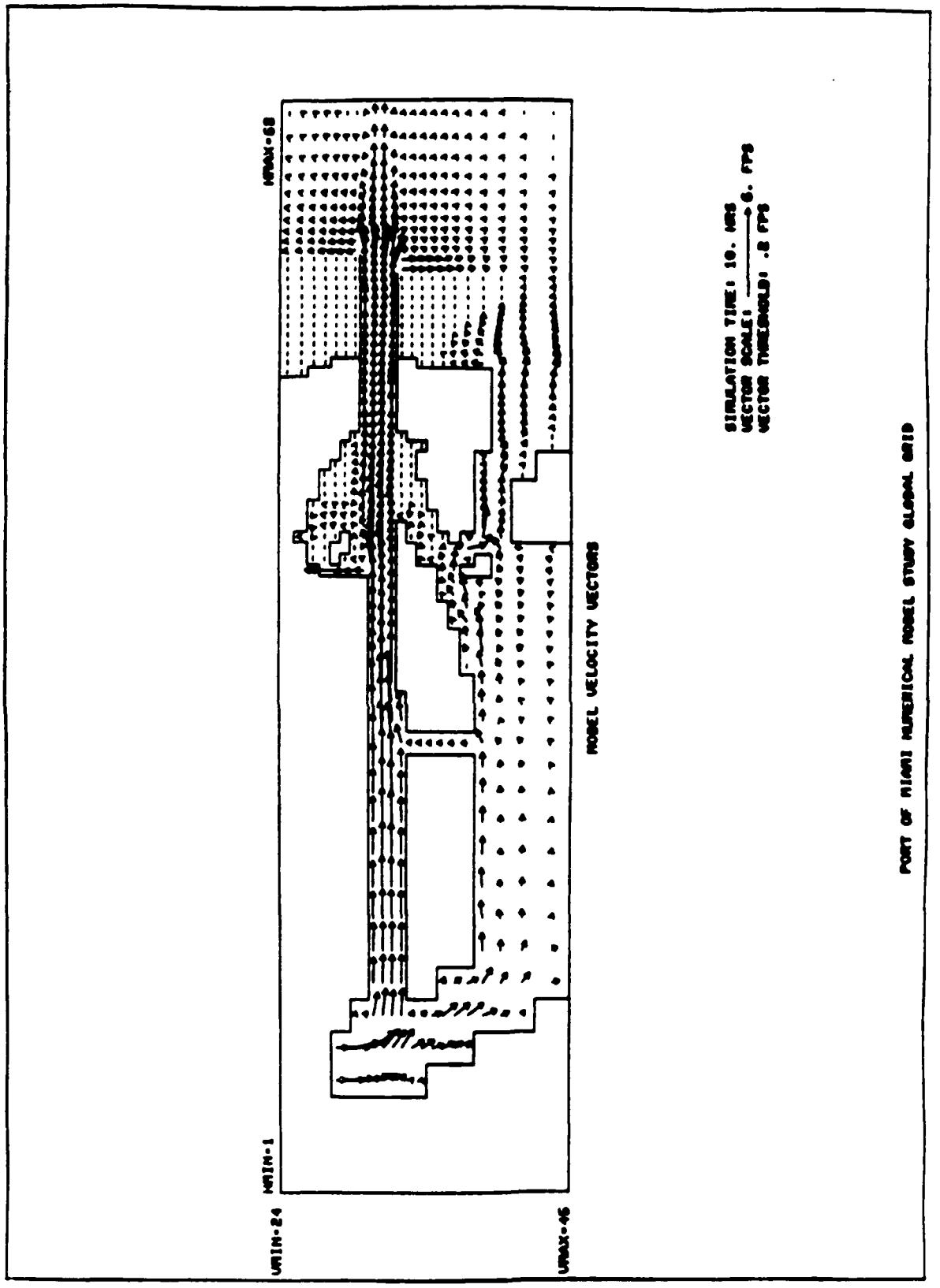
PORT OF MIAMI NUMERICAL MODEL STUDY GLOBAL GRID
MODEL VELOCITY VECTORS
SIMULATION TIME: 10. HRS
VECTOR SCALE: ——→6. FPS
VECTOR THRESHOLD: .5 FPS
MMAX-68
MMIN-1
NMIN-24
NMAX-46

PLATE 22

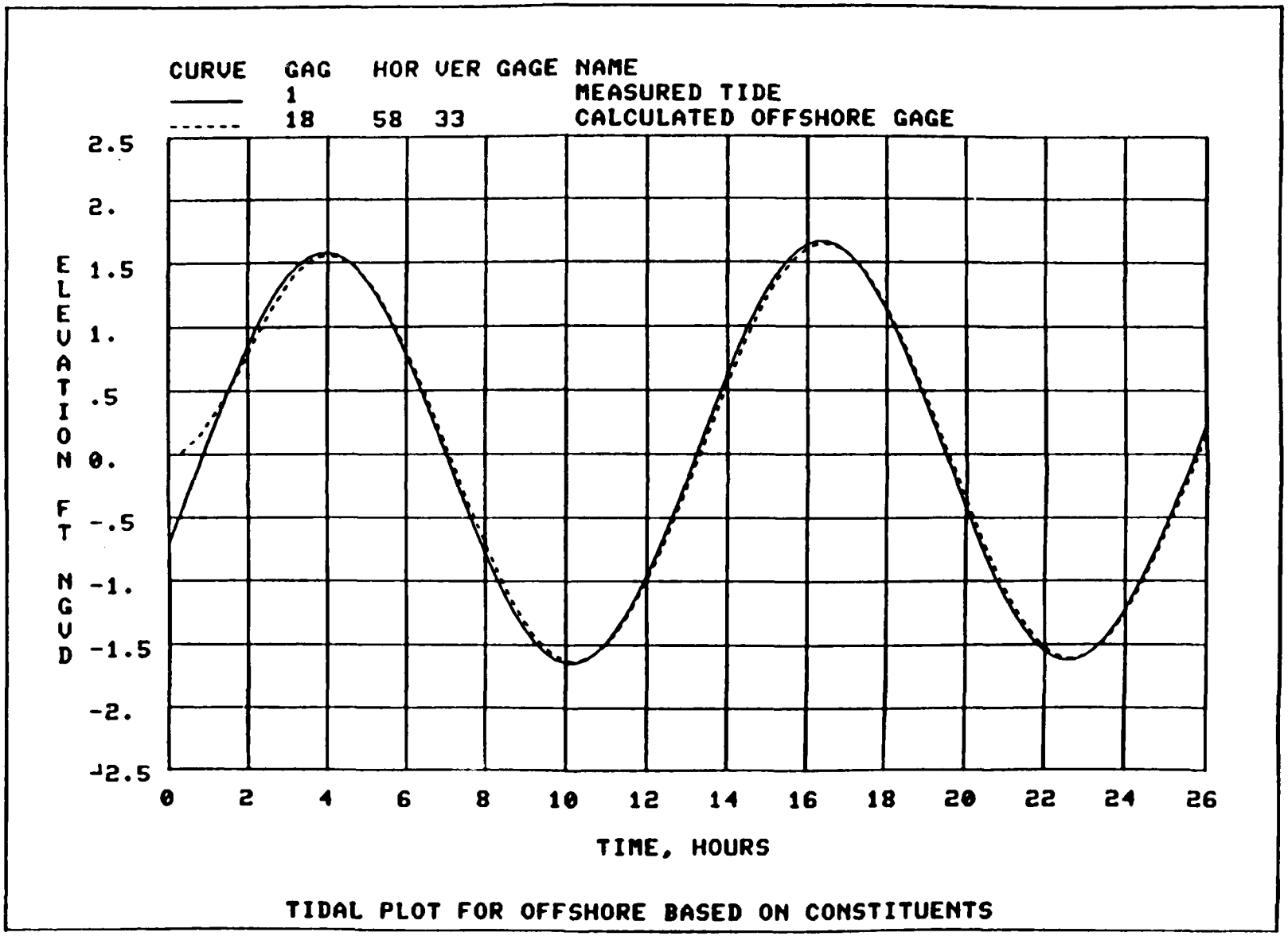

TIDAL PLOT FOR OFFSHORE BASED ON CONSTITUENTS

PLATE 23

PLATE 24

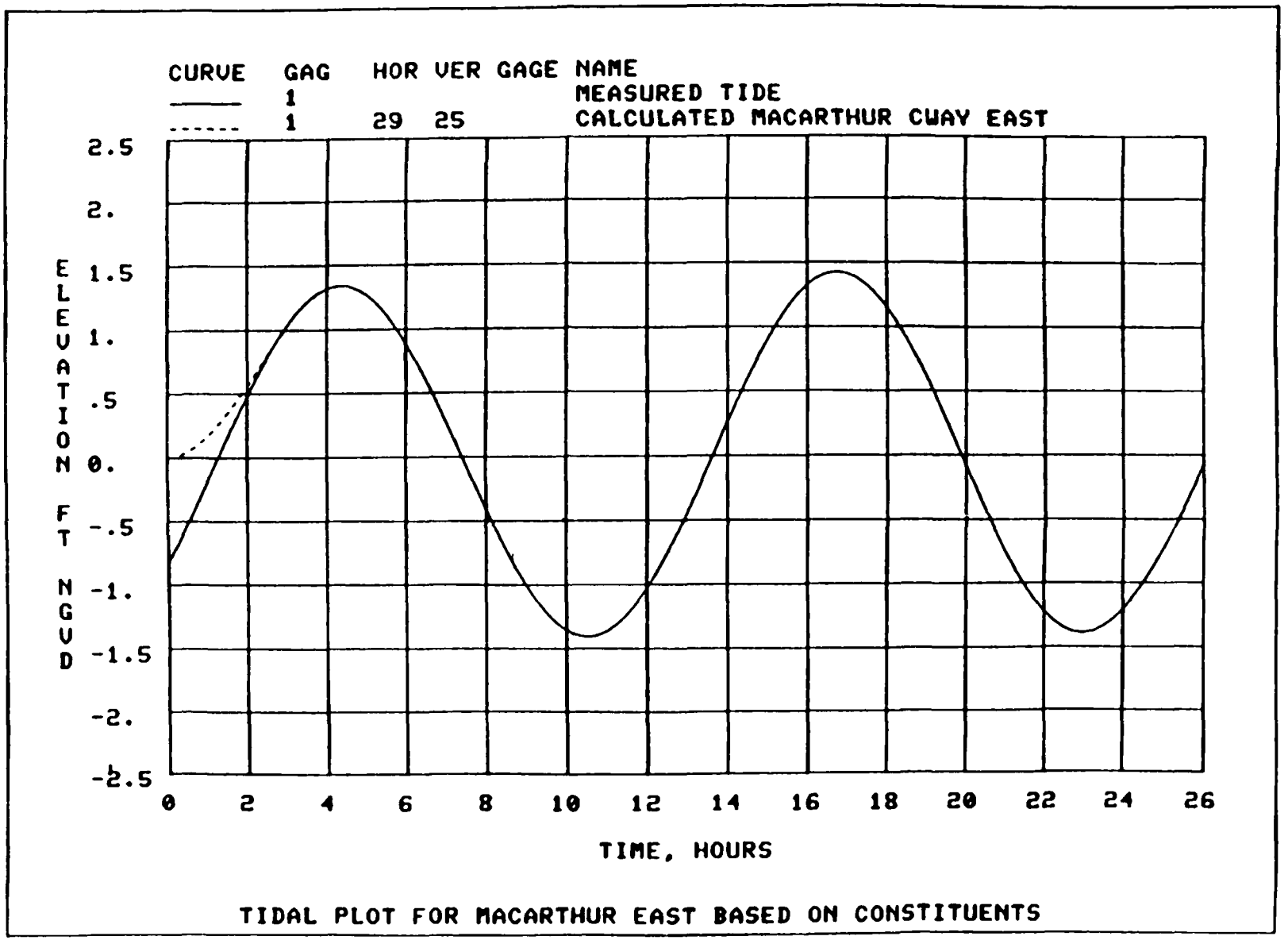

TIDAL PLOT FOR MACARTHUR EAST BASED ON CONSTITUENTS

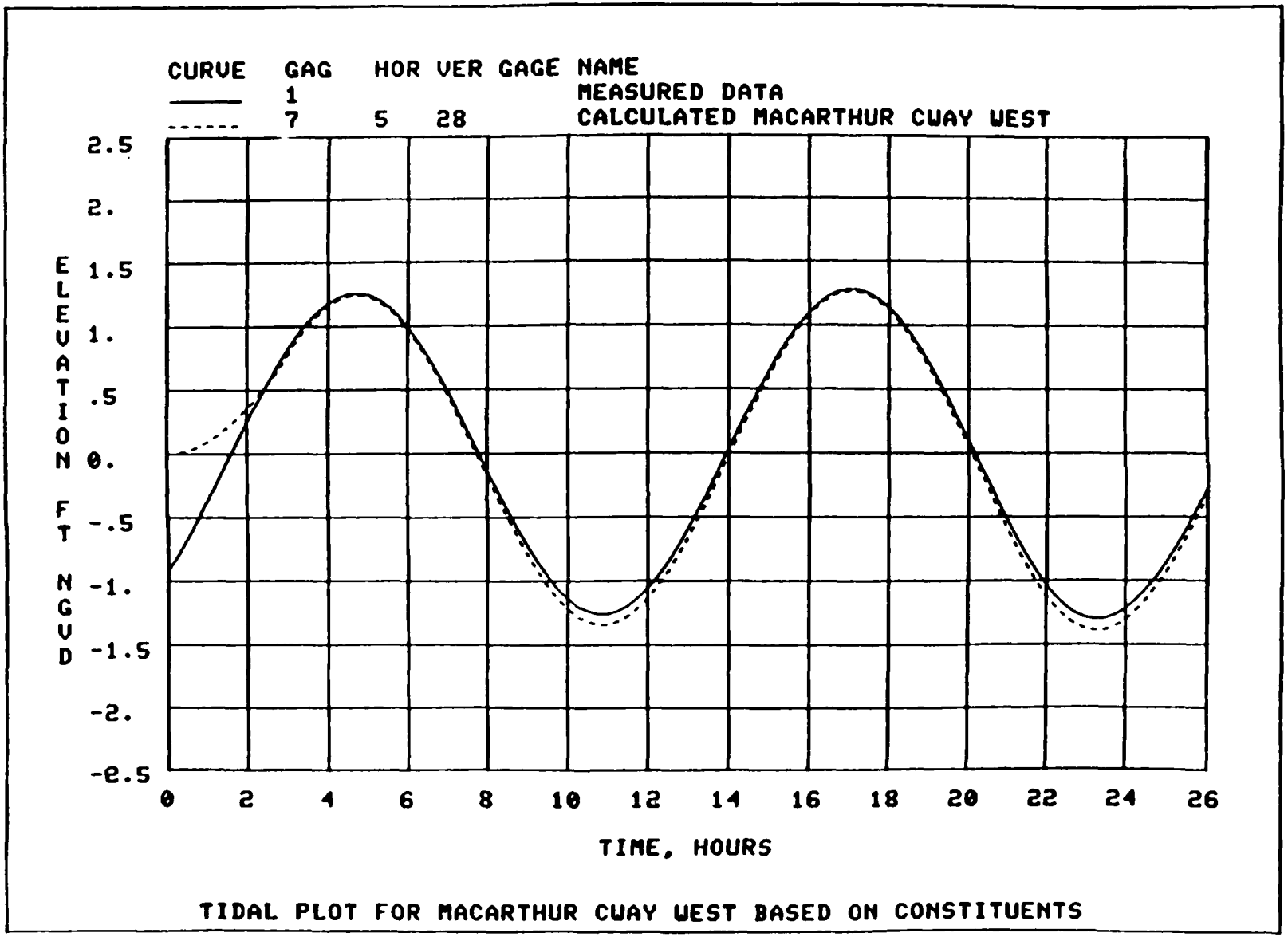

TIDAL PLOT FOR MACARTHUR CWAY WEST BASED ON CONSTITUENTS

PLATE 25

PLATE 26

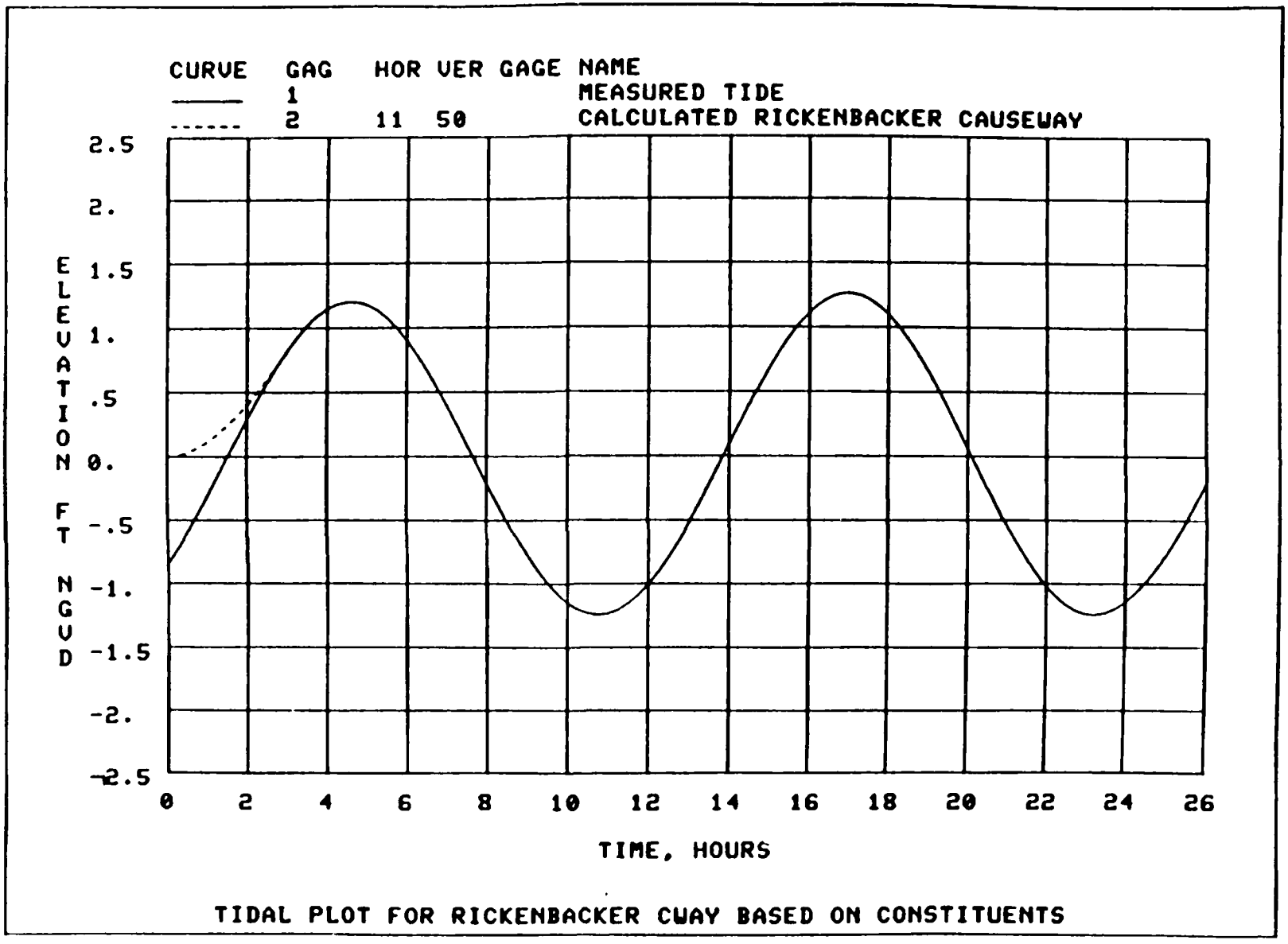

TIDAL PLOT FOR RICKENBACKER CWAY BASED ON CONSTITUENTS

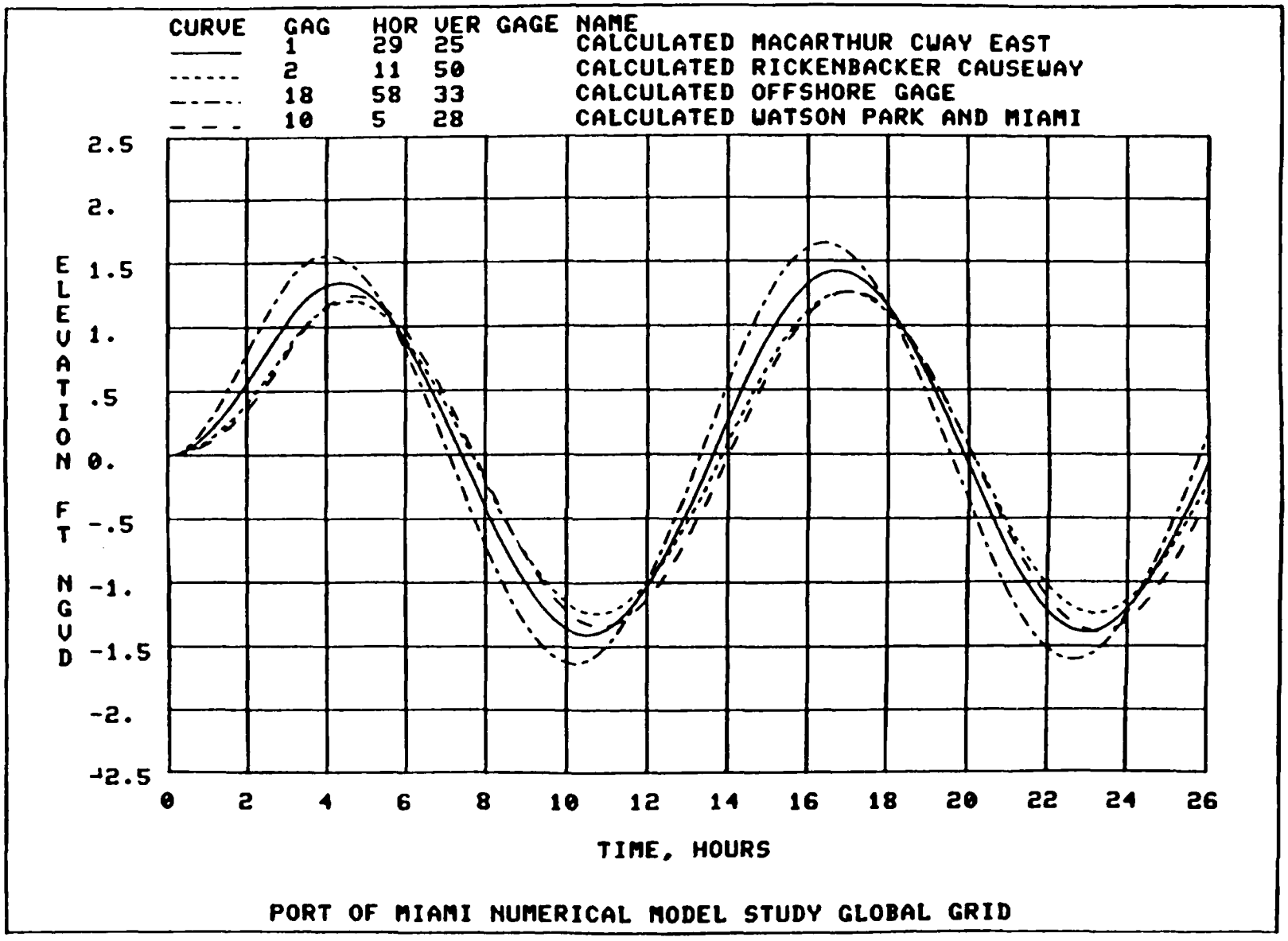
CURVE GAG HOR VER GAGE NAME
1 29 25 CALCULATED MACARTHUR CWAY EAST
2 11 50 CALCULATED RICKENBACKER CAUSEWAY
18 58 33 CALCULATED OFFSHORE GAGE
10 5 28 CALCULATED WATSON PARK AND MIAMI
ELEVATION FT NGVD
2.5
2.
1.5
1.
.5
0.
-.5
-1.
-1.5
-2.
-2.5
0 2 4 6 8 10 12 14 16 18 20 22 24 26
TIME, HOURS
PORT OF MIAMI NUMERICAL MODEL STUDY GLOBAL GRID

PLATE 27

PLATE 28

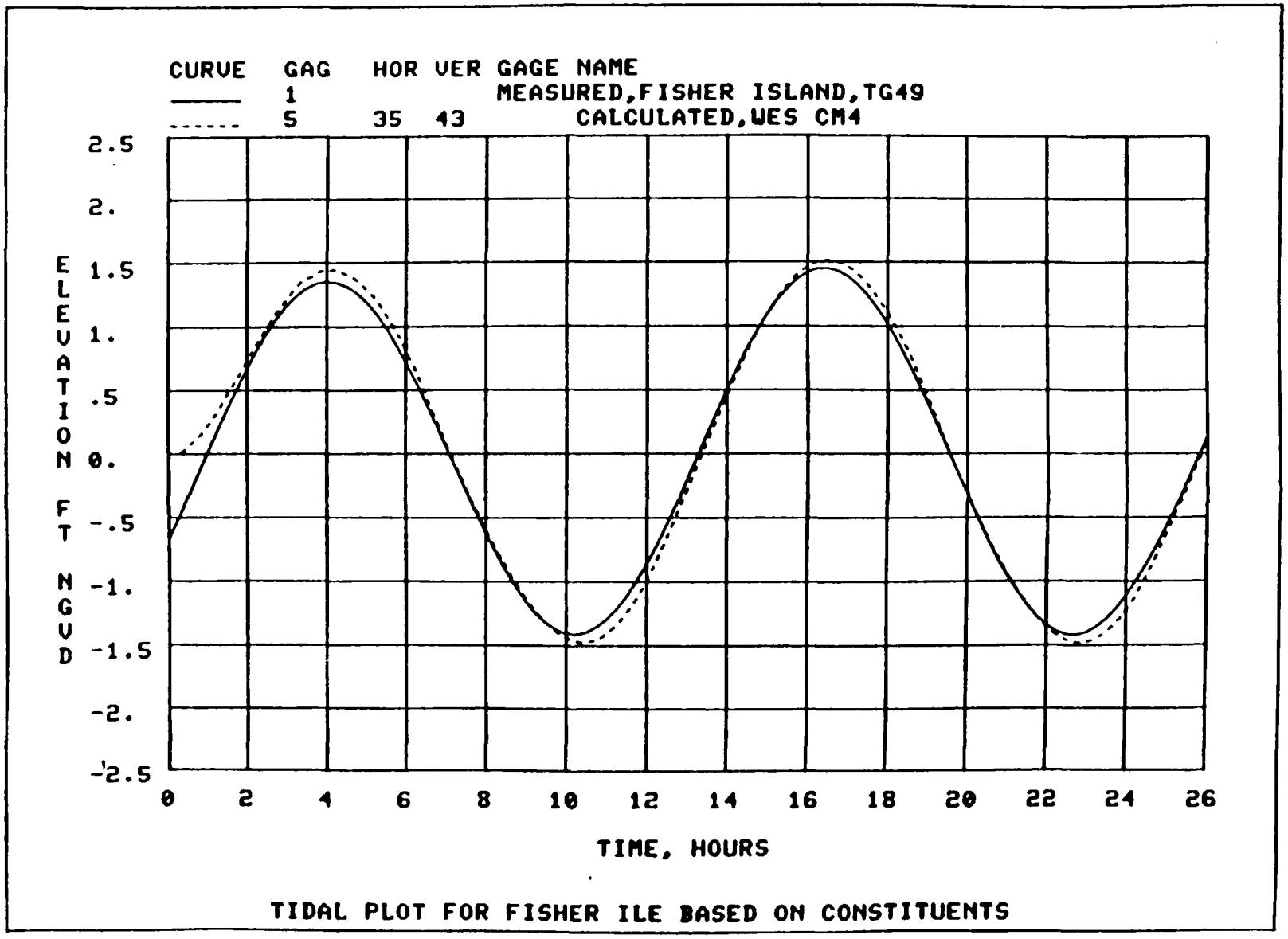

TIDAL PLOT FOR FISHER ILE BASED ON CONSTITUENTS

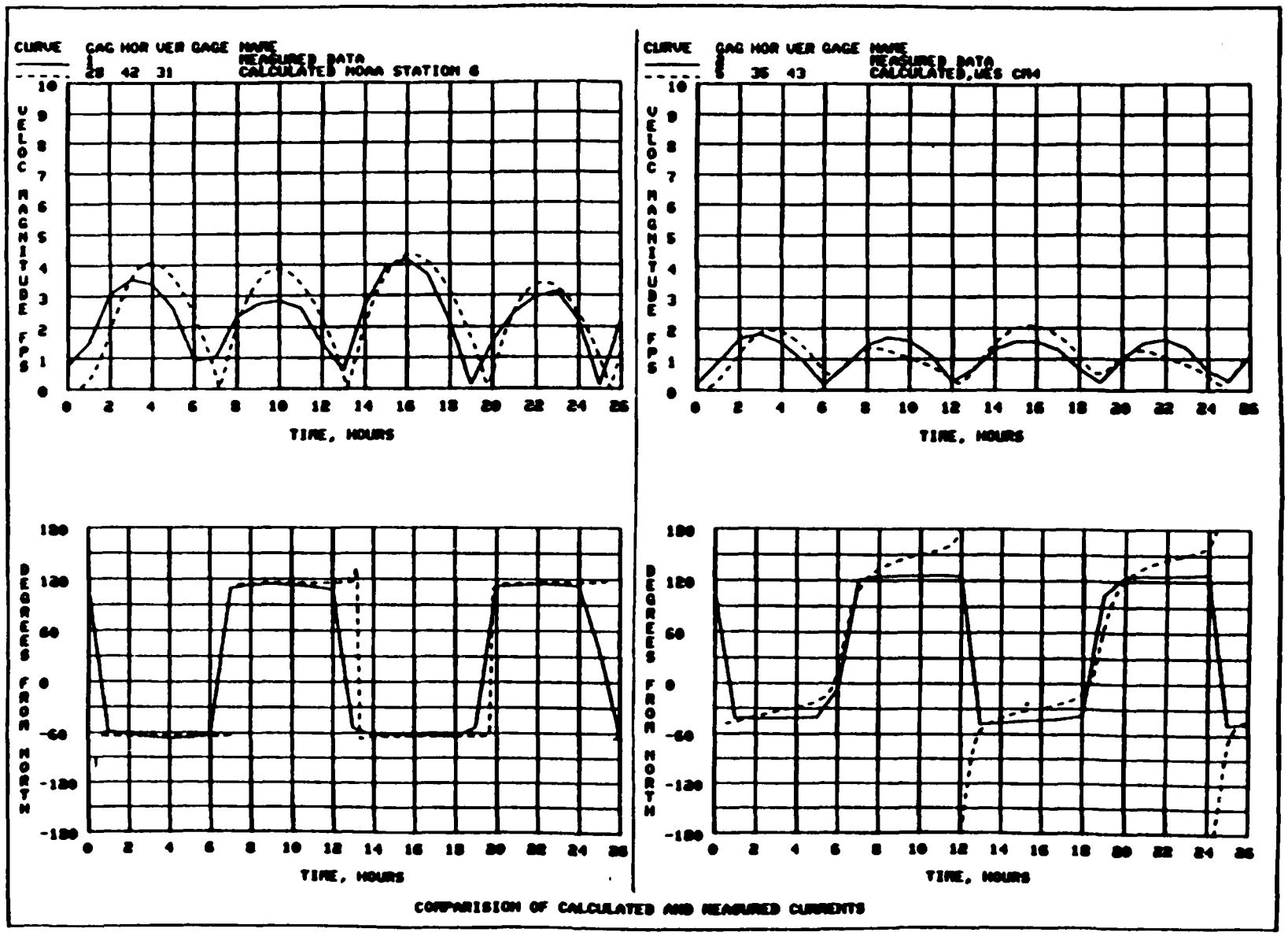

COMPARISION OF CALCULATED AND MEASURED CURRENTS

PLATE 29

PLATE 30

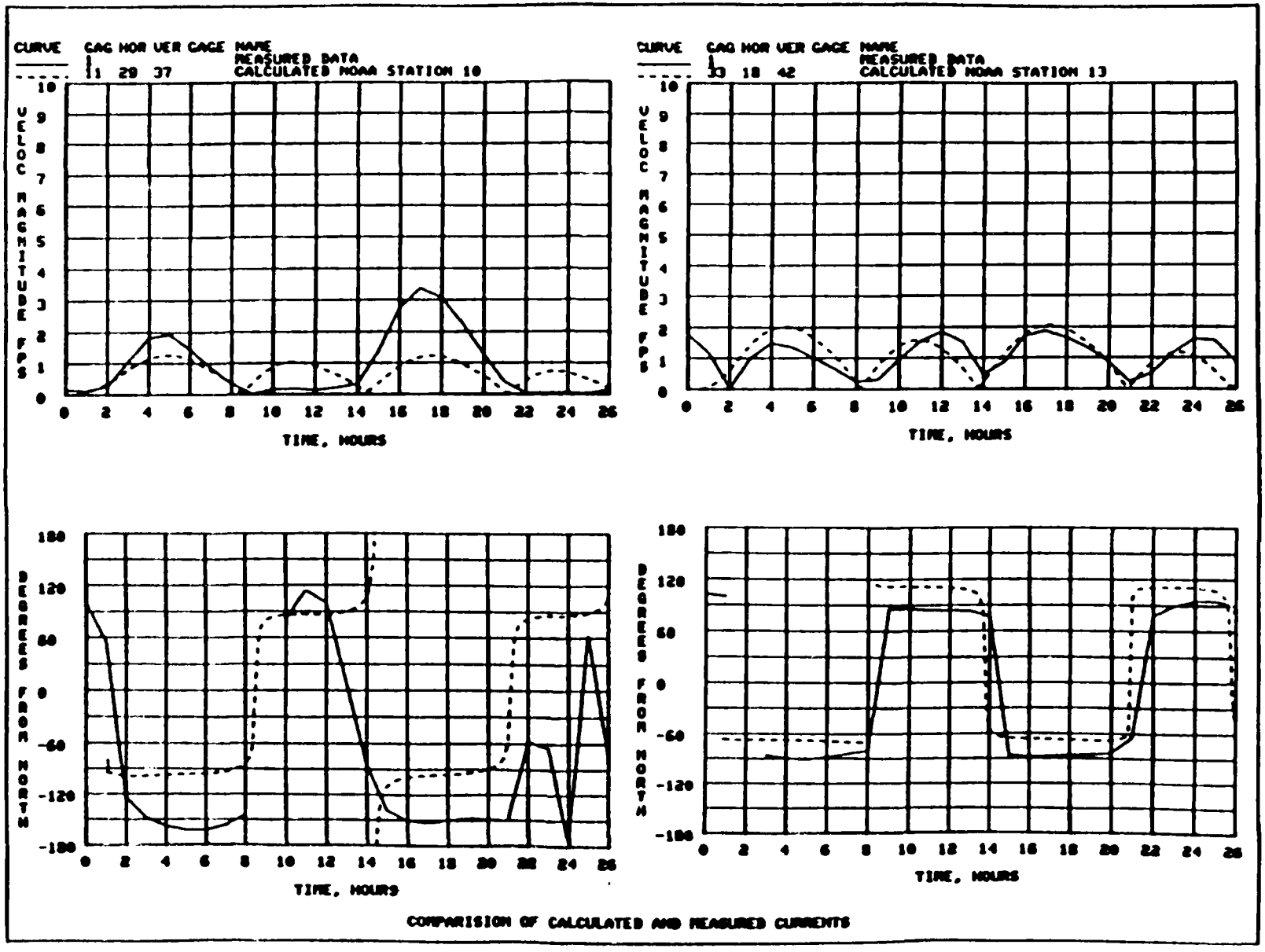

COMPARISION OF CALCULATED AND MEASURED CURRENTS

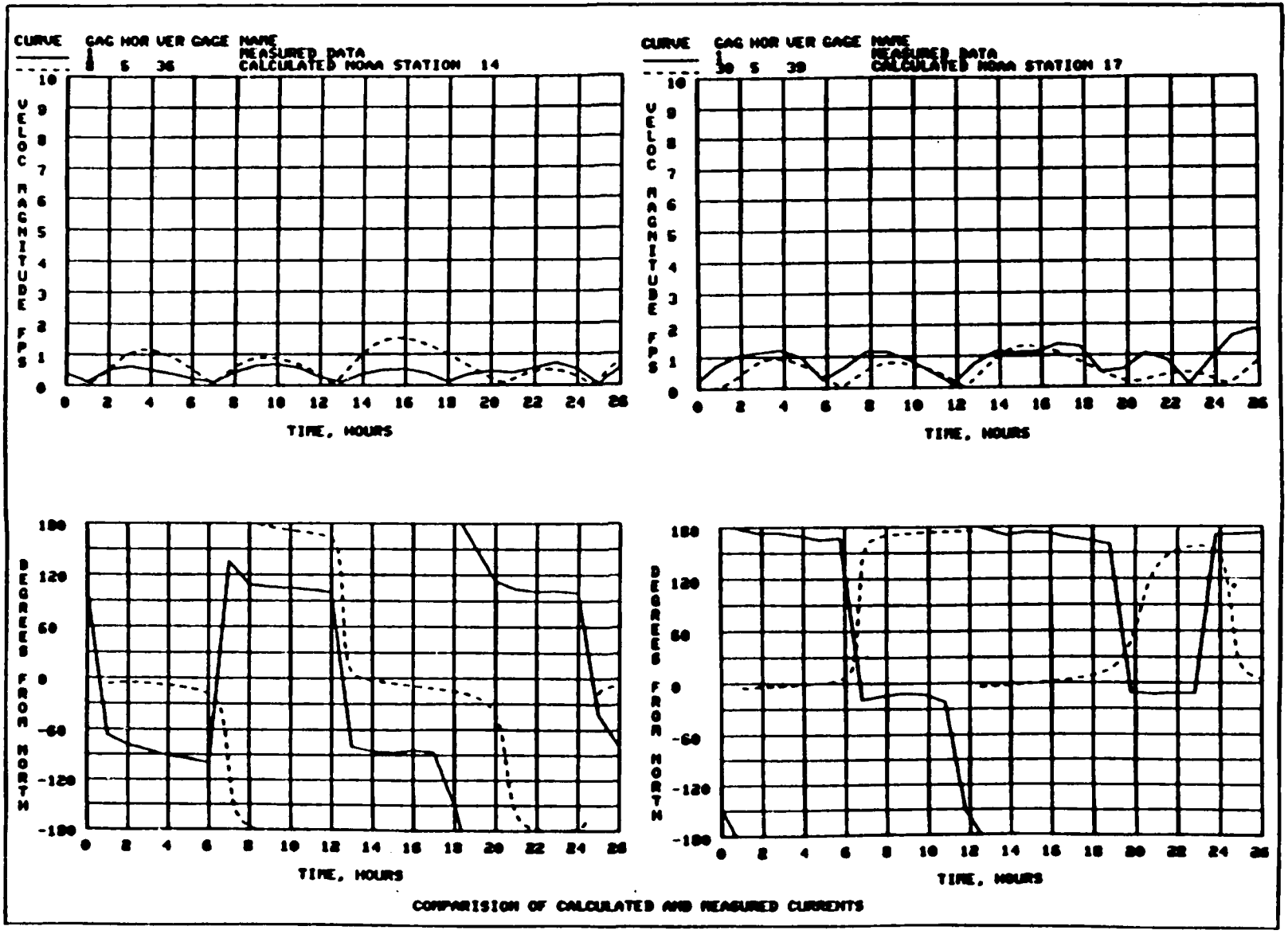

COMPARISION OF CALCULATED AND MEASURED CURRENTS

PLATE 31

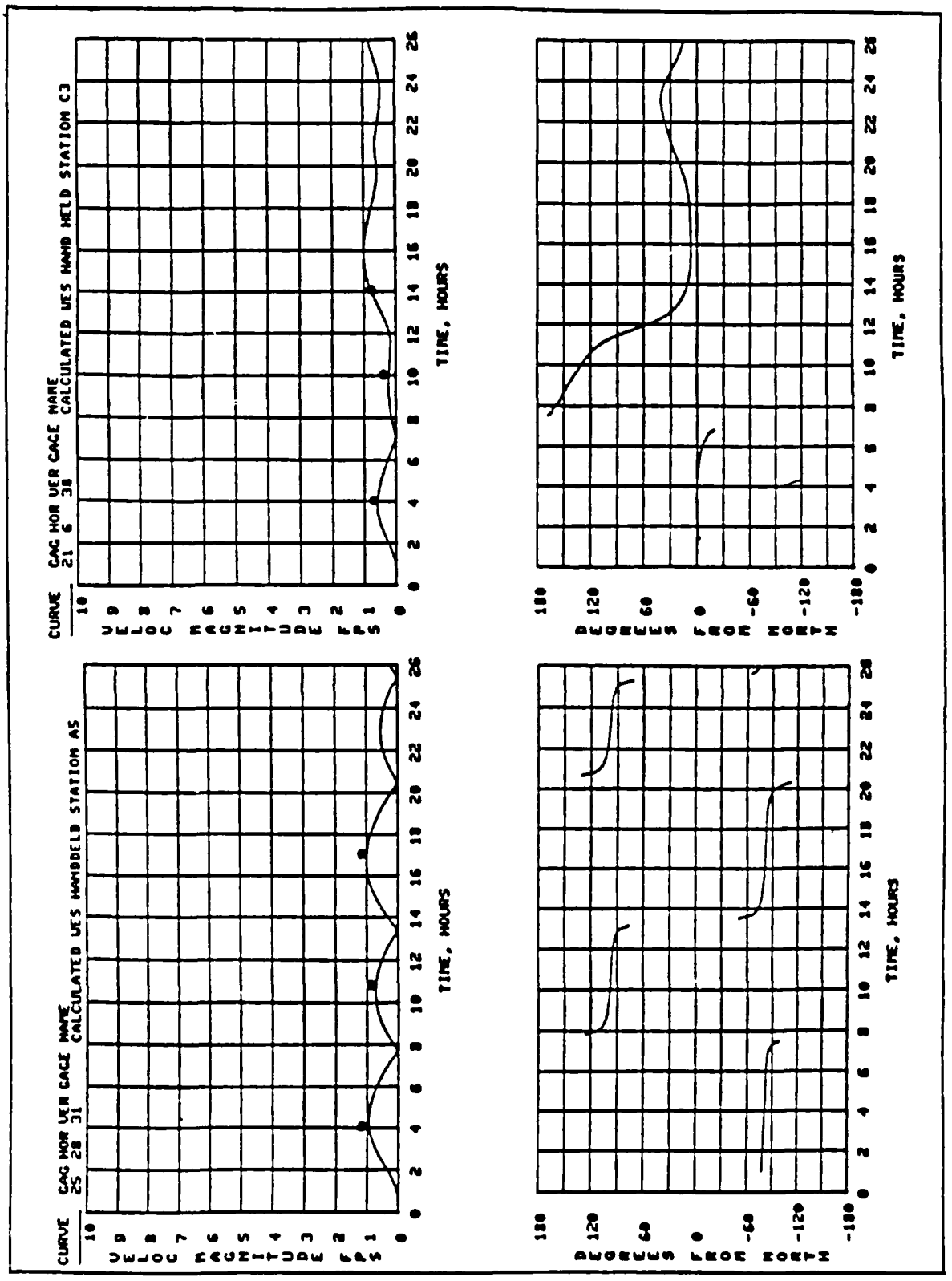
CURVE
CAC HOR VER CAGE NAME
CALCULATED UES HAND HELD STATION C3
21 6 38
VELOCITY MAGNITUDE FPS
TIME, HOURS
DEGREES FROM NORTH
CURVE
CAC HOR VER CAGE NAME
CALCULATED UES HANDHELD STATION A5
25 28 31
VELOCITY MAGNITUDE FPS
TIME, HOURS
DEGREES FROM NORTH

PLATE 32

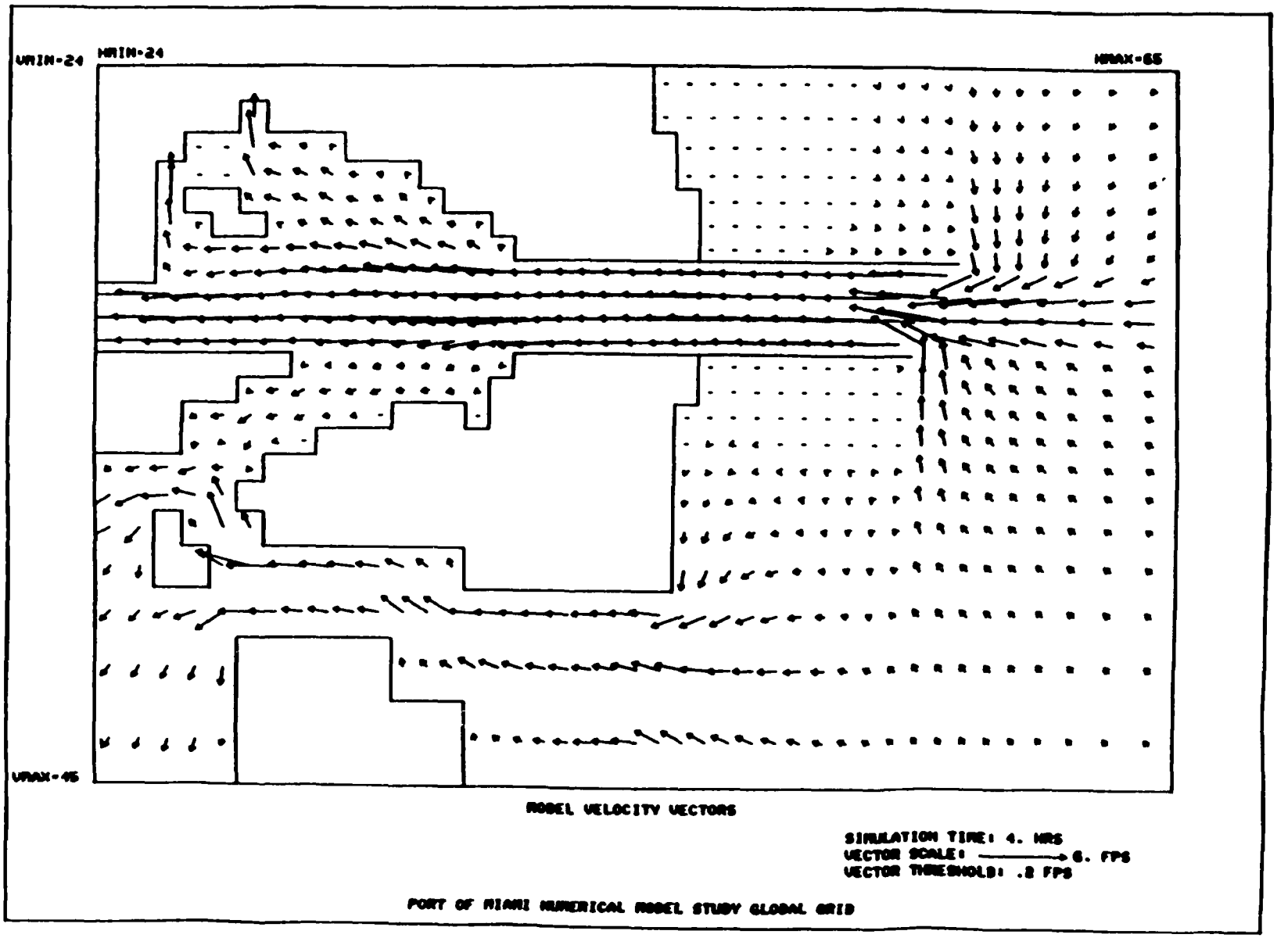
UMIN-24
MMIN-24
MMAX-65
UMAX-45
MODEL VELOCITY VECTORS
SIMULATION TIME: 4. HRS
VECTOR SCALE: 6. FPS
VECTOR THRESHOLD: .2 FPS
PORT OF MIAMI NUMERICAL MODEL STUDY GLOBAL GRID

PLATE 33

PLATE 34

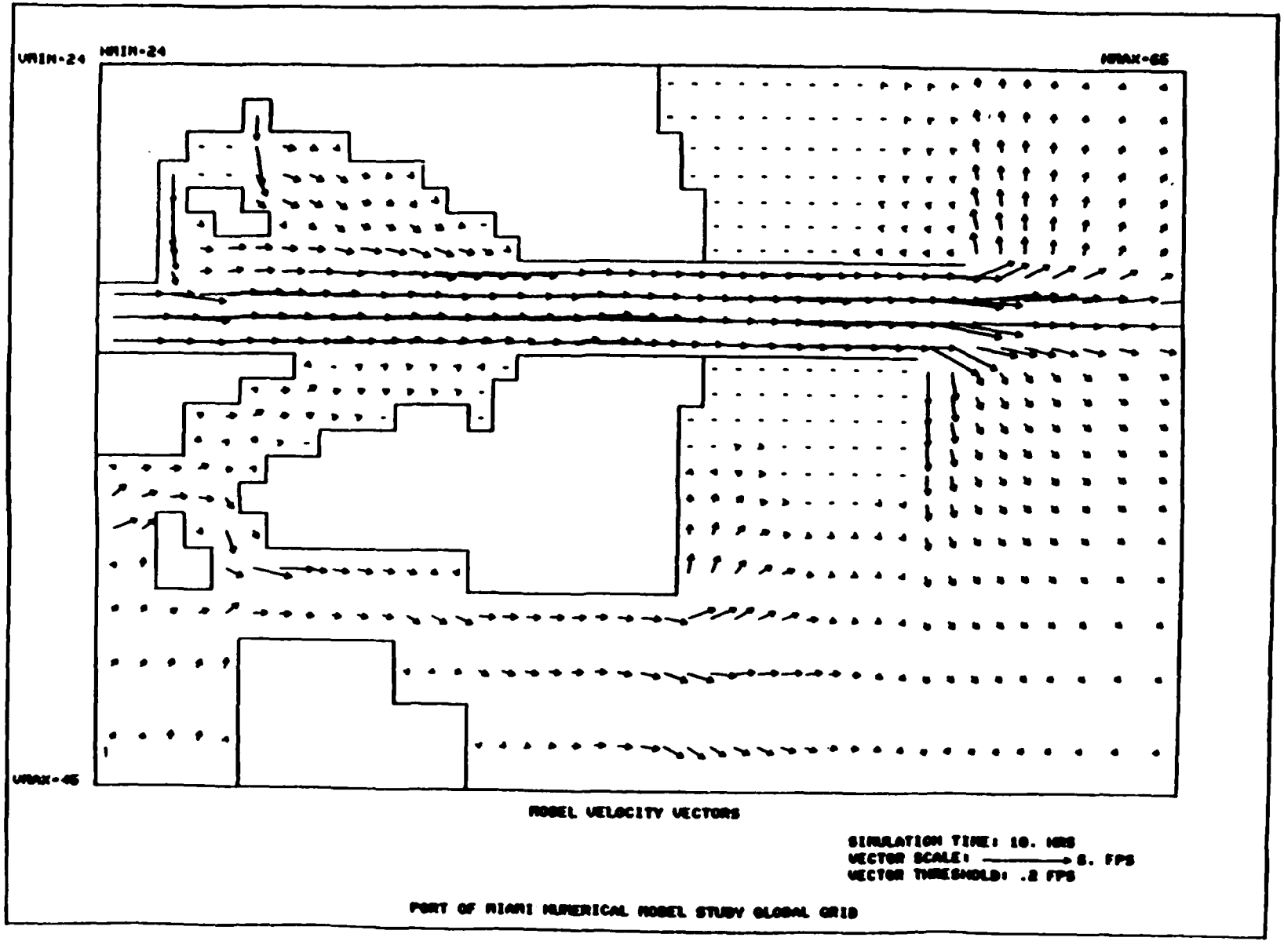

PORT OF MIAMI NUMERICAL MODEL STUDY GLOBAL GRID

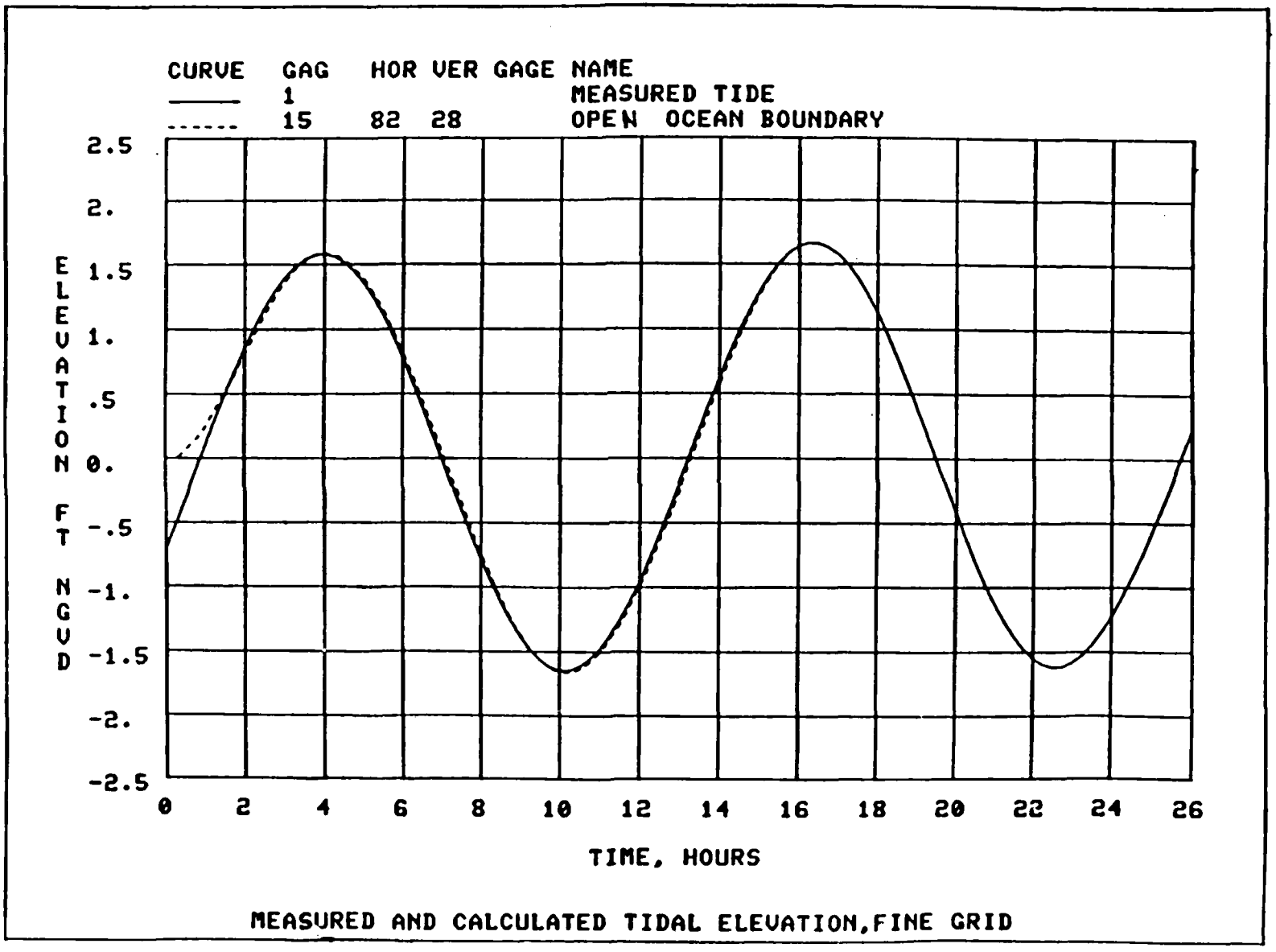

MEASURED AND CALCULATED TIDAL ELEVATION, FINE GRID

PLATE 35

PLATE 36

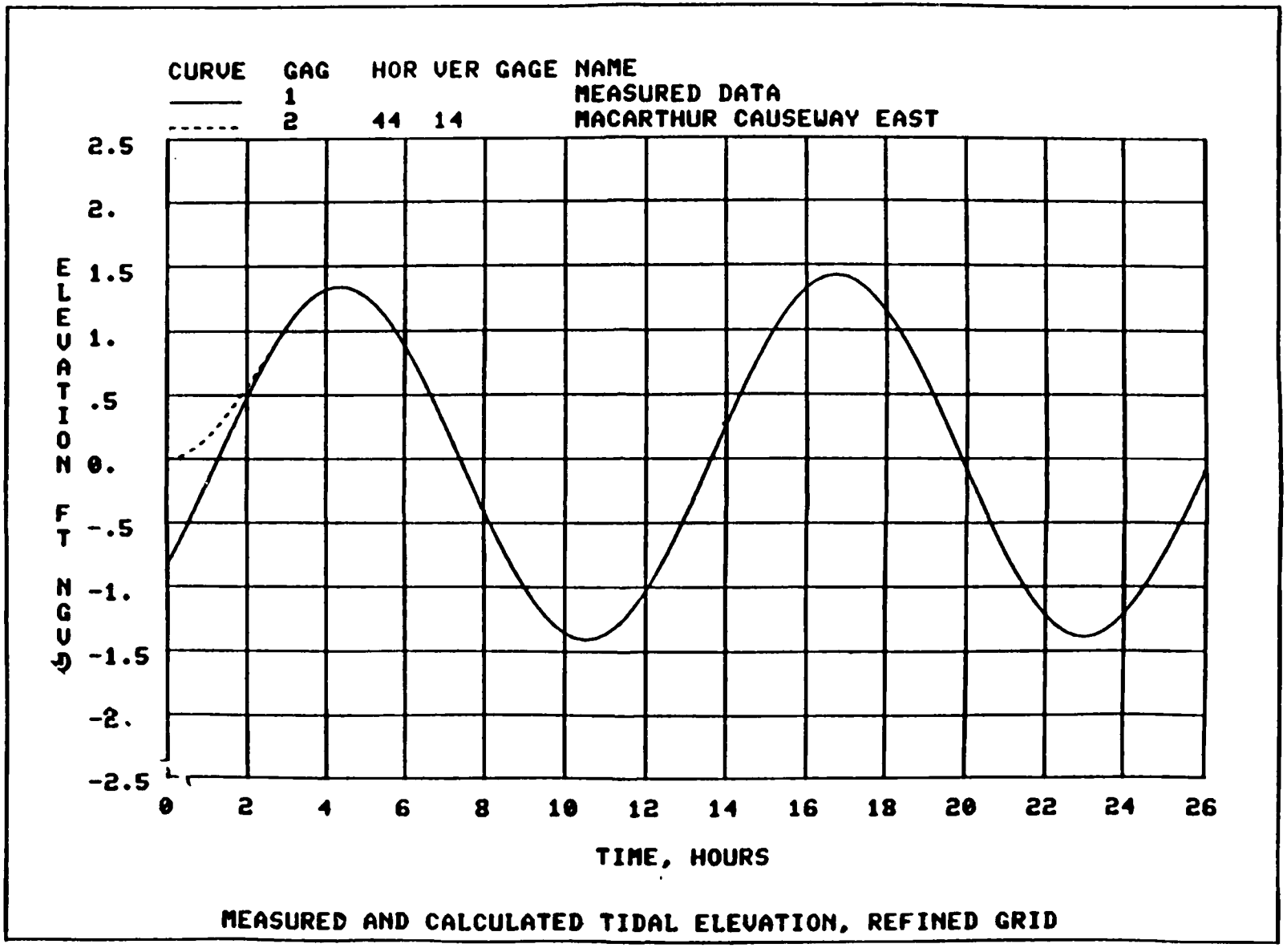

MEASURED AND CALCULATED TIDAL ELEVATION, REFINED GRID

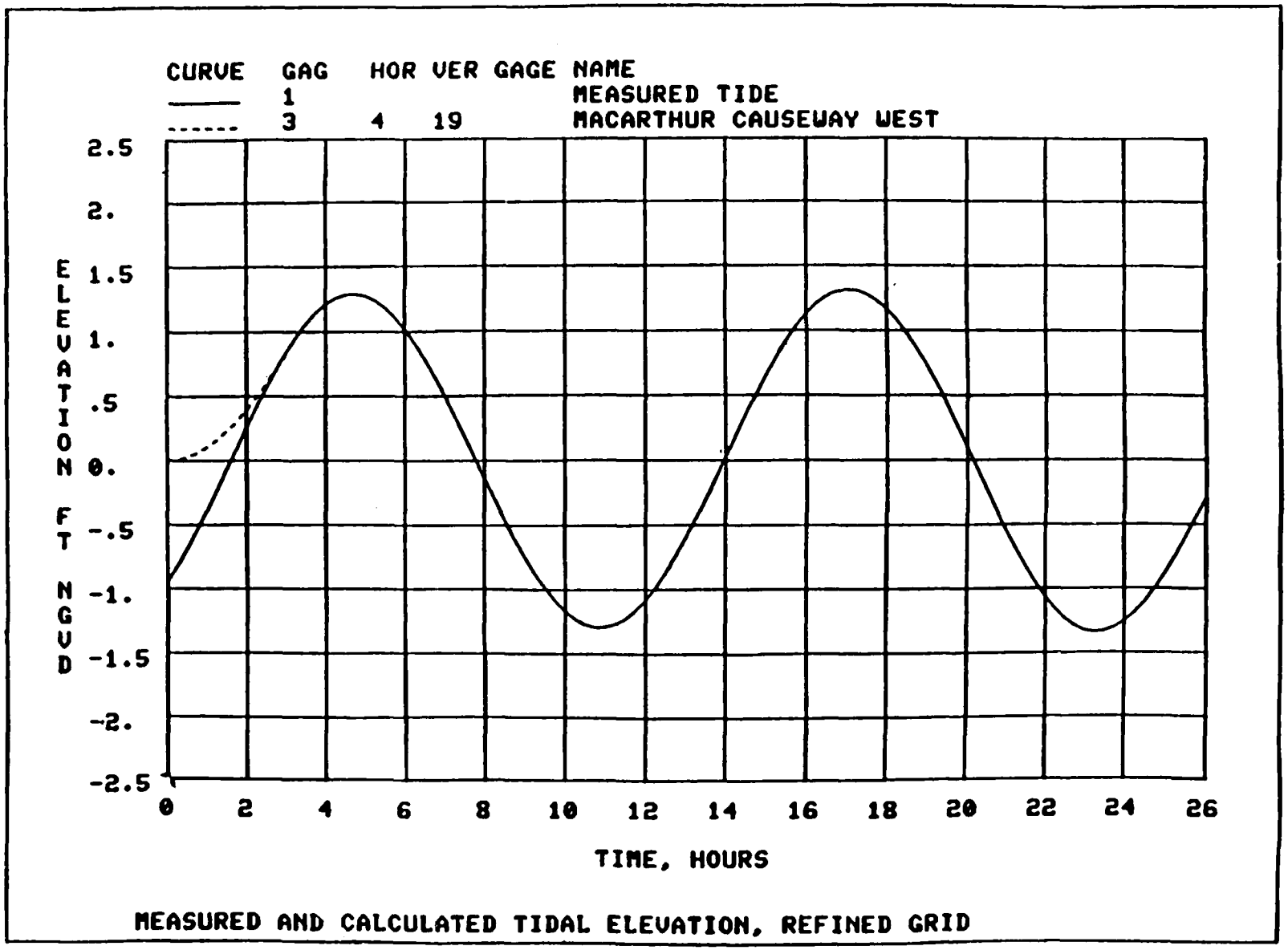

PLATE 37

MEASURED AND CALCULATED TIDAL ELEVATION, REFINED GRID

PLATE 38

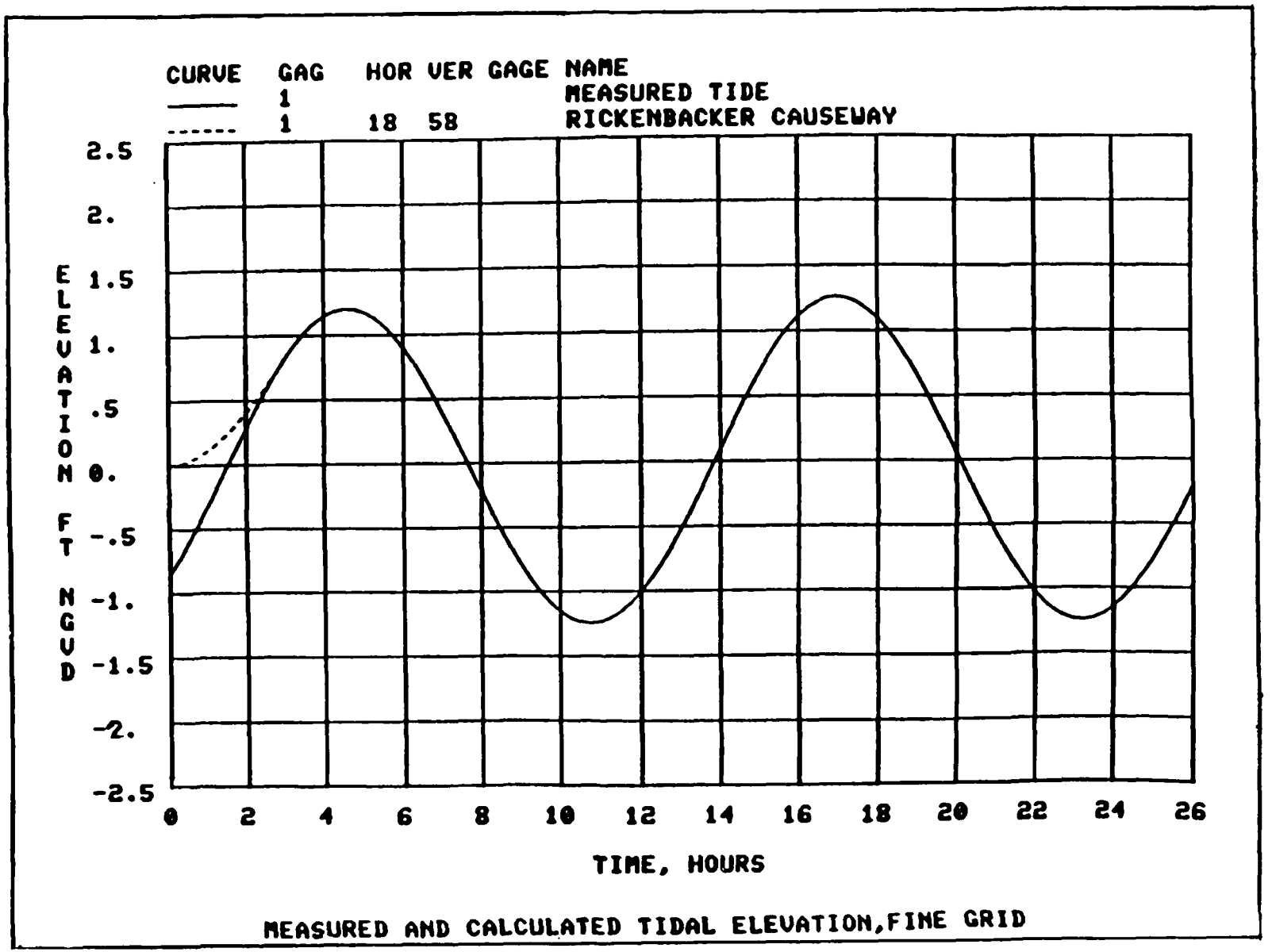

MEASURED AND CALCULATED TIDAL ELEVATION,FINE GRID

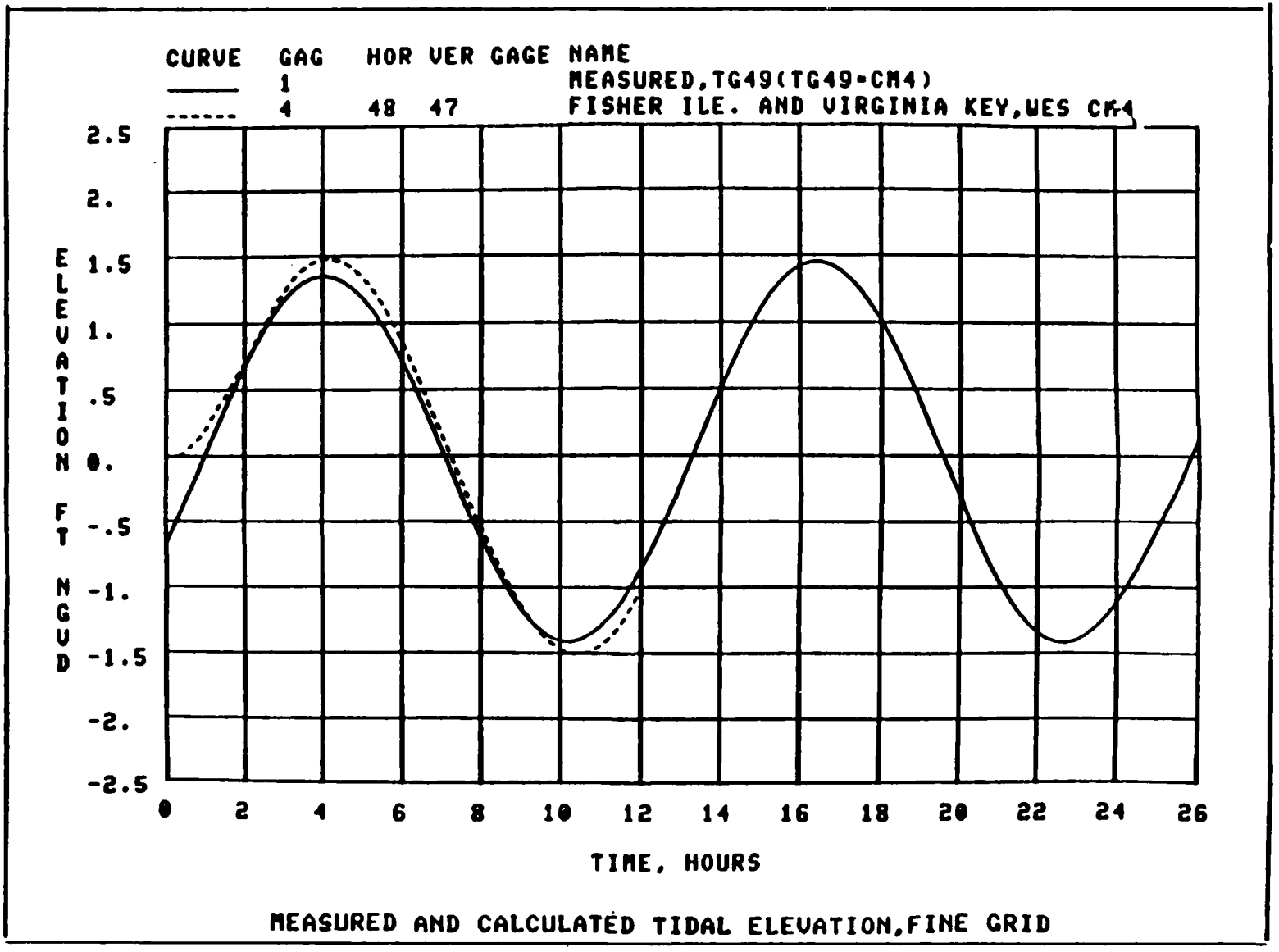

MEASURED AND CALCULATED TIDAL ELEVATION,FINE GRID

PLATE 39

PLATE 40

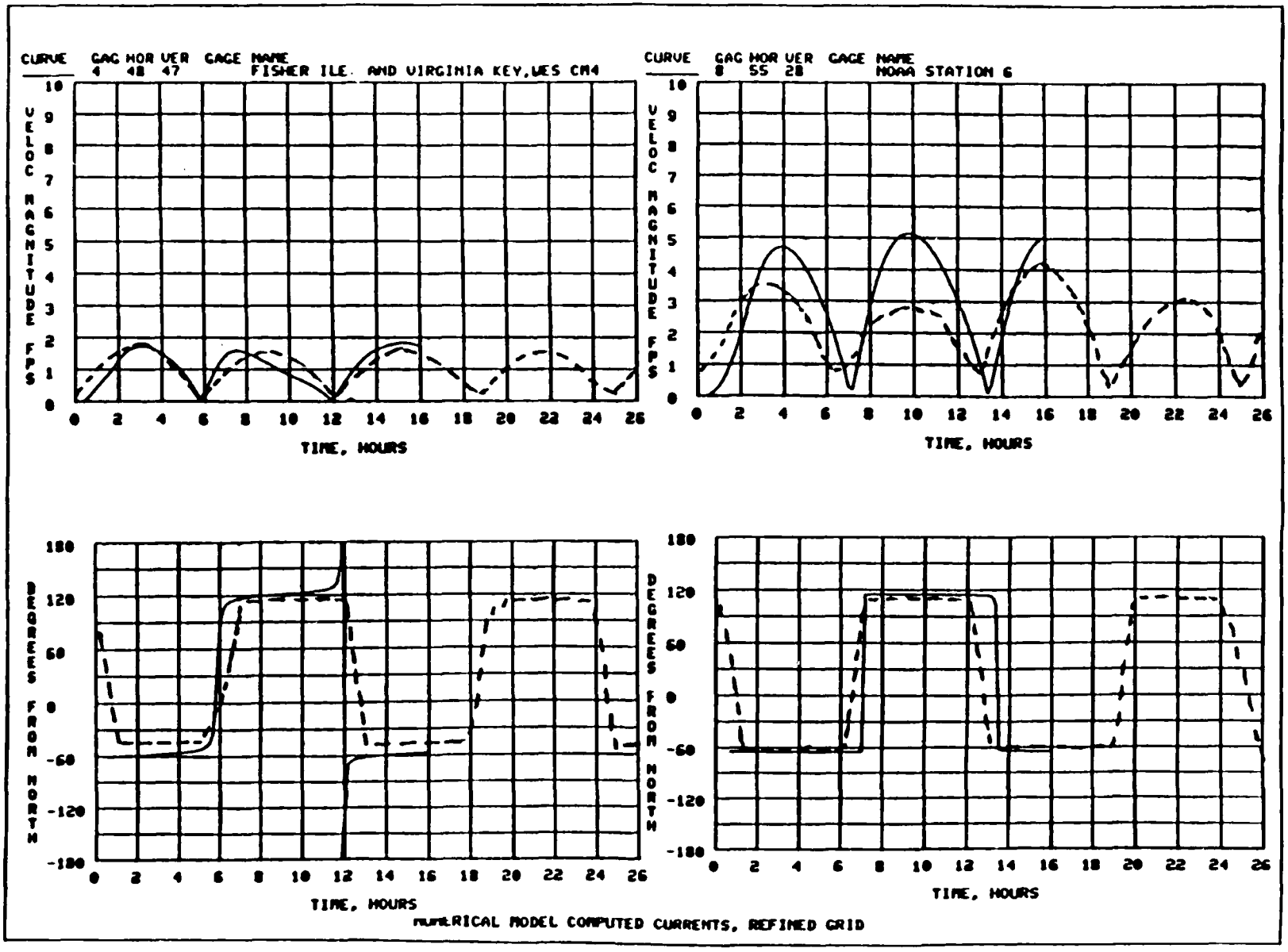
CURVE GAG HOR VER GAGE NAME
4 48 47 FISHER ILE. AND VIRGINIA KEY,UES CM4
CURVE GAG HOR VER GAGE NAME
8 55 28 NOAA STATION 6
VELOC MAGNITUDE FPS
DEGREES FROM NORTH
TIME, HOURS
NUMERICAL MODEL COMPUTED CURRENTS, REFINED GRID

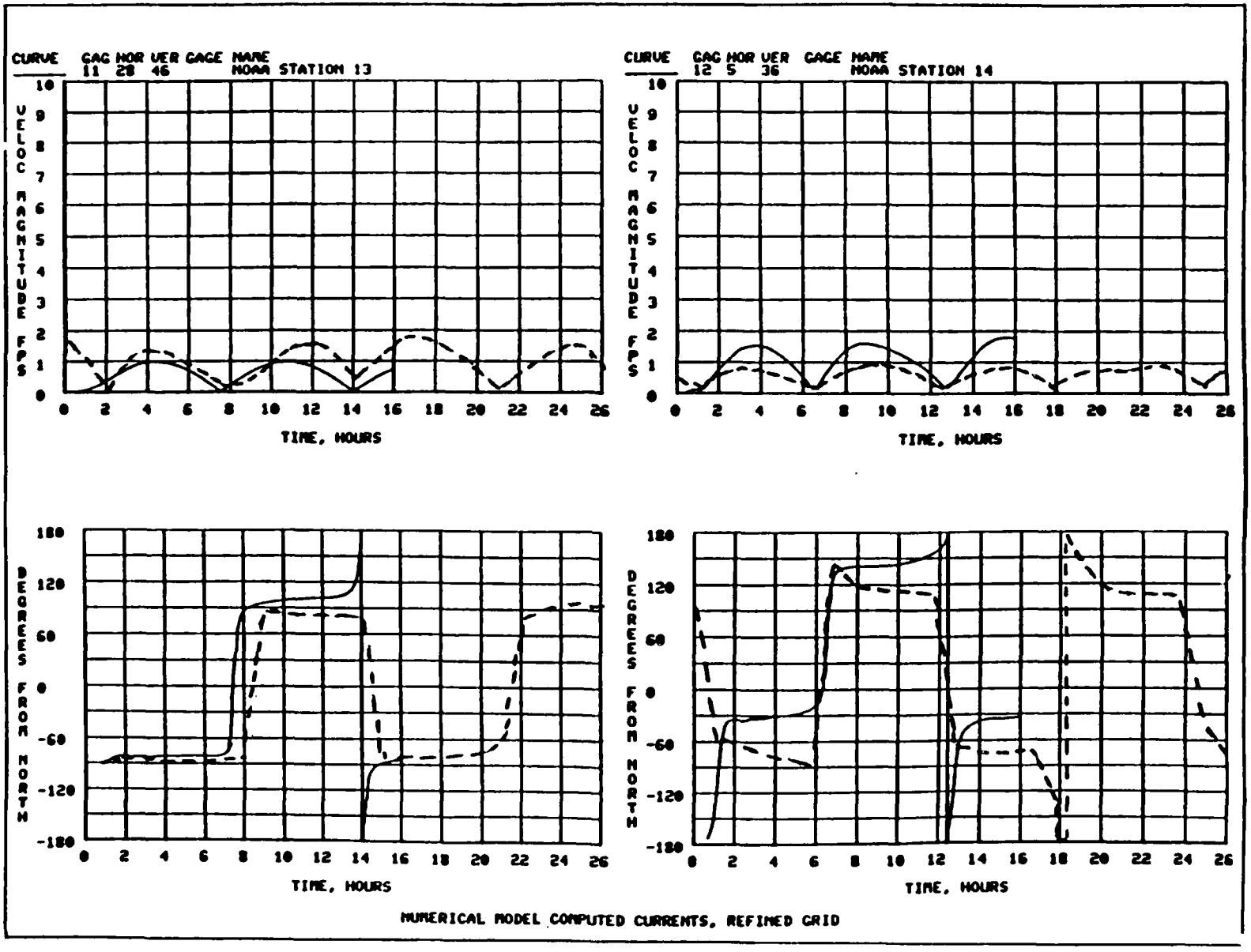

NUMERICAL MODEL COMPUTED CURRENTS, REFINED GRID

PLATE 41

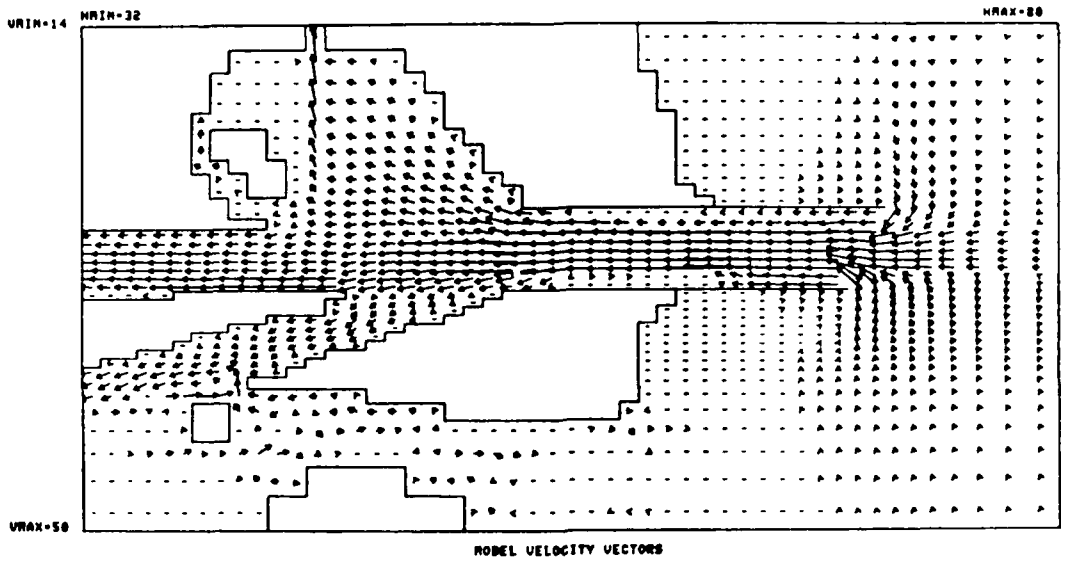

MODEL VELOCITY VECTORS

SIMULATION TIME: 6. HRS
VECTOR SCALE: ——→ 6. FPS
VECTOR THRESHOLD: .2 FPS

PORT OF MIAMI NUMERICAL STUDY, REFINED GRID

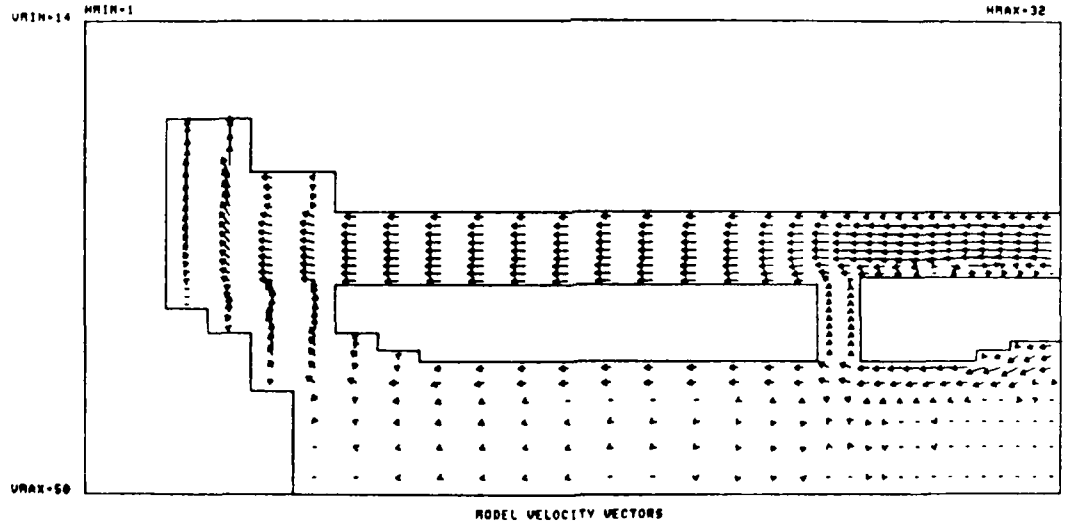

MODEL VELOCITY VECTORS

SIMULATION TIME: 6. HRS
VECTOR SCALE: ——→ 6. FPS
VECTOR THRESHOLD: .2 FPS

PORT OF MIAMI NUMERICAL STUDY, REFINED GRID

PLATE 42

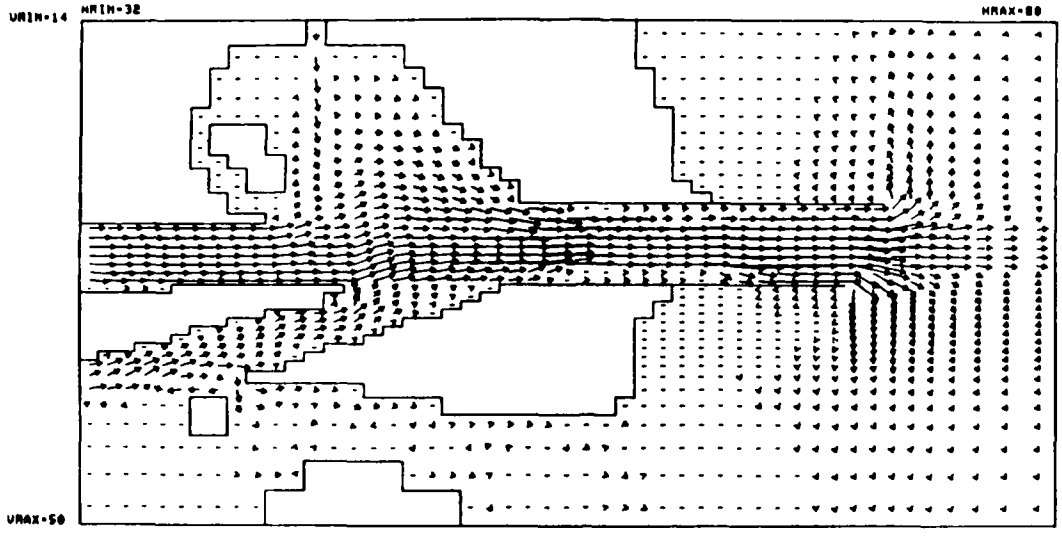

MODEL VELOCITY VECTORS

SIMULATION TIME: 12. HRS
VECTOR SCALE: ——→ 6. FPS
VECTOR THRESHOLD: .2 FPS

PORT OF MIAMI NUMERICAL STUDY, REFINED GRID

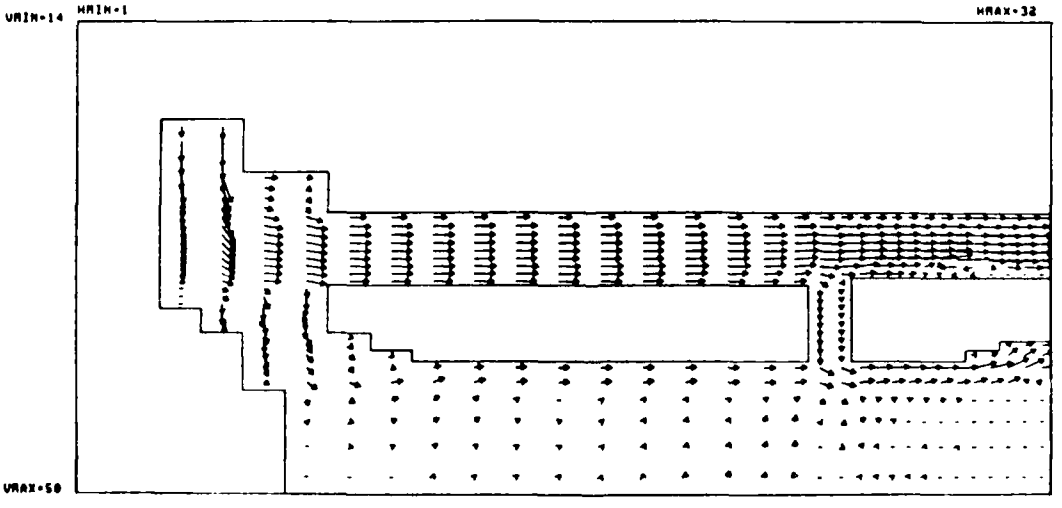

MODEL VELOCITY VECTORS

SIMULATION TIME: 12. HRS
VECTOR SCALE: ——→ 6. FPS
VECTOR THRESHOLD: .2 FPS

PORT OF MIAMI NUMERICAL STUDY, REFINED GRID

PLATE 43

PLATE 44

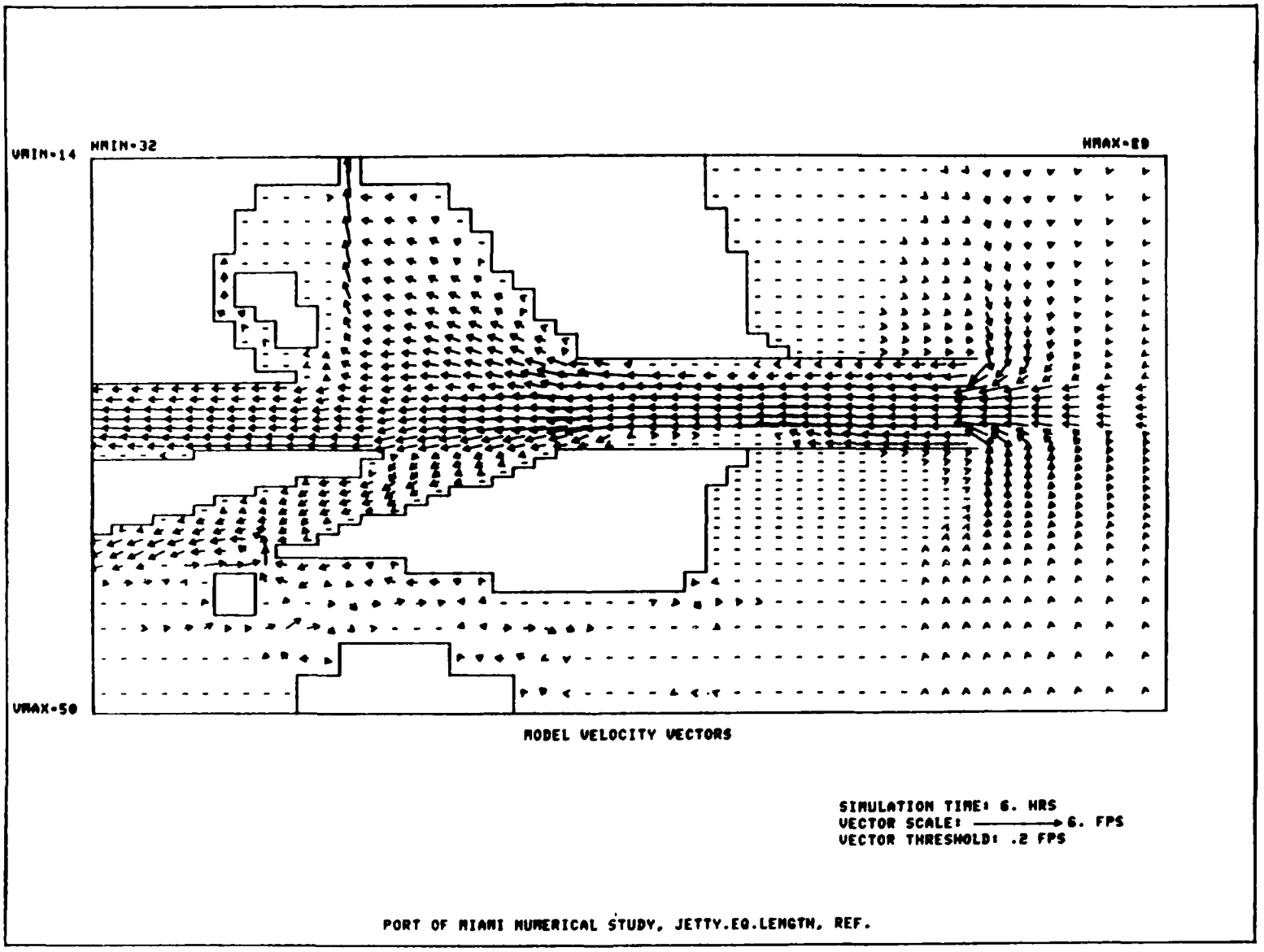
VMIN=14
MMIN=32
MMAX=89
VMAX=50
MODEL VELOCITY VECTORS
SIMULATION TIME: 6. HRS
VECTOR SCALE: 6. FPS
VECTOR THRESHOLD: .2 FPS
PORT OF MIAMI NUMERICAL STUDY, JETTY.EQ.LENGTH, REF.

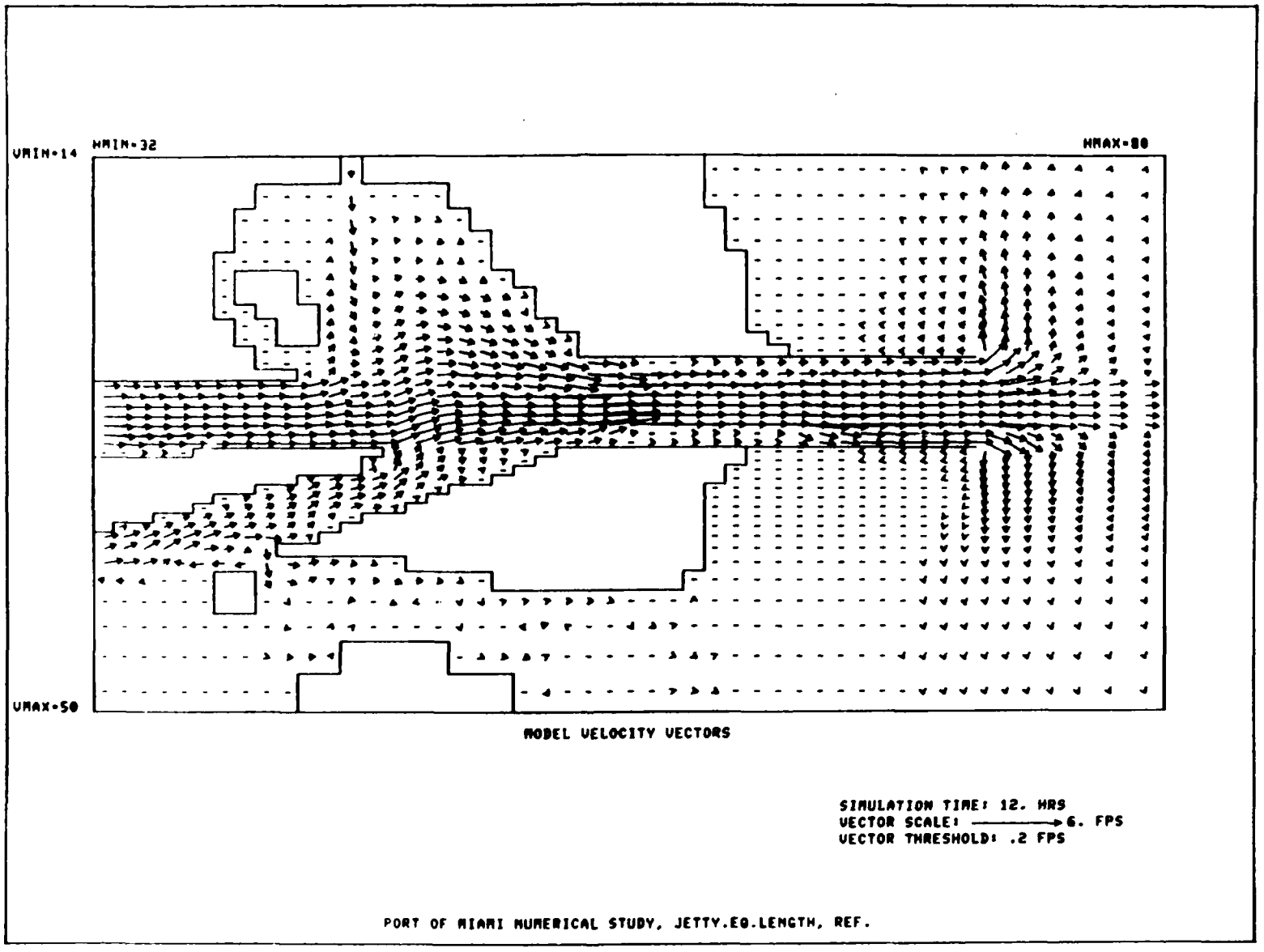
VMIN=14
MMIN=32
MMAX=88
VMAX=50
MODEL VELOCITY VECTORS
SIMULATION TIME: 12. HRS
VECTOR SCALE: ——→ 6. FPS
VECTOR THRESHOLD: .2 FPS
PORT OF MIAMI NUMERICAL STUDY, JETTY.EQ.LENGTH, REF.

PLATE 45

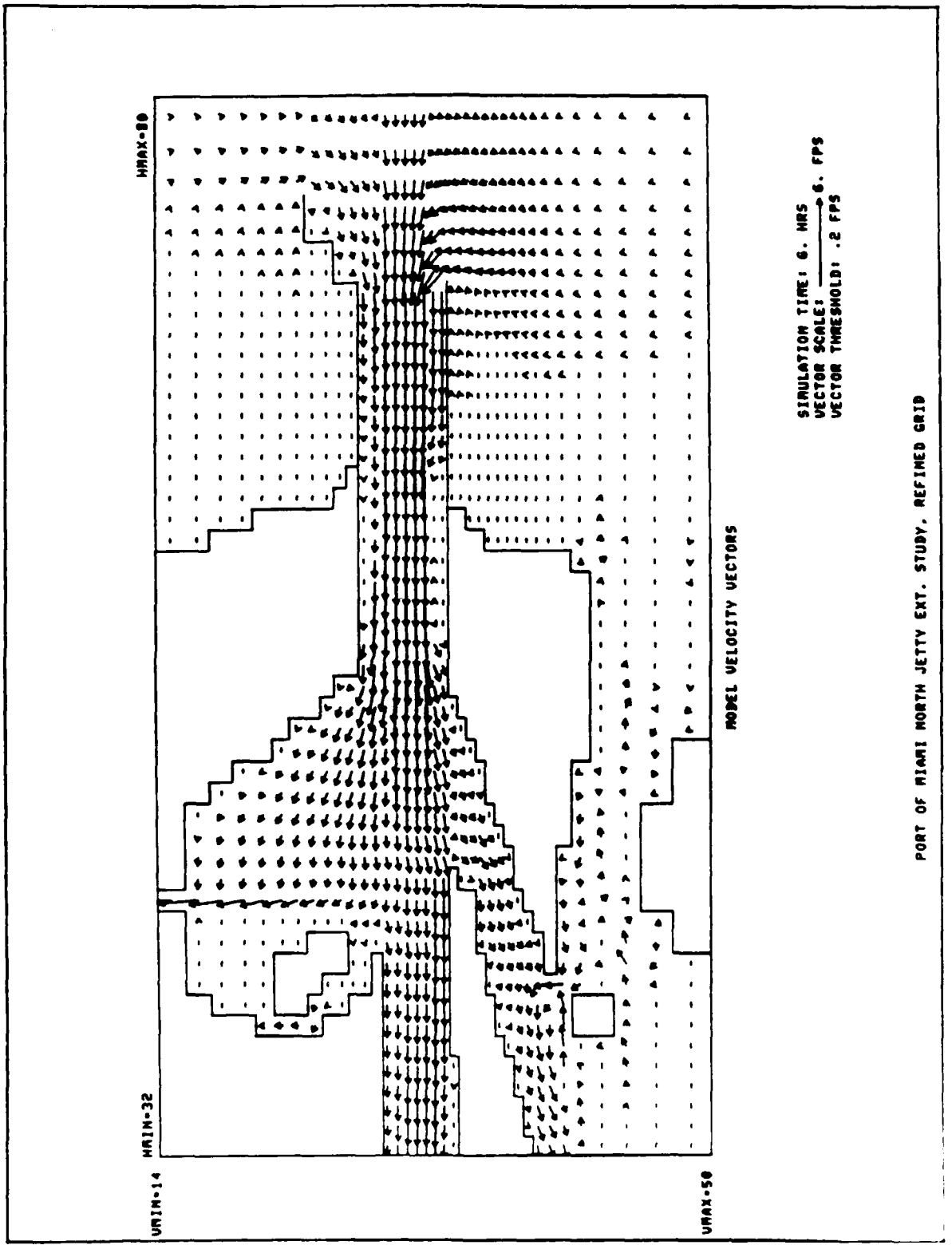
PORT OF MIAMI NORTH JETTY EXT. STUDY, REFINED GRID
MODEL VELOCITY VECTORS
SIMULATION TIME: 6. HRS
VECTOR SCALE: ——→ 6. FPS
VECTOR THRESHOLD: .2 FPS
HMAX=80
HMIN=32
UMIN=14
UMAX=50

PLATE 46

AD-A190 505 PORT OF MIAMI NUMERICAL MODEL STUDY(U) COASTAL 2/2
ENGINEERING RESEARCH CENTER VICKSBURG MS A SWAIN
JAN 88 CERC-MP-88-2

UNCLASSIFIED F/G 13/2 NL

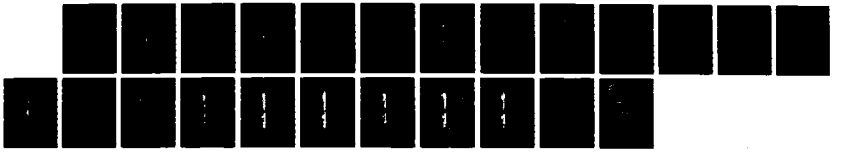

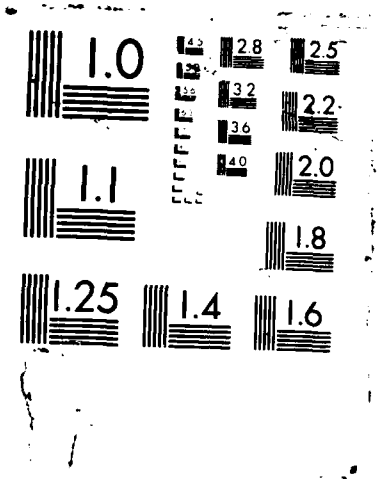
1.0
2.8
2.5
3.2
2.2
3.6
4.0
2.0
1.1
1.8
1.25
1.4
1.6

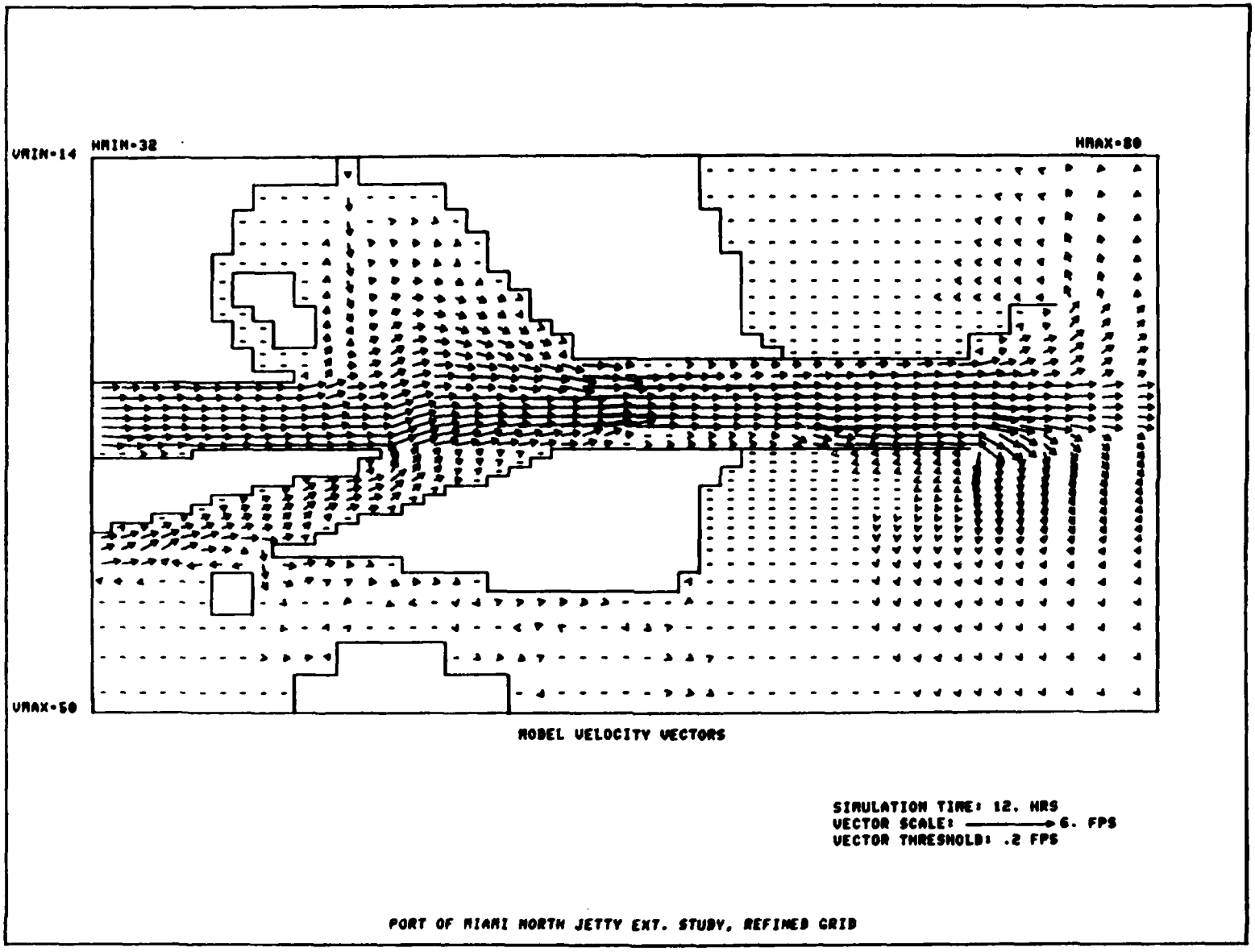

PORT OF MIAMI NORTH JETTY EXT. STUDY, REFINED GRID

PLATE 47

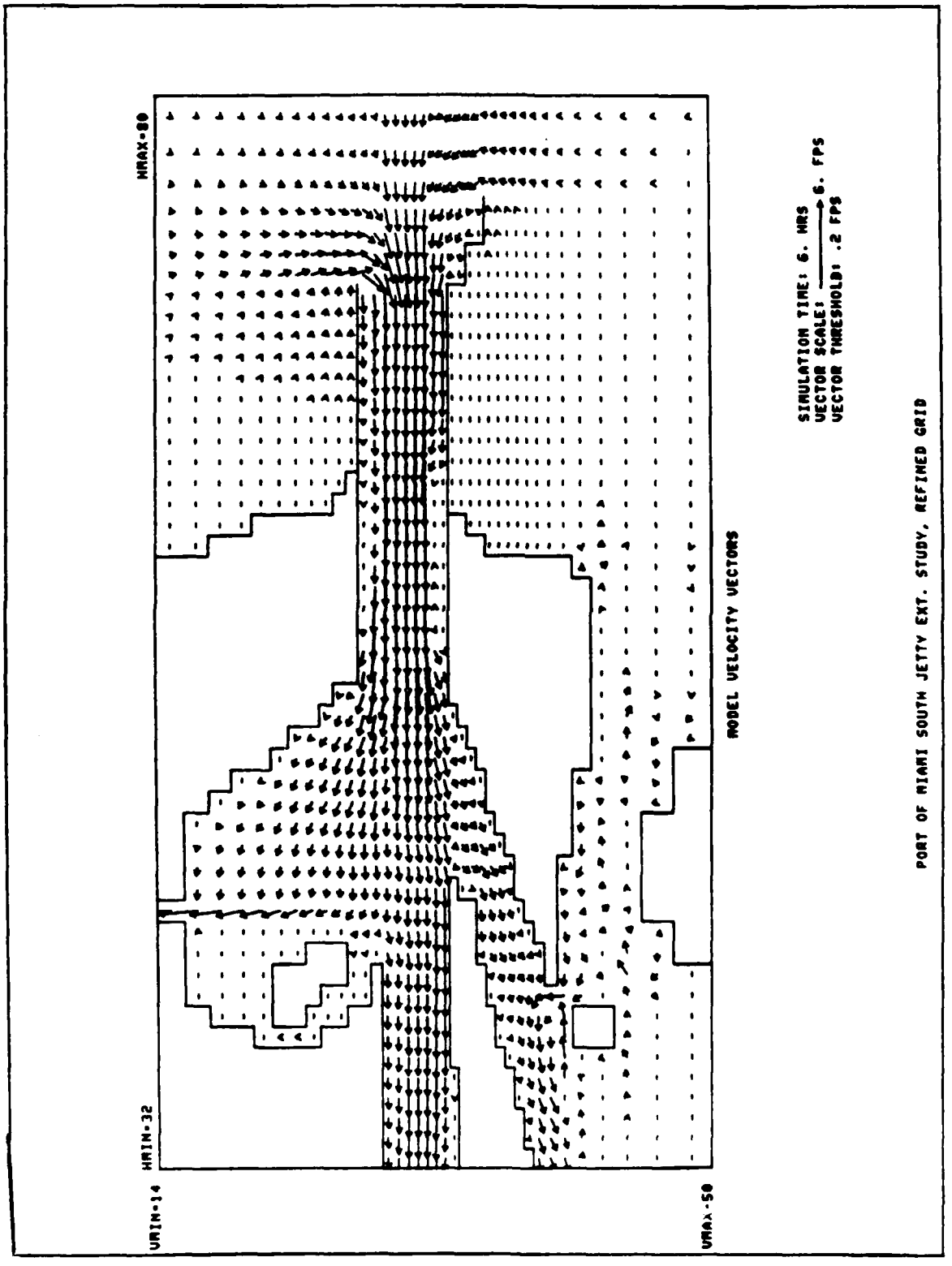
MRAX=80
MRIN=32
URIN=14
URAX=58
MODEL VELOCITY VECTORS
SIMULATION TIME: 6. HRS
VECTOR SCALE: ——→ 6. FPS
VECTOR THRESHOLD: .2 FPS
PORT OF MIAMI SOUTH JETTY EXT. STUDY, REFINED GRID

PLATE 48

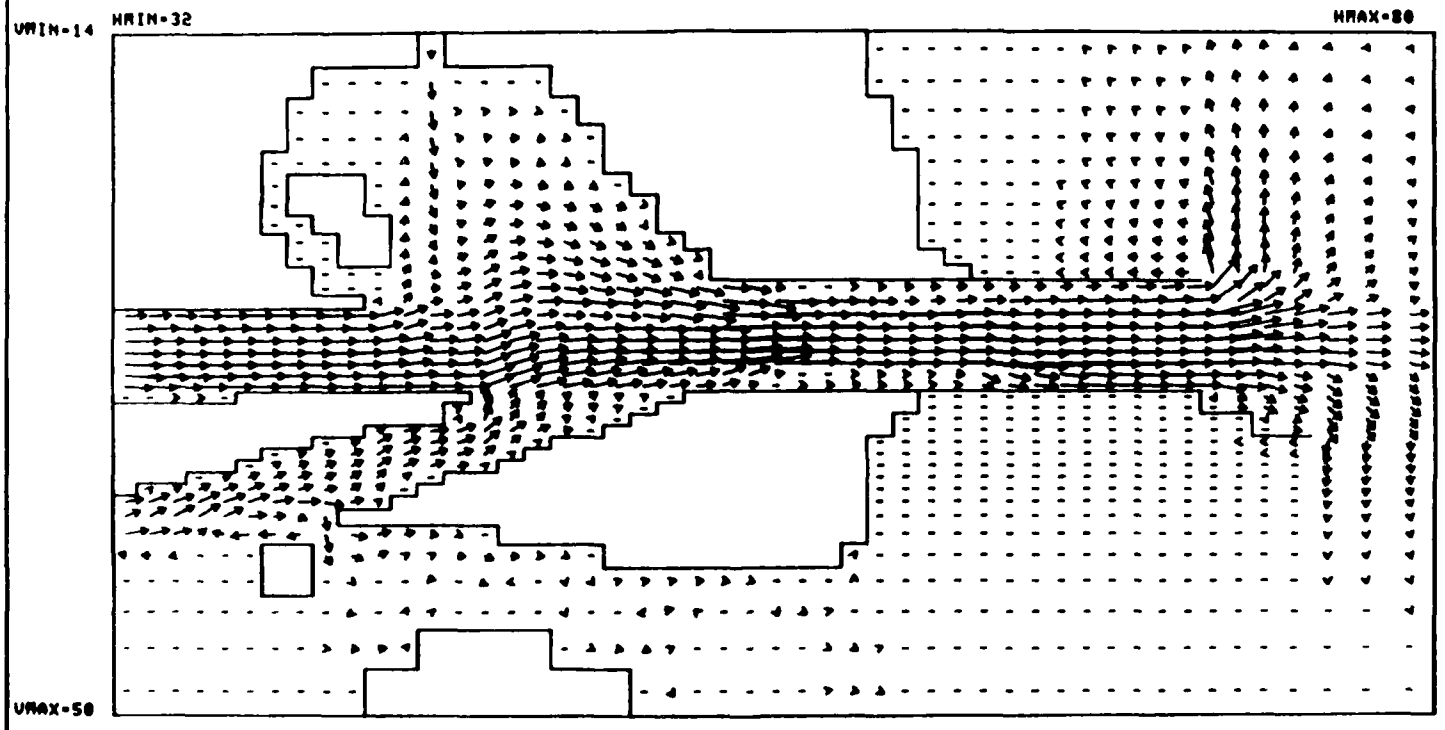

MODEL VELOCITY VECTORS

SIMULATION TIME: 12. HRS
VECTOR SCALE: ——→ 6. FPS
VECTOR THRESHOLD: .2 FPS

PLATE 49

PORT OF MIAMI SOUTH JETTY EXT. STUDY, REFINED GRID

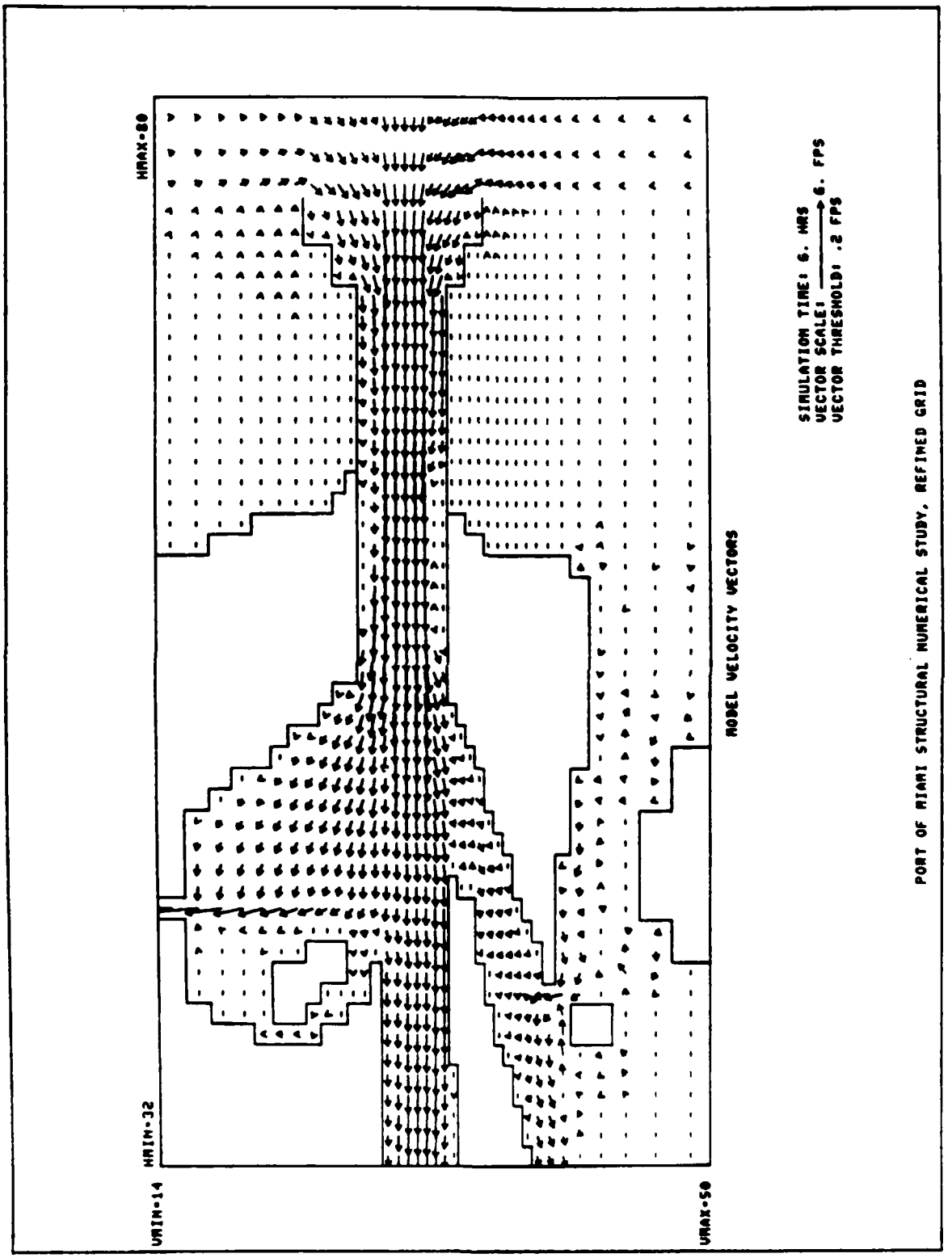
PORT OF MIAMI STRUCTURAL NUMERICAL STUDY, REFINED GRID
MODEL VELOCITY VECTORS
SIMULATION TIME: 6. HRS
VECTOR SCALE: ——→ 6. FPS
VECTOR THRESHOLD: .2 FPS
HMAX=80
HMIN=32
VMIN=14
VMAX=50

PLATE 50

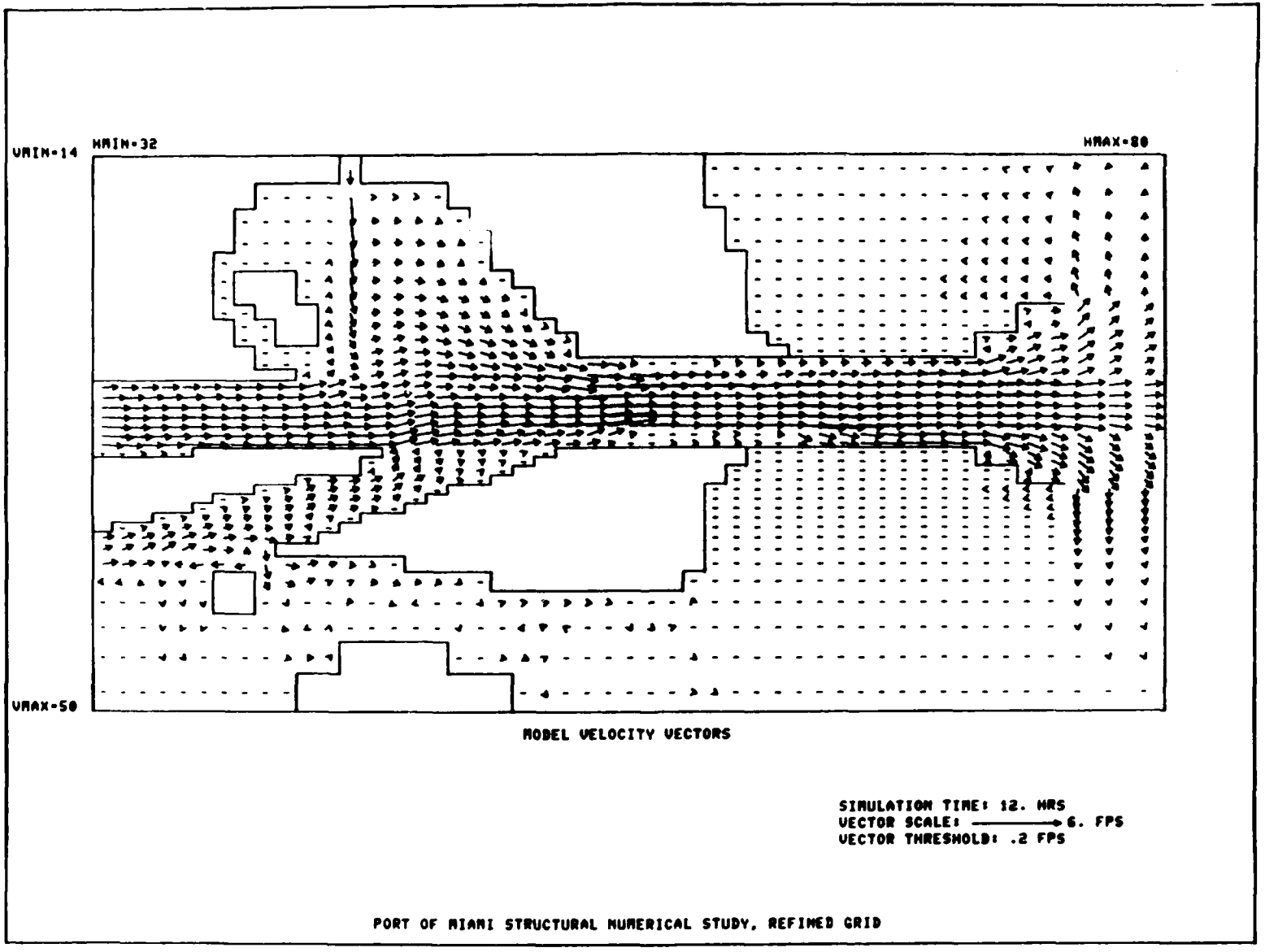
VMIN=14
MMIN=32
MMAX=80
VMAX=50
MODEL VELOCITY VECTORS
SIMULATION TIME: 12. HRS
VECTOR SCALE: 6. FPS
VECTOR THRESHOLD: .2 FPS
PORT OF MIAMI STRUCTURAL NUMERICAL STUDY, REFINED GRID

PLATE 51

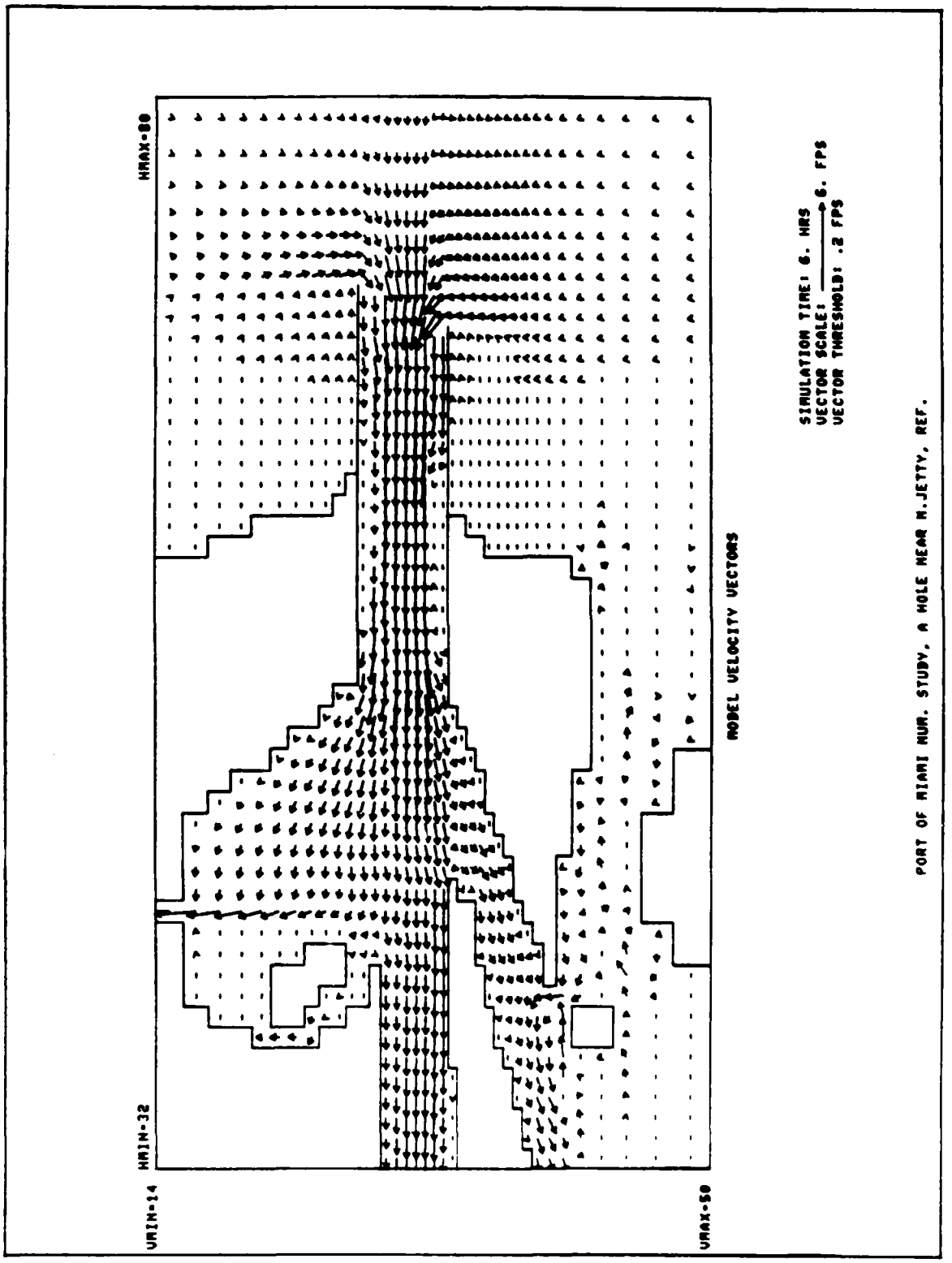
PORT OF MIAMI NUM. STUDY, A HOLE NEAR N.JETTY, REF.
MODEL VELOCITY VECTORS
SIMULATION TIME: 6. HRS
VECTOR SCALE: 6. FPS
VECTOR THRESHOLD: .2 FPS
HMAX=80
HMIN=32
VMIN=14
VMAX=50

PLATE 52

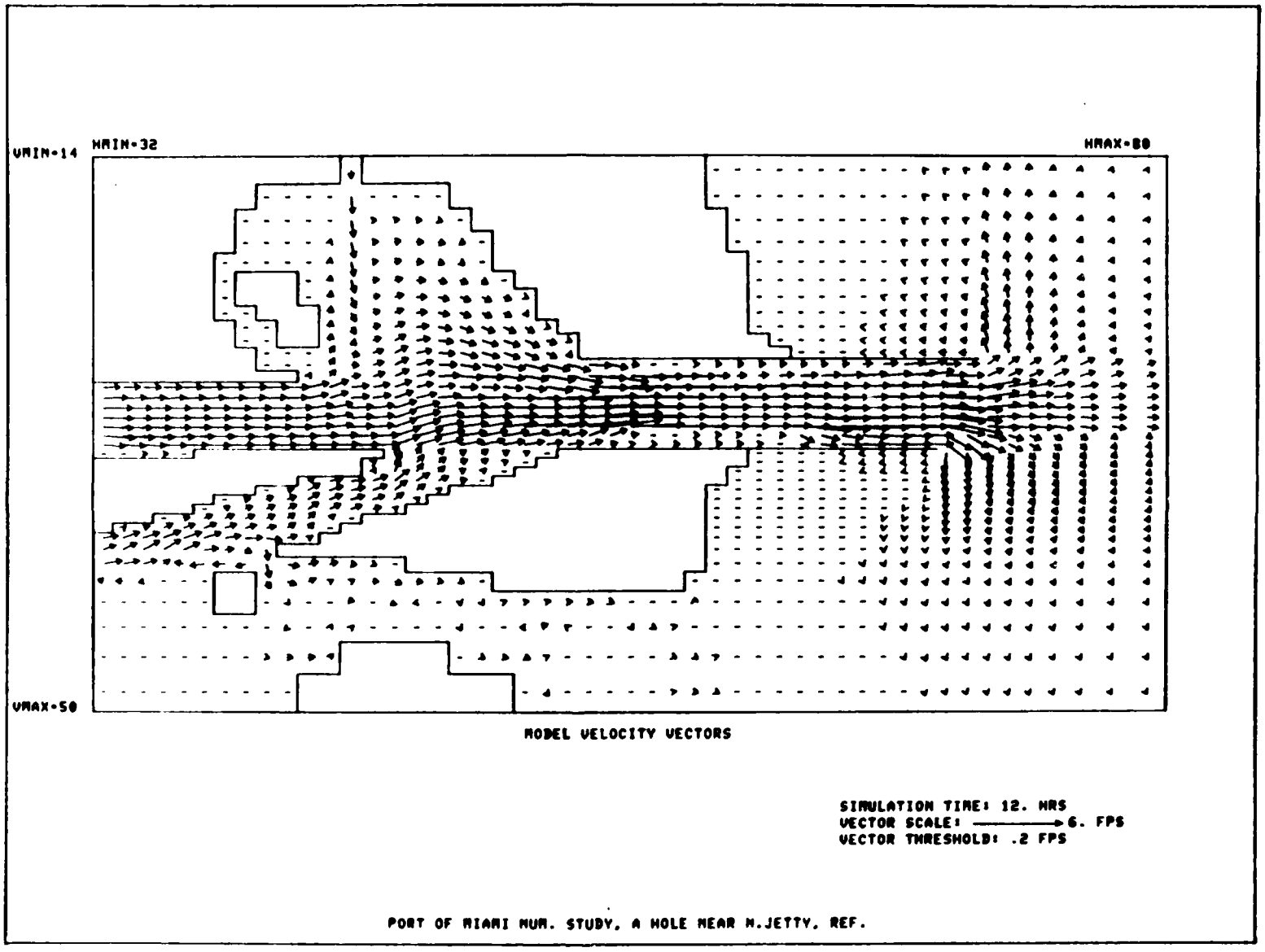
VMIN=14
HMIN=32
HMAX=80
VMAX=50
MODEL VELOCITY VECTORS
SIMULATION TIME: 12. HRS
VECTOR SCALE: 6. FPS
VECTOR THRESHOLD: .2 FPS
PORT OF MIAMI NUM. STUDY, A HOLE NEAR N.JETTY, REF.

PLATE 53

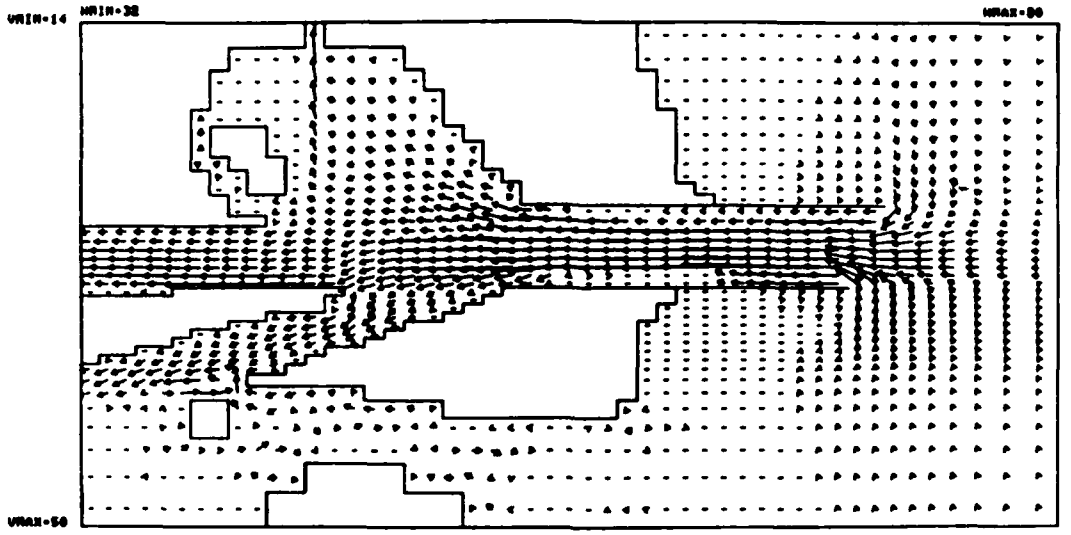

MODEL VELOCITY VECTORS

SIMULATION TIME: 6. HRS
VECTOR SCALE: ——→ 6. FPS
VECTOR THRESHOLD: .2 FPS

PORT OF MIAMI MONSTRUCTURAL STUDY, REFINED GRID

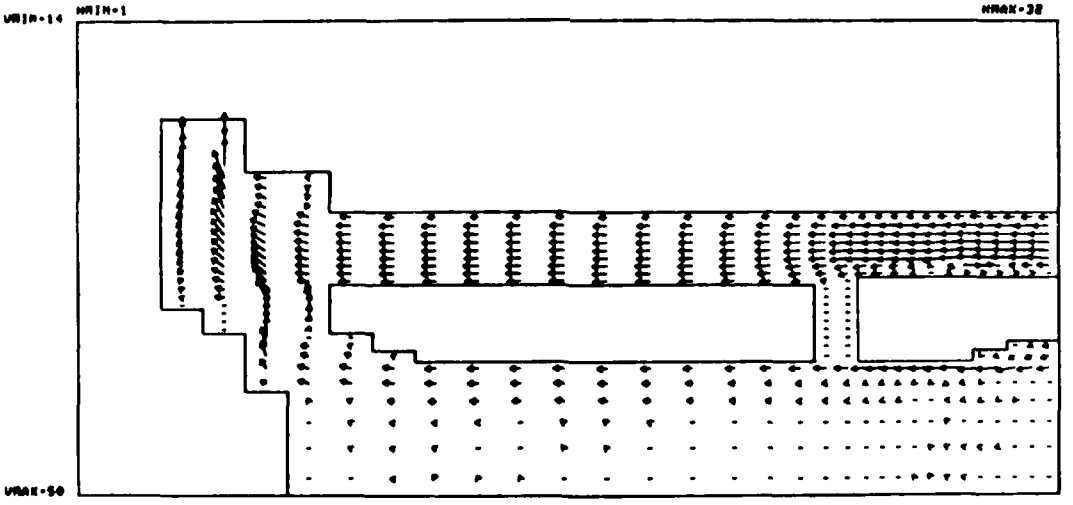

MODEL VELOCITY VECTORS

SIMULATION TIME: 6. HRS
VECTOR SCALE: ——→ 6. FPS
VECTOR THRESHOLD: .2 FPS

PORT OF MIAMI MONSTRUCTURAL NUMERICAL STUDY, REFINED GRID

PLATE 54

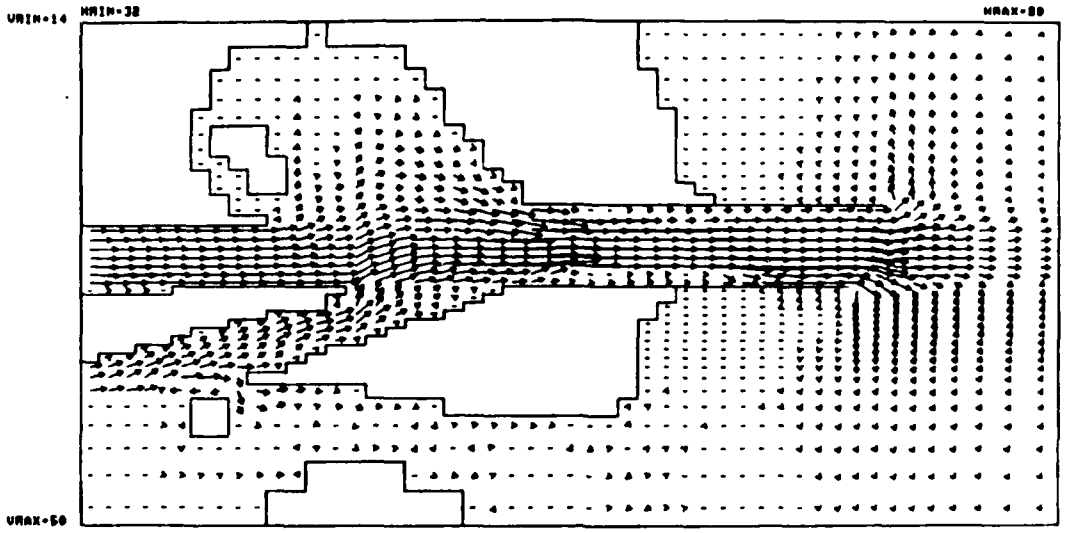

MODEL VELOCITY VECTORS

SIMULATION TIME: 12. HRS
VECTOR SCALE: ——→ 6. FPS
VECTOR THRESHOLD: .2 FPS

PORT OF MIAMI NONSTRUCTURAL STUDY, REFINED GRID

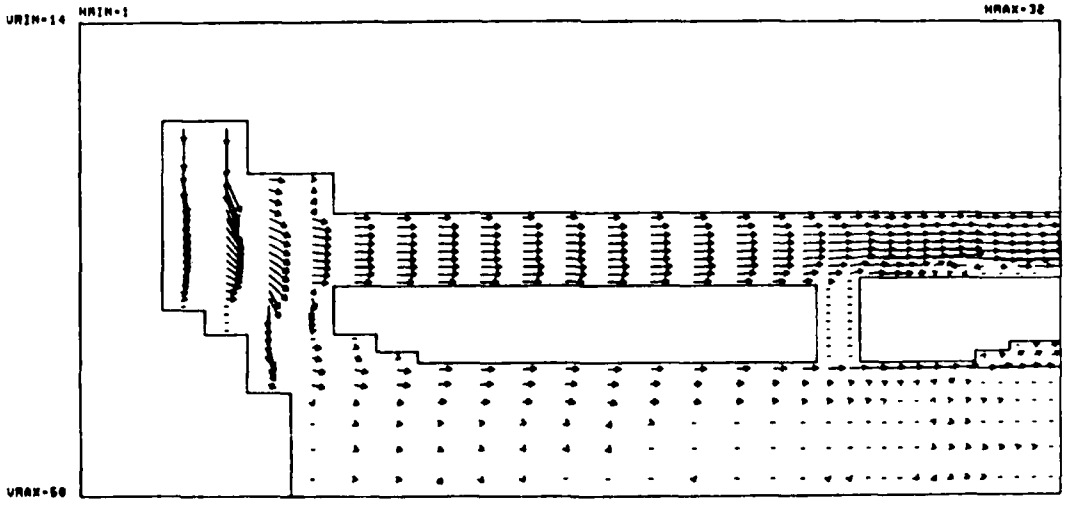

MODEL VELOCITY VECTORS

SIMULATION TIME: 12. HRS
VECTOR SCALE: ——→ 6. FPS
VECTOR THRESHOLD: .2 FPS

PORT OF MIAMI NONSTRUCTURAL NUMERICAL STUDY, REFINED GRID

PLATE 55

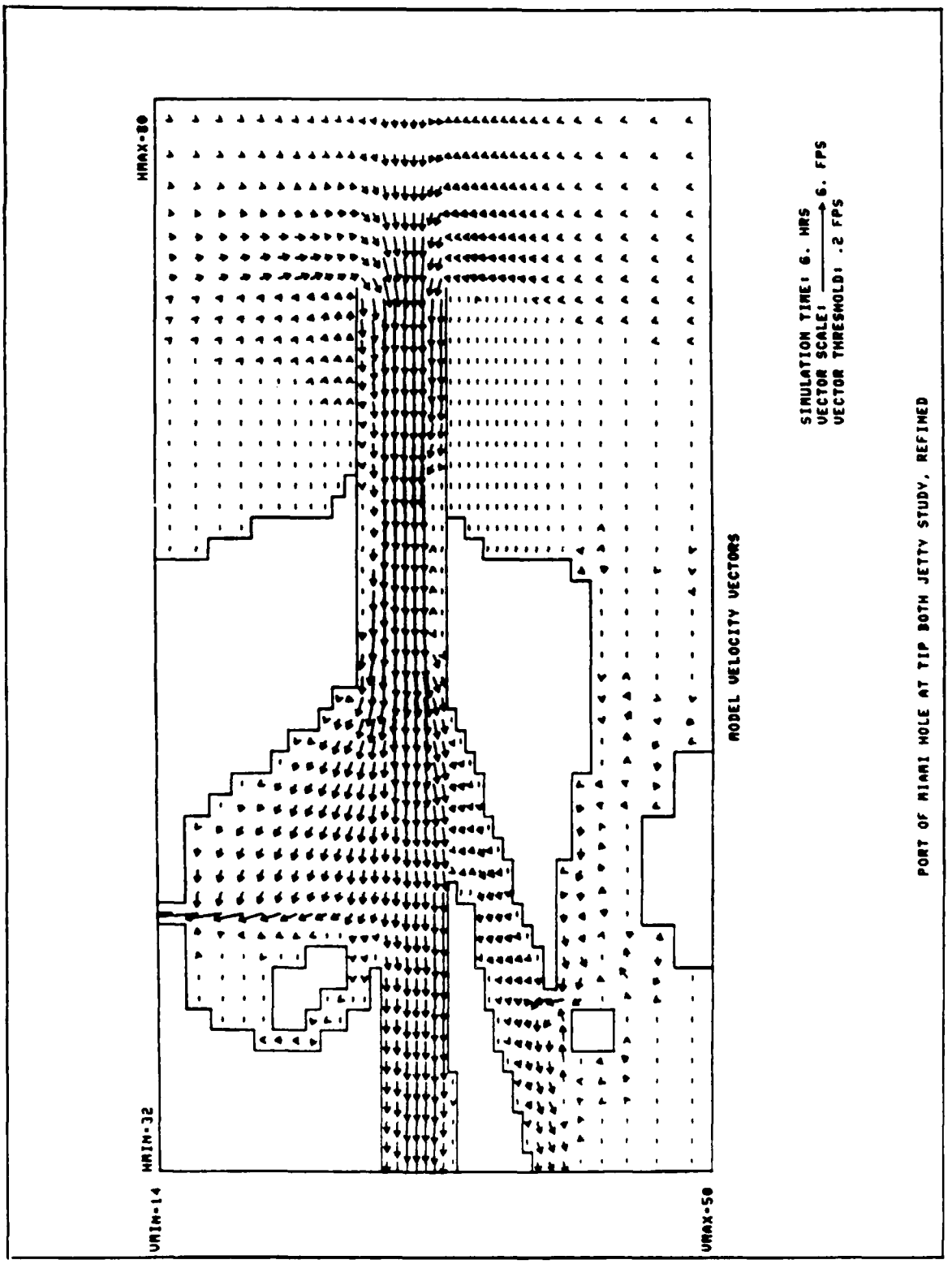
PORT OF MIAMI HOLE AT TIP BOTH JETTY STUDY, REFINED
MODEL VELOCITY VECTORS
SIMULATION TIME: 6. HRS
VECTOR SCALE: 6. FPS
VECTOR THRESHOLD: .2 FPS
HMAX-80
HMIN-32
VMIN-14
VMAX-50

PLATE 56

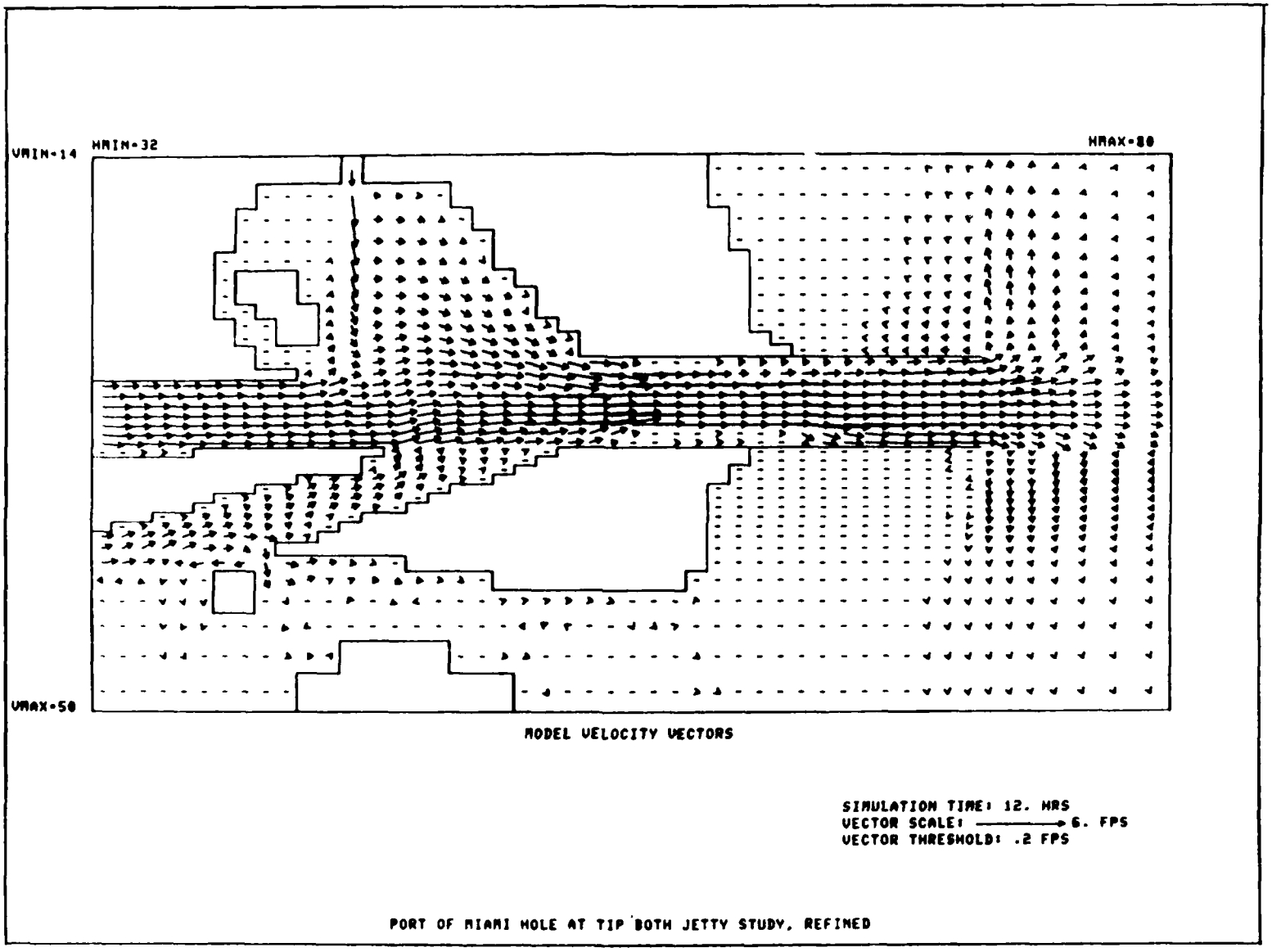

PORT OF MIAMI HOLE AT TIP BOTH JETTY STUDY, REFINED

PLATE 57

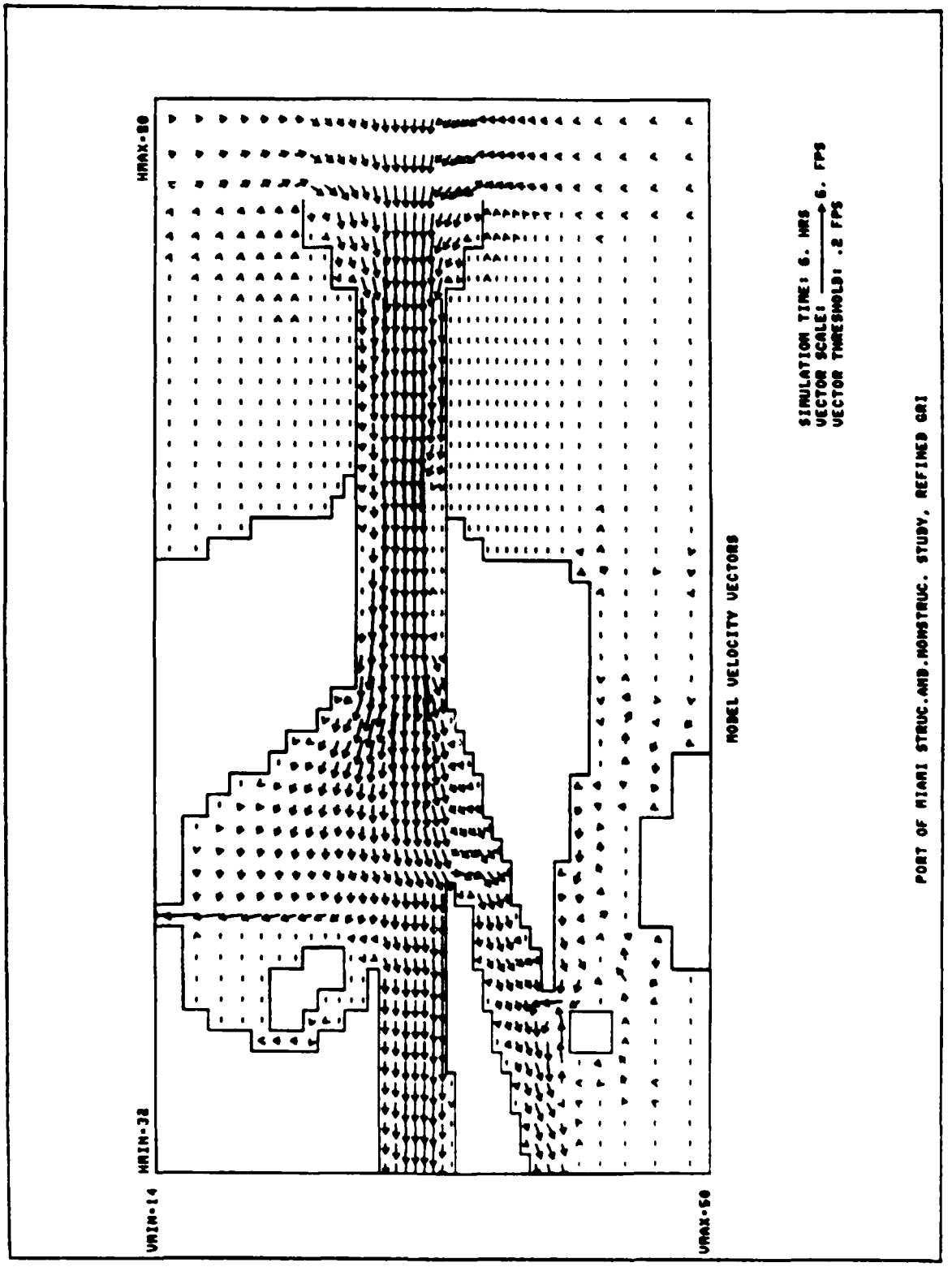
PORT OF MIAMI STRUC.AND.NONSTRUC. STUDY, REFINED GRI
MODEL VELOCITY VECTORS
SIMULATION TIME: 6. HRS
VECTOR SCALE: 6. FPS
VECTOR THRESHOLD: .2 FPS
HMAX=80
HMIN=38
VMIN=14
VMAX=50

PLATE 58

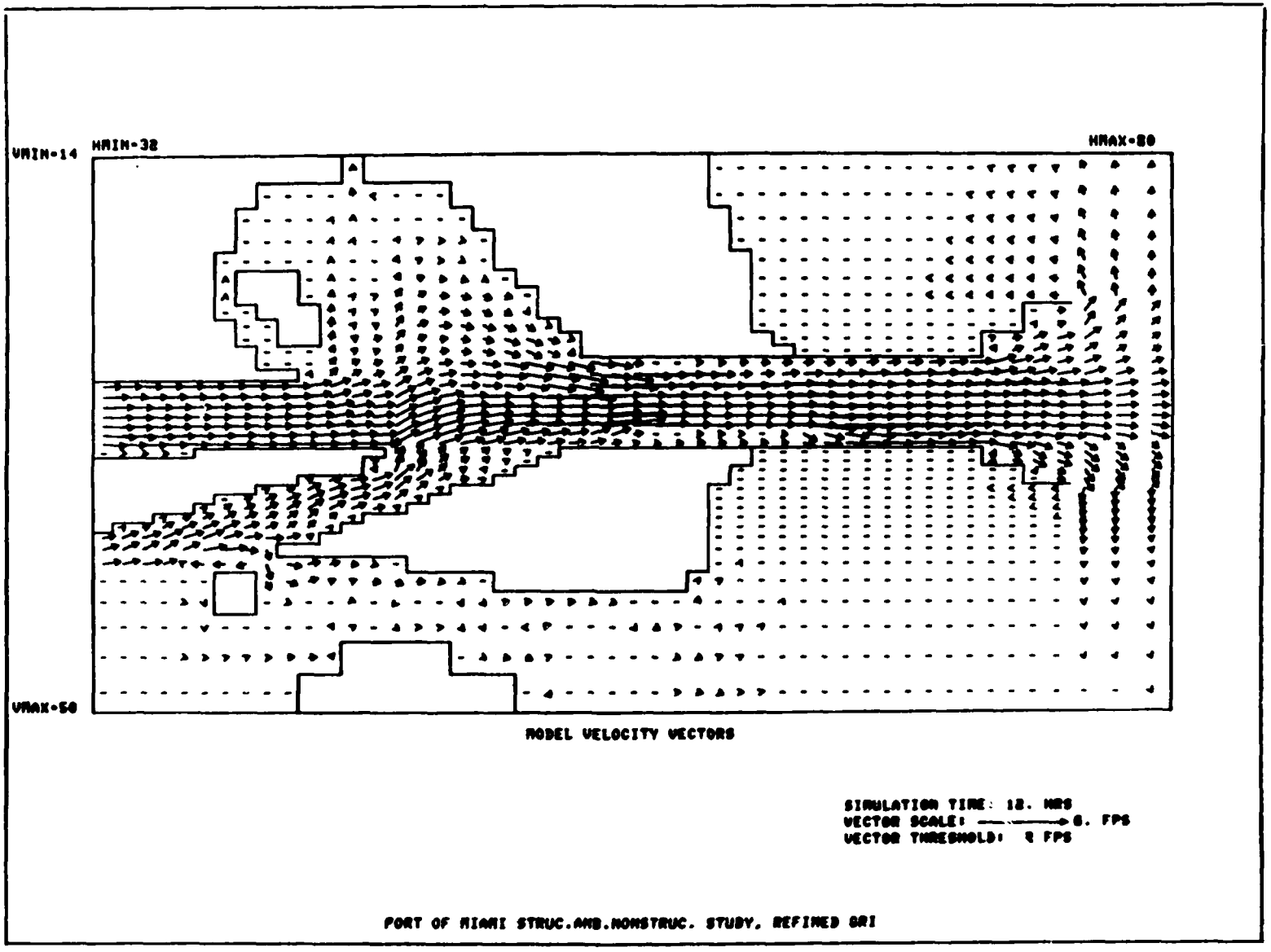
VMIN=14
HMIN=38
HMAX=80
VMAX=58
MODEL VELOCITY VECTORS
SIMULATION TIME: 12. HRS
VECTOR SCALE: 8. FPS
VECTOR THRESHOLD: 0 FPS
PORT OF MIAMI STRUC.AND.NONSTRUC. STUDY, REFINED GRI

PLATE 59

PLATE 60

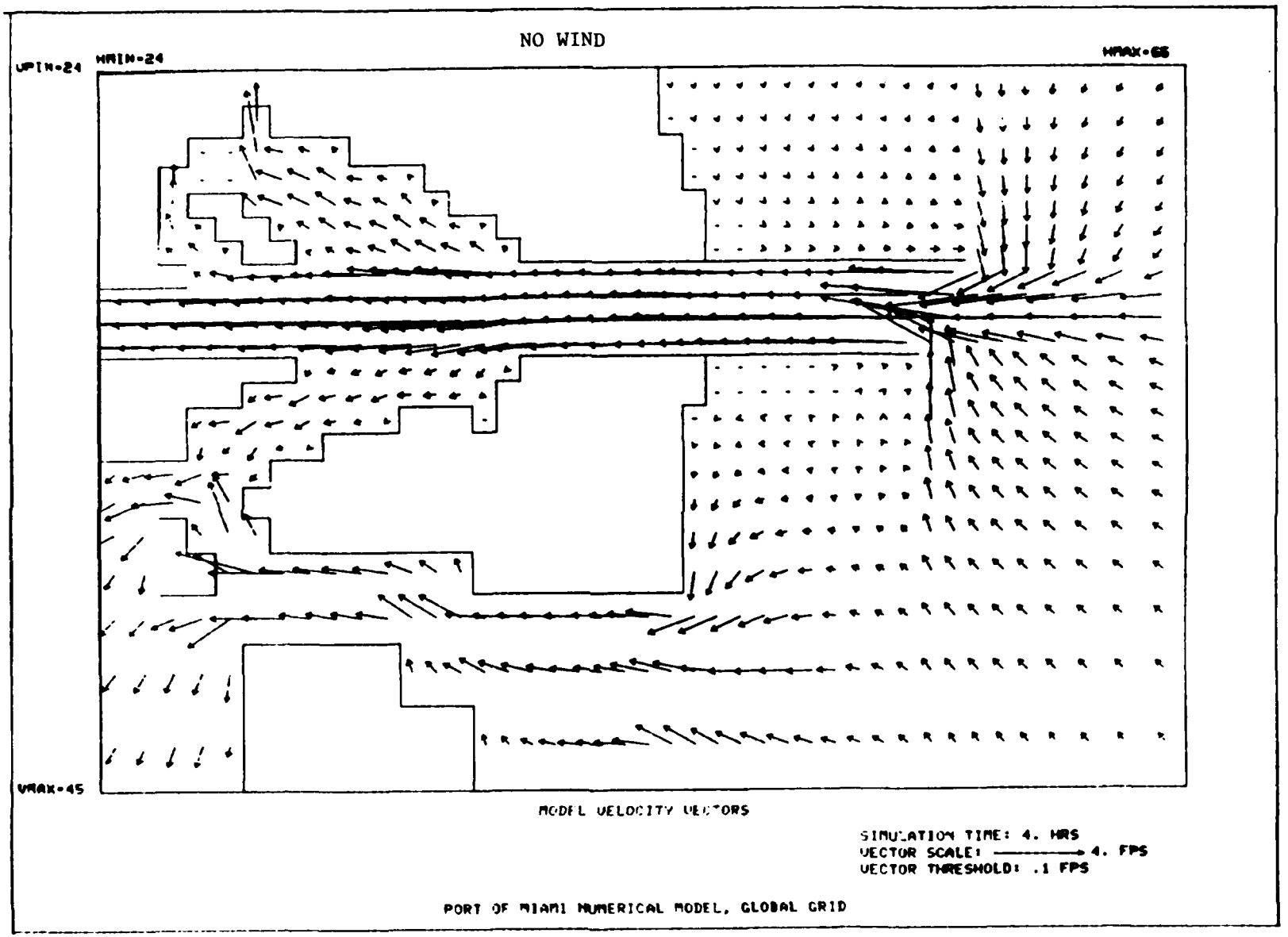
NO WIND
UMIN=24
VMIN=24
UMAX=65
VMAX=45
MODEL VELOCITY VECTORS
SIMULATION TIME: 4. HRS
VECTOR SCALE: 4. FPS
VECTOR THRESHOLD: .1 FPS
PORT OF MIAMI NUMERICAL MODEL, GLOBAL GRID

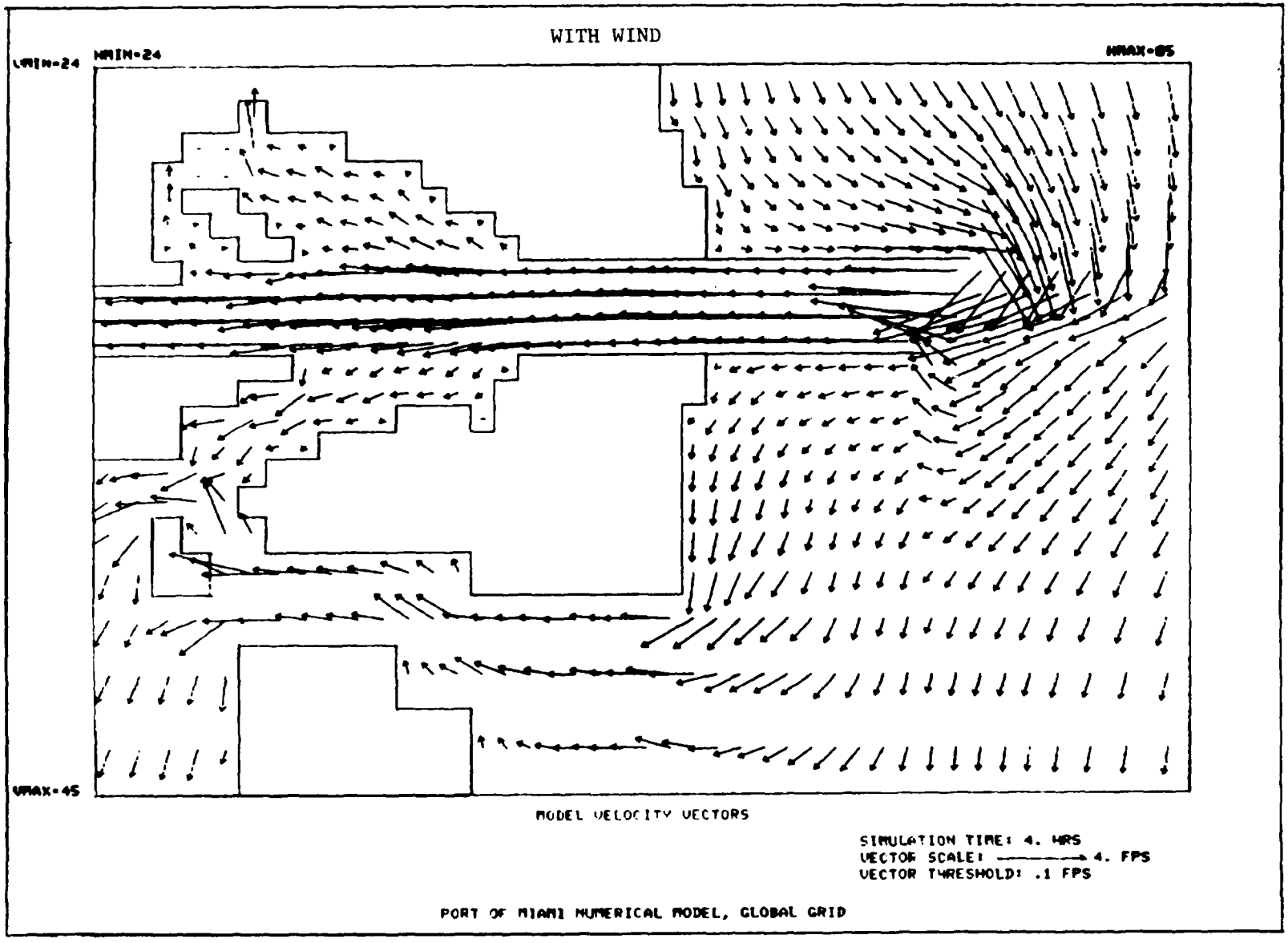
WITH WIND
MRIN=24
MRIN=24
MMAX=85
MMAX=45
MODEL VELOCITY VECTORS
SIMULATION TIME: 4. HRS
VECTOR SCALE: 4. FPS
VECTOR THRESHOLD: .1 FPS
PORT OF MIAMI NUMERICAL MODEL, GLOBAL GRID

PLATE 61

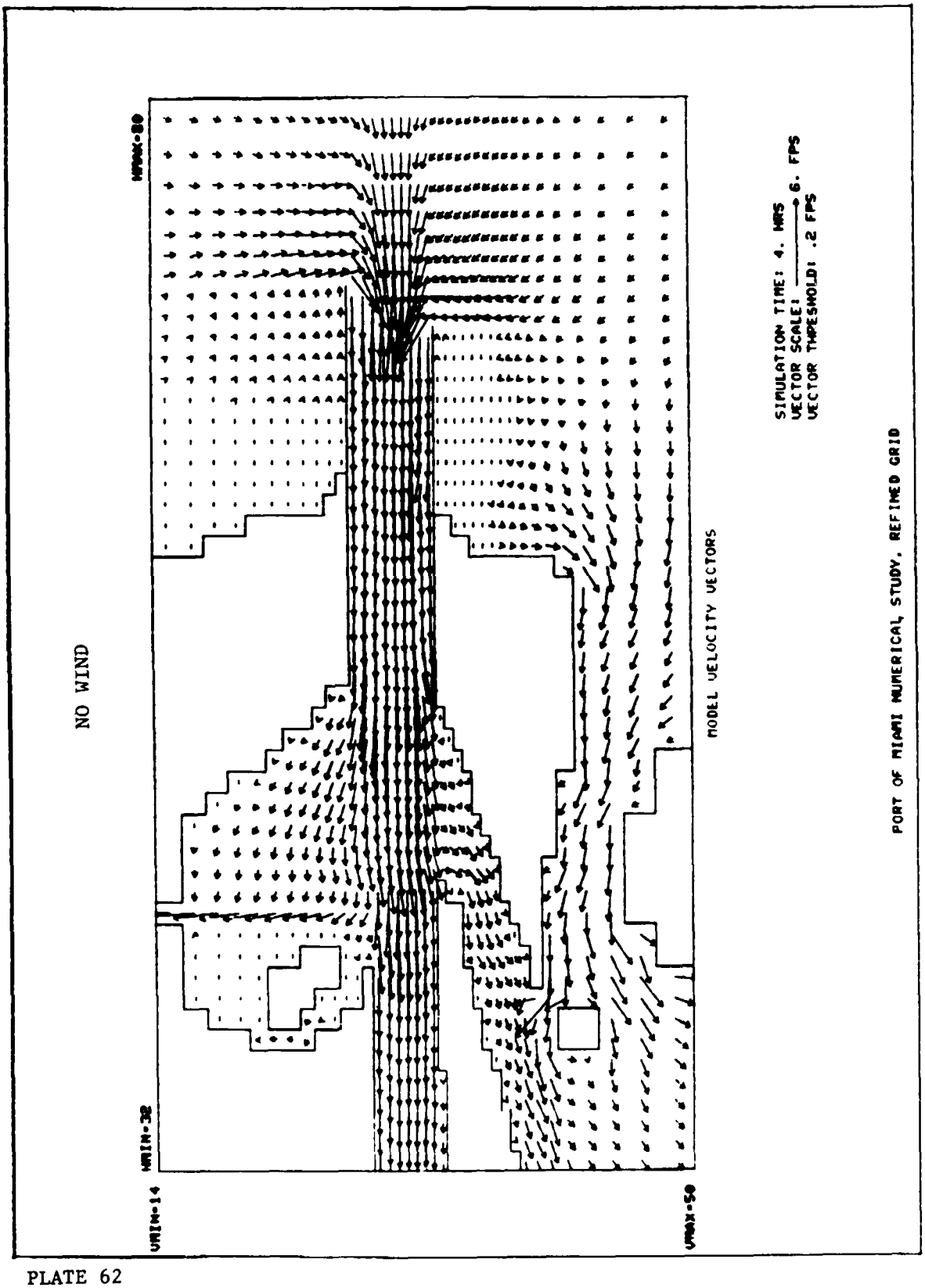
NO WIND
MODEL VELOCITY VECTORS
SIMULATION TIME: 4. HRS
VECTOR SCALE: ——→ 6. FPS
VECTOR THRESHOLD: .2 FPS
PORT OF MIAMI NUMERICAL STUDY, REFINED GRID
MMAX=80
MMIN=32
NMIN=14
NMAX=50

PLATE 62

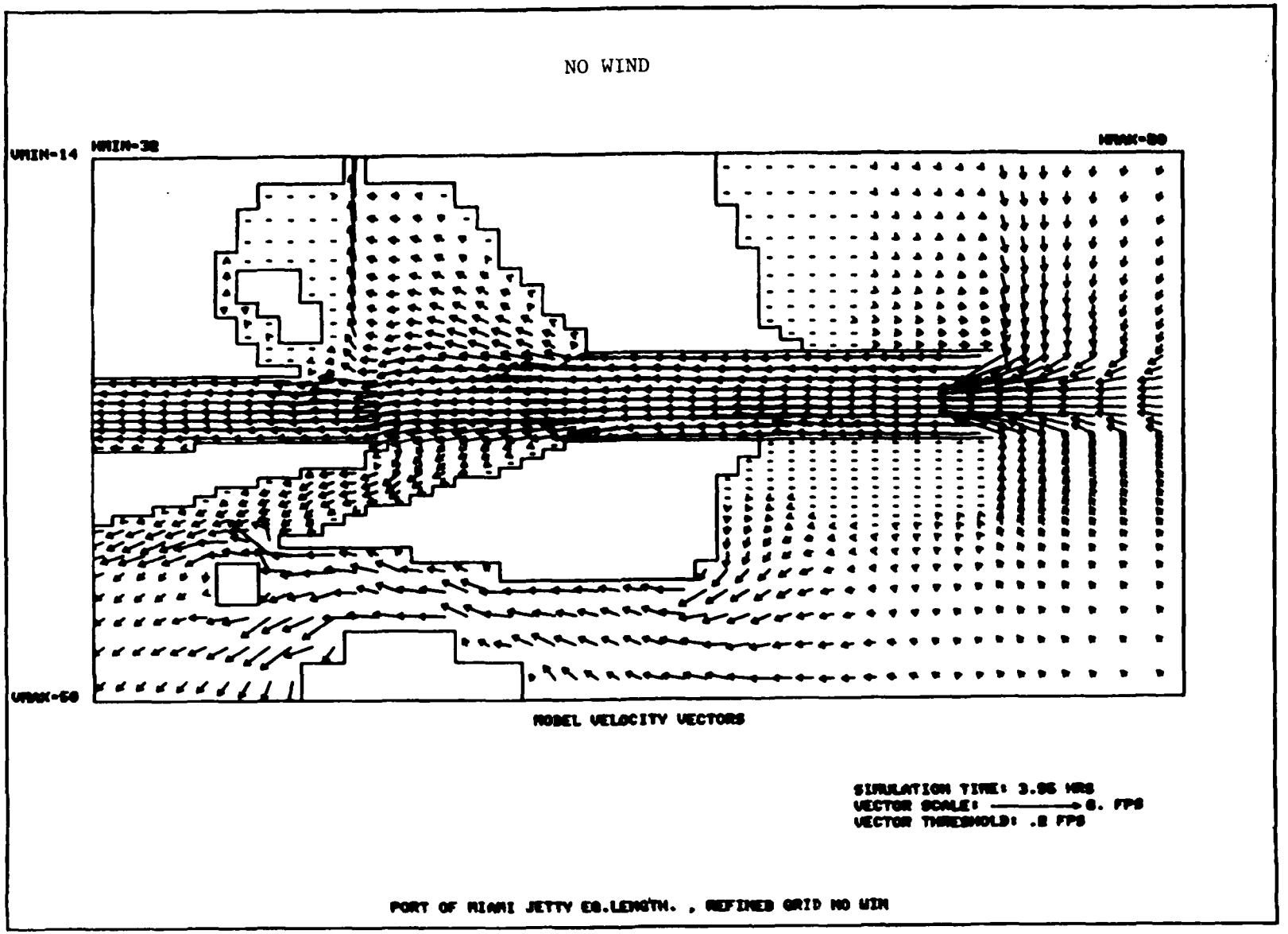
NO WIND
UMIN-14
MMIN-38
MMAX-80
UMAX-60
MODEL VELOCITY VECTORS
SIMULATION TIME: 3.05 HRS
VECTOR SCALE: 6. FPS
VECTOR THRESHOLD: .2 FPS
PORT OF MIAMI JETTY EQ.LENGTH. , REFINED GRID NO WIN

PLATE 63

PLATE 64

NO WIND

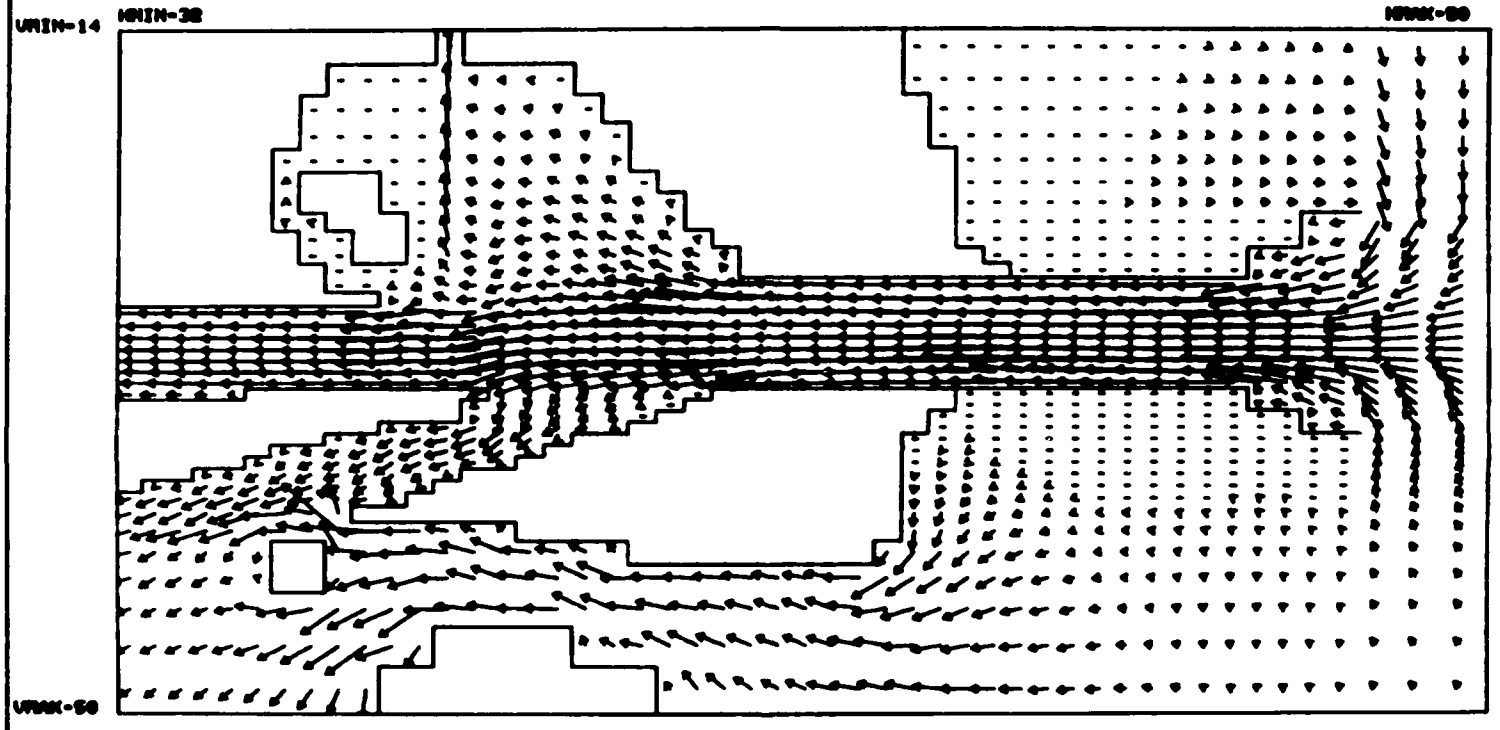

MODEL VELOCITY VECTORS

SIMULATION TIME: 3.95 HRS
VECTOR SCALE: ——→ 6. FPS
VECTOR THRESHOLD: .2 FPS

PORT OF MIAMI STRC.AND.MONSTR. , REFINED GRID NO WIN

WITH WIND

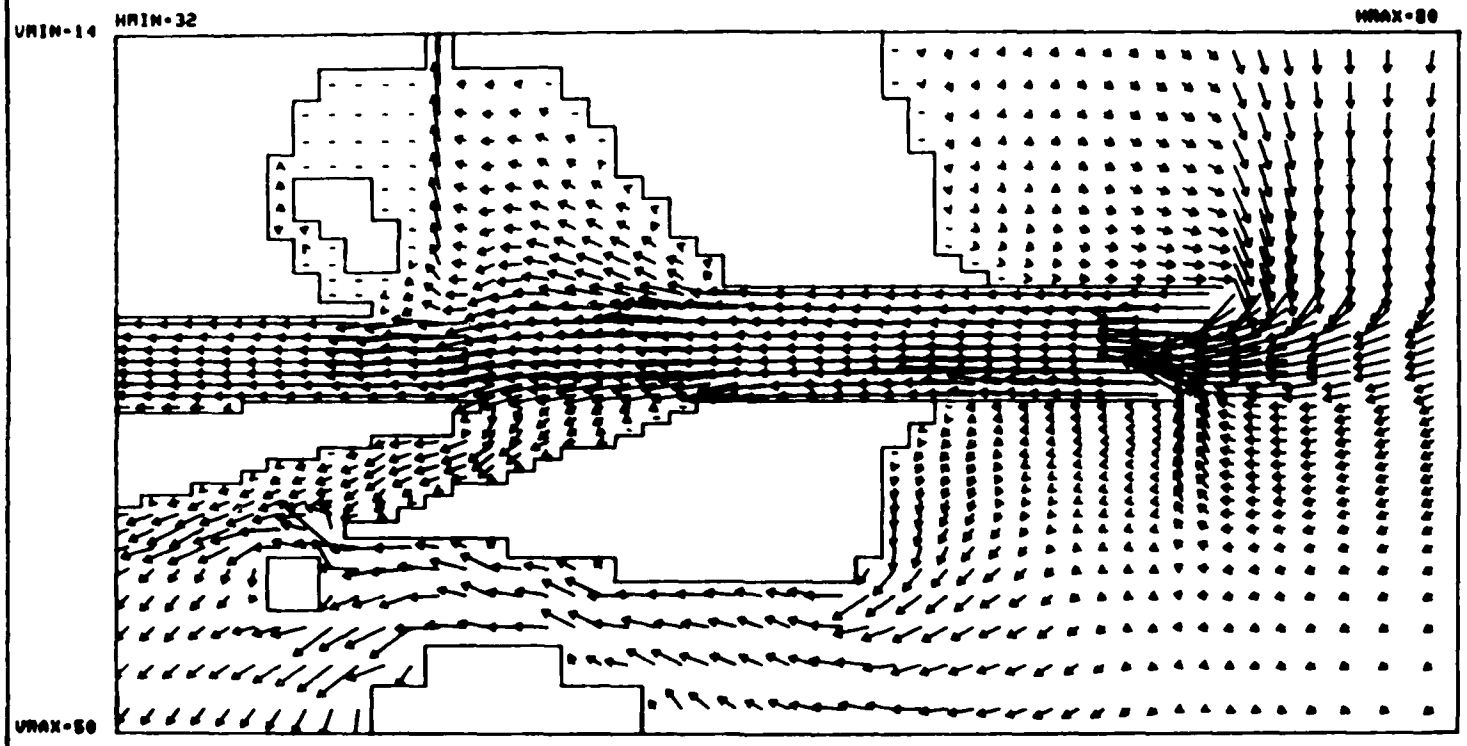

RODEL VELOCITY VECTORS

SIMULATION TIME: 3.85 HRS
VECTOR SCALE: ——→ 6. FPS
VECTOR THRESHOLD: .2 FPS

PORT OF MIAMI NUMERICAL STUDY, REFINED GRID

PLATE 65

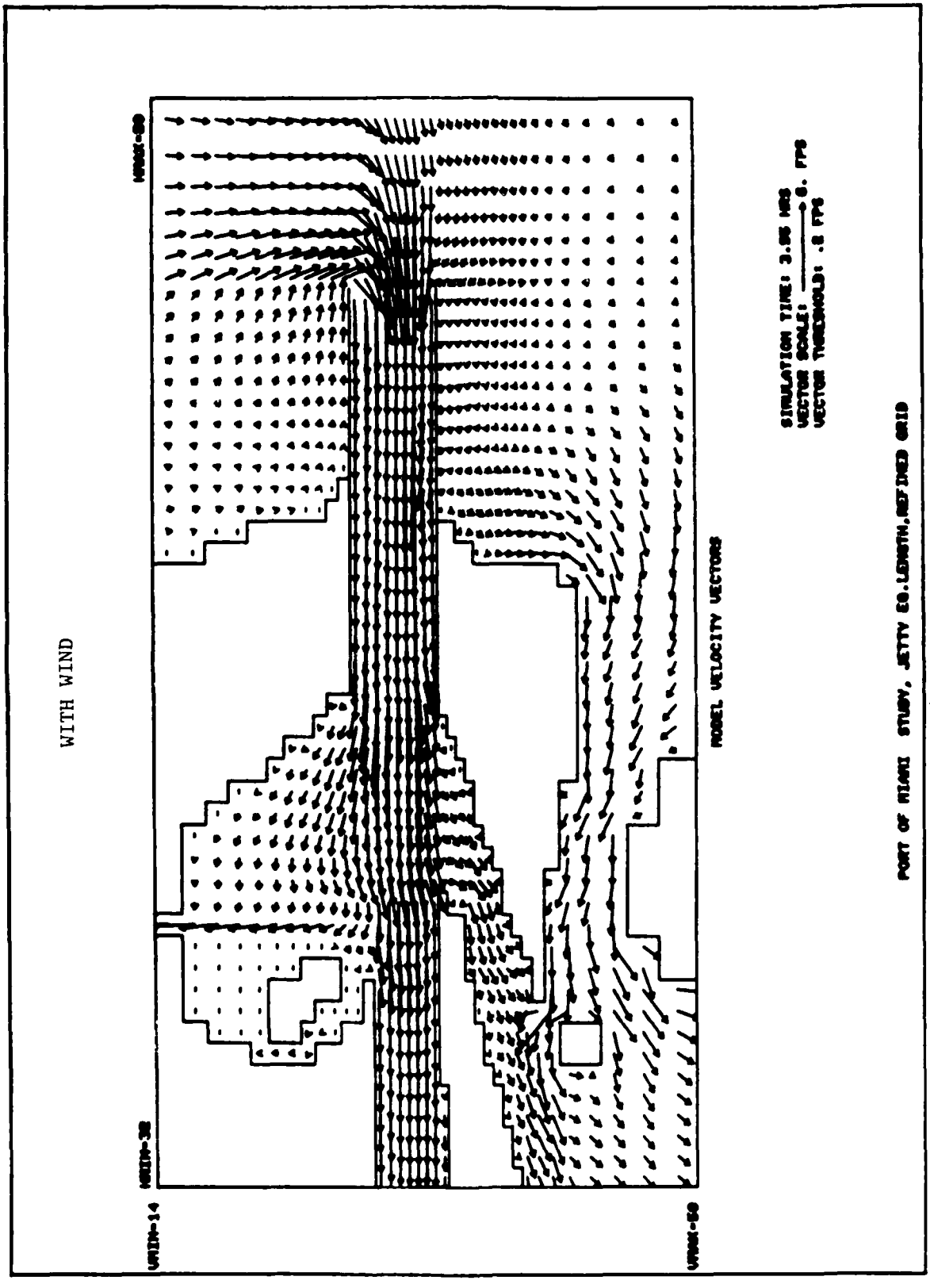
WITH WIND
MODEL VELOCITY VECTORS
SIMULATION TIME: 3.85 HRS
VECTOR SCALE: 6. FPS
VECTOR THRESHOLD: .5 FPS
PORT OF MIAMI STUDY, JETTY EQ.LENGTH,REFINED GRID

PLATE 66

WITH WIND

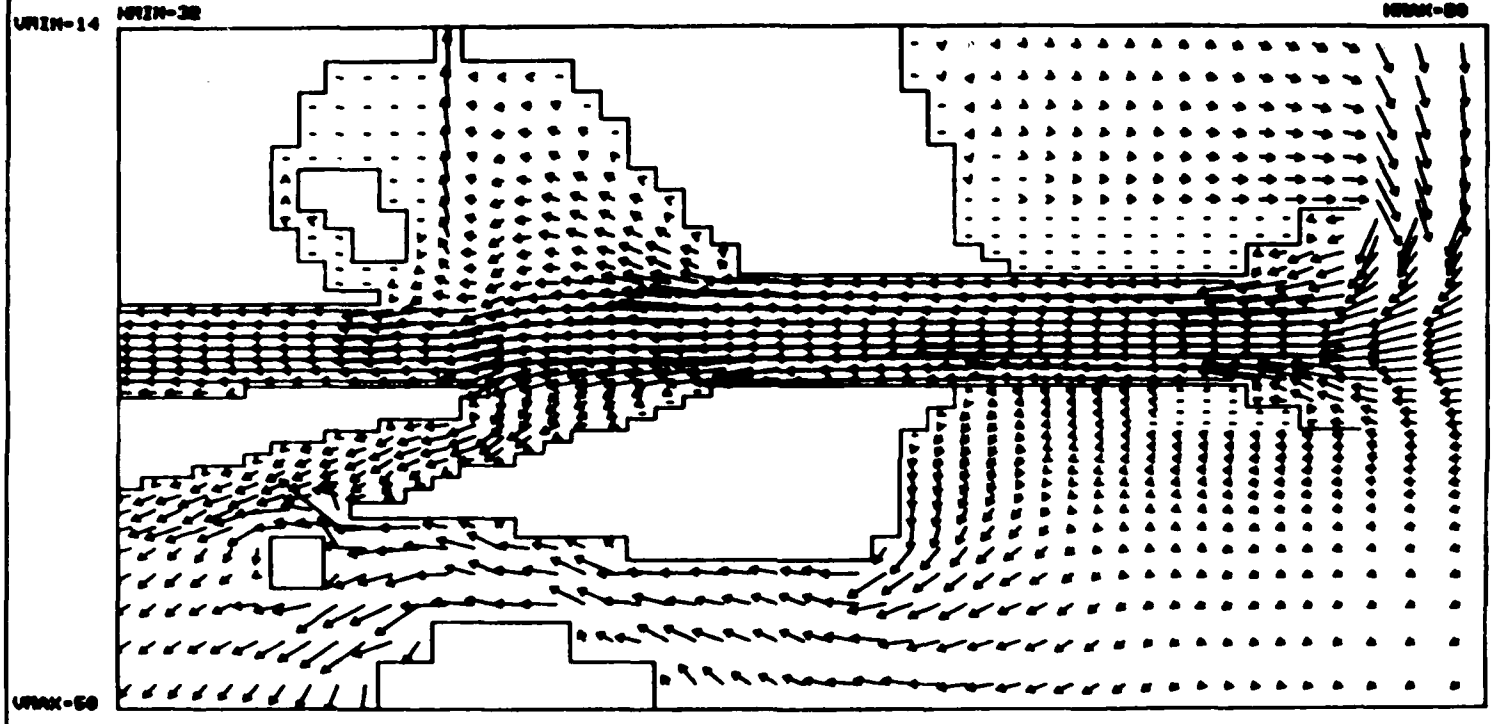

MODEL VELOCITY VECTORS

SIMULATION TIME: 3.85 HRS
VECTOR SCALE: ——→ 6. FPS
VECTOR THRESHOLD: .2 FPS

PORT OF MIAMI STRUC.AND.MONSTRUC. STUDY, REFINED GRI

PLATE 67

APPENDIX A: NOTATION

a,b,c	Regional constants derived from stretching transformation of coordinate system
A,B	Coefficient matrices
C	Chezy friction coefficient
d	Total depth of water column $d = \eta - h$
f	Coriolis parameter
g	Acceleration due to gravity
h	Local ground (cell) elevation above datum
k	Integer time-step counter
n	Dimensionless parameter used to characterize stability criterion
R	Rate of water volume change in the system (for example through rainfall or evaporation)
t	Time
u	Vertically averaged water velocity in x-direction
U	Matrix consisting of η, u, and v, as functions of x, y, and t
v	Vertically averaged water velocity in x-direction
V	Largest velocity encountered at a computational cell
x,y	Cartesian coordinate system axes
X	Smaller value of x and y
Z	Computational grid lines defined by positive integer value
Δt	Time-step
$\Delta x, \Delta y$	Length of computational cell in x- and y-direction
ϵ	Eddy viscosity coefficient
η	Water surface elevation above datum
η_a	Hydrostatic water elevation due to atmospheric pressure differences
$\lambda_x \lambda_y$	Two-dimensional differences operators
ρ	Air density
τ	Surface stress of wind
*	Intermediate time-step level
∂	Positive integer representing computational grid line
δ_x, δ_y	Centered difference operators

END

DATE

FILMED

4-88

DTIC